Detecting Plant Functional Traits of Grassland Vegetation Using Spectral Reflectance Measurements

Dissertation

zur

Erlangung des Doktorgrades (Dr. rer. nat.)

der

Mathematisch-Naturwissenschaftlichen Fakultät

der

Rheinischen Friedrich-Wilhelms-Universität Bonn

vorgelegt von

Jens Lothar Hollberg

aus Hilden

Bonn, August 2017

Angefertigt mit Genehmigung der Mathematisch-Naturwissenschaftlichen Fakultät der

Rheinischen Friedrich-Wilhelms-Universität Bonn

Abstract

Grasslands cover more than 30% of the earth's terrestrial surface, host a diverse flora and fauna and provide the habitat for many endemic animal- and plant-species. However, changes in climate and an intensified agricultural use threaten grassland ecosystems in many places. To allow an effective conservation of grassland vegetation communities, ecologists monitor variations in their plant functional traits (FTs). FTs are morphological, physiological or phenological properties of plants, which are measured at the individual plant level. Using FTs it is possible to evaluate the responses of vegetation communities to changes in the environment (e.g. to climate conditions) and to management actions, such as nutrient supply, cutting frequency and grazing intensity. Thereby, FTs enable scientists to assess variations in grassland status, independent of the taxonomic identity of the occurring plant species.

However, manual measurements of FTs are costly as well as time-consuming and often require destructive sampling techniques. Grassland ecologists and agronomists are thus seeking for novel methods to efficiently monitor and map changes in grassland FTs. Previous studies indicate that remote sensing (RS) may provide a universal solution to the mentioned problems and further allows to collect spatially contiguous and multitemporal information on functionally important plant properties.

To test the performance of RS systems for detecting FTs, the Rengen Grassland Experiment in Germany was selected as study site. Due to more than 70 years of constant fertilization along a gradient from limed only to fully fertilized (treated with lime, nitrogen, phosphorus and potassium), characteristic plant communities have developed, which differ considerably in their FTs. In this experimental setting, the spectral reflectance of five different plant communities was collected over a period of three years using an Analytical Spectral Devices Inc. FieldSpec 3 (FS 3) spectroradiometer. This instrument provides information on the portion of incident light reflected from a surface in 2150 sections (i.e. spectral bands) in the visible and infrared regions of the electromagnetic spectrum. Within one day distance in time to the acquisition of RS data, 23 different FTs were measured using manual methods (i.e. those currently used by ecologists).

The aims of this work were to (1) develop a method to reliably distinguish grassland vegetation communities using spectral reflectance measurements, (2) estimate the FTs in these communities based on canopy reflectance and (3) evaluate the potential of RS sensors featuring different spectral resolutions (i.e. numbers and widths of spectral bands) and ranges (i.e. regions of the electromagnetic spectrum measured) for detecting the FTs of grassland.

In the first step, it was investigated if and how the five grassland communities can be distinguished using 15 different remotely sensed vegetation indices (VIs). It was found that the performance of single VIs for differentiating the studied plant canopies fluctuated considerably over time. Consequently, it was not possible to distinguish the communities with a high accuracy throughout all phases of their phenological development using solely one VI. However, at those points in time when VIs sensitive to one biophysical variable (e.g. to biomass) featured only low classification accuracies, VIs sensitive to other variables (e.g. to plant water content) still allowed a successful classification. Although these results indicate that a differentiation of grassland communities using single VIs is possible, the identification of the most suitable VIs at a specific phenological state requires extensive previous analyses. This complexity is further enhanced as the performances of VIs for grassland classification significantly vary between different growths and years. To solve this problem, a multi-VI approach using the random forests algorithm is proposed, which automatically selects the ideal sets of VIs for distinguishing grasslands. This approach enables a stable and accurate classification of grassland communities throughout the entire growing season, irrespective of the plant phenological state.

In the second step, it was studied how well the FTs of the different grassland communities can be estimated based on RS data. Using partial least squares regression (PLSR) it was possible to create one single model for estimating one FT of all studied grassland canopies and at all phenological stages based on its spectral reflectance. Among the 23 investigated FTs, nine were modelled with high accuracy (R² validation, $R^2_{val} \geq 0.6$), including plant height, fraction of photosynthetically active radiation absorbed, carbon-to-nitrogen ratio, tiller fresh matter, nitrogen content, compressed sward height, SPAD-value of the leaves, neutral detergent fiber content of the plant and leaf area. Models for plant fresh matter, leaf fresh matter, leaf dry matter and leaf dry matter content reached moderate accuracies ($0.6 > R^2_{val} \geq 0.4$). Only low accuracies ($R^2_{val} < 0.4$) were determined for the models relating the spectral reflectance to plant dry matter, tiller dry matter, plant dry matter content, tiller dry matter content, plant-, tiller- and leaf water content, carbon content, leaf-stem-ratio and specific leaf area. It is thus concluded that field spectrometry allows to collect information on many (13 of 23) tested FTs of different grassland communities over entire growing seasons with moderate to high accuracy. This method is thus of large importance for agricultural and ecological research because it makes a cost-efficient, time-saving and non-destructive monitoring of FTs possible.

Within the third part of this study, the potential of different RS systems for detecting FTs was assessed. Based on spectral reflectance data recorded with a full-range FS 3, the bands of the half-range field spectroradiometer ASD HandHeld 2 (HH2, 785 bands), the hyperspectral satellite sensor EnMAP (EnM, 242 bands) and three multispectral satellite sensors, including Sentinel-2 (S-2, 13 bands), Landsat 7 (L 7, seven bands) and RapidEye (RE, five bands), were simulated. Thirteen FTs were successfully modeled ($R^2_{val} > 0.4$) using FS 3, 11 using EnM and ten using HH 2 data. Based on multispectral information, $R^2_{val} > 0.4$ were reached with S-2 for nine, L 7 for four and RE data for none of the 23 FTs. These results show that hyperspectral RS systems enable scientists to create models featuring higher accuracies for detecting FTs than multispectral systems. We infer that that a broad spectral range of a sensor is an important factor for producing accurate estimates of FTs. A high number of spectral bands may further allow to improve model performances.

It is concluded that hyperspectral RS systems provide the potential to collect spatio-temporal information on grassland FTs. Such information may support grassland scientists in adapting the management strategies to changes in climate and land-use intensity and to secure a sustainable cultivation of grassland ecosystems.

Zusammenfassung

Grünland bedeckt mehr als 30% der Landoberfläche der Erde, beheimatet eine artenreiche Flora und Fauna und bildet sie das Habitat vieler endemischer Tier- und Pflanzenarten. Jedoch sind diese Ökosysteme durch eine Intensivierung der Landwirtschaft sowie durch den Klimawandel vielerorts bedroht. Um eine nachhaltige Entwicklung der Vegetationsgesellschaften von Grünlandökosystemen zu ermöglichen, bewerten Ökologen Veränderungen der funktionalen Merkmale der anzutreffenden Vegetation. Funktionale Merkmale sind morphologische, physiologische oder phänologische Pflanzeneigenschaften, die am Individuum (d.h. an einer einzelnen Pflanze) gemessen werden. Mit Hilfe dieser Merkmale ist es möglich, die Reaktion von Pflanzengesellschaften auf Veränderungen der Umweltbedingungen, insbesondere der Bodeneigenschaften und des Klimas, zu quantifizieren. Anhand dieses Ansatzes können daher, auch ohne vorherige taxonomische Zuordnung der Arten, Zustandsänderungen der Pflanzenbestände erkannt und Entscheidungen zu Düngung, Mahd und Beweidung getroffen werden.

Die manuelle Messung von Funktionalen Merkmalen ist jedoch kostspielig, denn sie erfordert einen hohen Arbeitsaufwand sowie eine destruktive Probenentnahme. Daher suchen Agronomen und Ökologen nach neuen Verfahren, um Veränderungen der funktionalen Merkmale von Grünland überwachen und kartieren zu können. Frühere Untersuchungen deuten darauf hin, dass die fernerkundliche Detektion funktionaler Merkmale von Grünlandbeständen deren manuelle Erfassung ergänzen oder sogar ersetzen kann. Daher stellt die Fernerkundung eine mögliche Lösung der zuvor genannten Probleme dar und kann zudem eine räumliche und zeitlich hoch aufgelöste Erfassung von funktionalen Merkmalen ermöglichen.

Um das Potential der Fernerkundung für eine solche Detektion funktionaler Merkmalen zu evaluieren, wurde das Rengen Grasland Experiment als Versuchsstandort gewählt. Durch die mehr als 70 Jahre andauernden Unterschiede in der Düngung entlang eines Gradienten von ausschließlicher Kalkung bis hin zur Volldüngung (Zugabe von Kalk, Stickstoff, Phosphor und Kalium), entwickelten sich charakteristische Pflanzengesellschaften, die sich erheblich in der Zusammensetzung ihrer funktionalen Merkmale unterscheiden. In diesem Experiment wurde die spektrale Reflexion von fünf verschiedenen Pflanzengesellschaften mit einem Analytical Spectral Devices Inc. FieldSpec 3 (FS 3) Spektroradiometer über einen Zeitraum von drei Jahren gemessen. Dieses Instrument ermittelt den Anteil des von einer Oberfläche reflektierten einfallenden Lichts in 2150 einzelnen Abschnitten (d.h. spektralen Bändern) im sichtbaren sowie im infraroten Bereich des elektromagnetischen Spektrums. Innerhalb von maximal einem

Tag Abstand zu den Spektralmessungen wurden 23 verschiedene numerische funktionale Merkmale mit Hilfe manueller (d.h. der derzeit von Ökologen genutzter) Methoden gemessen.

Die Ziele der vorliegenden Untersuchung waren (1) eine Methode zu entwickeln, mit der verschiedene Intensitätsstufen bewirtschafteter Grünlandbestände anhand ihrer spektralen Reflexion unterschieden werden können, (2) die funktionalen Merkmale dieser Grünlandbestände mit hyperspektralen Reflexionsmessungen zu ermitteln und (3) das Potential von Fernerkundungssensoren mit verschiedenen spektralen Auflösungen (d.h. verschiedenen Anzahlen und Breiten der spektralen Bänder) sowie gemessenen Spektralbereichen für eine Detektion der funktionalen Merkmale zu evaluieren.

Dazu untersuchten wir zunächst, wie die Pflanzengesellschaften des Rengen Grasland Experiments mit 15 verschiedenen fernerkundlichen Vegetationsindizes (VIs) differenziert werden können. Die Güte der einzelnen VIs zur Unterscheidung der Pflanzenbestände variierte dabei deutlich über die Zeit. Daher war es mit keinem einzelnen VI möglich, die Pflanzengesellschaften während allen phänologischen Stadien sicher zu differenzieren. Sofern aber ein VI, der auf Veränderungen bestimmter Pflanzeneigenschaften (z.B. der Biomasse) reagiert, schlechte Ergebnisse lieferte, ermöglichten solche VIs, die auf Veränderungen anderer Pflanzeneigenschaften (z.B. den Wassergehalt der Pflanze) reagieren, weiterhin eine sichere Unterscheidung. Dies zeigt, dass eine Differenzierung der verschiedenen Grünlandgesellschaften mit sorgfältig gewählten einzelnen VIs möglich ist. Allerdings erfordert die Selektion geeigneter VIs für eine Klassifikation zu bestimmten phänologischen Stadien eine umfangreiche vorhergehende Untersuchung. Die Schwierigkeit dabei besteht darin, dass die Eignung von VIs für einen solchen Zweck sich deutlich zwischen verschiedenen Aufwüchsen sowie Jahren unterscheiden kann. Daher wurde mit Hilfe des Random-Forests-Algorithmus ein Multi-VI-Ansatz entwickelt, mit dem die für die Differenzierung bestimmter Grünlandbestände bestgeeigneten VIs für die entsprechenden phänologischen Stadien automatisch selektiert werden. Dadurch wird eine akkurate und über die gesamte Wachstumssaison (d.h. unabhängig vom phänologischen Status der Vegetation) stabile Unterscheidung von Pflanzengesellschaften ermöglicht.

Im zweiten Schritt untersuchten wir, wie die numerischen funktionalen Merkmale der verschiedenen Grünlandbestände auf Basis von Fernerkundungsdaten ermittelt werden können. Mit Hilfe von Partial Least Squares Regression (PLSR) war es möglich, jeweils ein Modell zu entwickeln, das die Detektion eines funktionales Merkmals für alle untersuchten Pflanzengesellschaften zu allen phänologischen Stadien über Veränderungen in der

gemessenen spektralen Reflexion erlaubt. Unter den 23 untersuchten funktionalen Merkmalen wurden neun mit hoher Genauigkeit (R² validation, $R^2_{val} \geq 0.6$) ermittelt, inklusive der Pflanzenhöhe, des Anteils der photosynthetisch aktiven absorbierten Strahlung, des Kohlenstoff-Stickstoff Verhältnisses, der Frischmasse der Stängel, des Stickstoff-Gehaltes der Pflanze, der komprimierten Bestandshöhe, des SPAD-Werts der Blätter, des Gehalts an neutraler Detergentienfaser der Pflanze sowie der Blattfläche. Die Modelle für die Detektion der Frischmasse der Pflanzen sowie der Frischmasse, der Trockenmasse und des Trockenmassegehalts der Blätter erreichten eine moderate Genauigkeit ($0.6 > R^2_{val} \geq 0.4$). Niedrige Genauigkeiten ($R^2_{val} < 0.4$) wurden von den Modellen für die Ermittlung der Trockenmasse der Pflanze und des Stängels, des Trockenmassegehalts der Pflanze und des Stängels, des Wassergehalts von Pflanze, Stängel und Blättern, des Kohlenstoffgehalts der Pflanze, des Blatt-Stängel Verhältnisses sowie der spezifischen Blattfläche erreicht. Diese Ergebnisse lassen den Schluss zu, dass mit Hilfe der Feldspektrometrie die Messung vieler (13 von 23) funktionaler Merkmale verschiedener Grünlandgesellschaften über komplette Vegetationszyklen mit moderaten bis hohen Genauigkeiten möglich ist. Somit ist diese kostengünstige, zeitsparende und nicht-destruktive Methode für die Beantwortung agrarwissenschaftlicher und ökologischer Fragestellungen von großem Wert.

Im dritten Teil der Arbeit wurde das Potenzial verschiedener Fernerkundungssensoren für die Detektion von funktionalen Merkmalen untersucht. Auf Basis von Reflexionsdaten, die mit dem FS 3 aufgenommen wurden, wurden die Bänder eines ASD Handheld 2 Spektroradiometers (HH 2, 725 Bänder), eines hyperspektralen Satellitensensors (EnMAP; EnM, 242 Bänder) sowie von drei multispektralen Satellitensensoren, inklusive Sentinel-2 (S-2, 13 Bänder), Landsat 7 (L 7, acht Bänder) und RapidEye (RE, fünf Bänder) simuliert. Es wurden 13 funktionale Merkmale erfolgreich ($R^2_{val} > 0.4$) mit FS 3 Daten, 11 mit EnM Daten und zehn mit HH 2 Daten ermittelt. Mit multispektralen Daten hingegen, wurden nur neun funktionale Merkmale mit S-2, vier mit L 7 und keins mit RE erfolgreich erfasst. Für die Detektion der funktionalen Merkmale erreichten die hyperspektralen Sensoren folglich höhere Genauigkeiten als die multispektralen Sensoren. Zudem wird darauf geschlossen, dass die Breite des spektralen Messbereichs eines Sensors für die Präzision der Ermittlung funktionaler Merkmale von großer Bedeutung ist. Eine größere Anzahl an Spektralbändern ermöglicht eine zusätzliche Erhöhung der Genauigkeit der Modelle.

Diese Ergebnisse zeigen, dass hyperspektrale Fernerkundungssysteme das Potential haben, Ökologen flächendeckende Informationen über die funktionalen Merkmale von

Grünlandbeständen mit hoher zeitlicher Auflösung zu liefern. Solche Informationen können dazu beitragen, die Bewirtschaftung von Grünlandökosystemen an Veränderungen der klimatischen Bedingungen und Nutzungsintensitäten anzupassen sowie deren nachhaltige Kultivierung sicherzustellen.

Table of contents

List of figures

List of tables

List of acronyms

ASD	Analytical Spectral Devices Inc.
BRDF	bidirectional reflectance distribution function
C	carbon
Ca	plot fertilized with lime only as calcium oxide (CaO)
CaN	plot fertilized with calcium oxide and nitrogen (CaO/N),
CaNP	plot fertilized with calcium oxide, nitrogen and phosphorus (CaO/N/P_2O_5)
CaNPKCl	plot fertilized with calcium oxide, lime, nitrogen, phosphorus and potassium (CaO/N/P_2O_5/KCl)
CaNPK$_2$SO$_4$	plot fertilized with calcium oxide, lime, nitrogen, phosphorus and potassium (CaO/N/P_2O_5/K_2SO_4)
C/N	ratio of the mass of carbon to the mass of nitrogen in a substance
CSH	compressed sward height
EnM	Environmental Mapping and Analysis Program satellite sensor
EnMAP	Environmental Mapping and Analysis Program satellite
FOV	field of view
fPAR$_{abs}$	fraction of photosynthetically active radiation absorbed
FS 3	Analytical Spectral Devices Inc. FieldSpec 3 spectroradiometer
fSWIR	far shortwave infrared (1800-2500 nanometers)
FT	plant functional trait
GNDVI	green normalized difference vegetation index
HH 2	Analytical Spectral Devices Inc. HandHeld 2 spectroradiometer
HyspIRI	Hyperspectral Infrared Imager
IR	infrared
LA	leaf area
LAI	leaf area index
LCI	leaf chlorophyll index
LDM	leaf dry matter
LDMC	leaf dry matter content
LFM	leaf fresh matter
lidar	light detection and ranging
LOO-CV	leave-one-out cross validation
LS	leaf-tiller ratio
LS 7	Landsat 7 Enhanced Thematic Mapper + satellite sensor
LWC	leaf water content
MESMA	multiple endmember spectral mixture analysis
N	nitrogen
NDF	neutral detergent fiber content
NDVI	normalized difference vegetation index
nGNDVI	narrowband green normalized difference vegetation index
NIR	near infrared (700-1399 nanometers)
nLCI	narrowband leaf chlorophyll index
nNDLI	narrowband normalized difference lignin index
nNDNI	narrowband normalized difference nitrogen index
nNDVI	narrowband normalized difference vegetation index
nNPCI	narrowband normalized pigment chlorophyll index
nNPQI	narrowband normalized phaeophytization index
NPCI	normalized pigment chlorophyll index
NPQI	normalized phaeophytization index
nPRI	narrowband photochemical reflectance index

nREP	narrowband red edge position
nRMSE$_{cal}$	normalized root mean squared error in calibration
nRMSE$_{val}$	normalized root mean squared error in validation
nSIPI	narrowband structure intensive pigment index
nSWIR	near shortwave infrared (1400-1799 nanometers)
nWC	narrowband water content
nWI	narrowband water index
PCA	principal component analysis
PCR	principal component regression
PDM	plant dry matter
PDMC	plant dry matter content
PFM	plant fresh matter
PFT	plant functional type
PH	plant height
PWC	plant water content
radar	radio detection and ranging
R²	coefficient of determination
R²$_{cal}$	coefficient of determination in calibration
R²$_{val}$	coefficient of determination in validation
RE	RapidEye satellite sensor
RGE	Rengen Grassland Experiment
RS	remote sensing
RTM	radiative transfer model
S-2	Sentinel-2 satellite sensor
SD	standard deviation
SLA	specific leaf area
SPAD	SPAD value (estimated chlorophyll content)
SWIR	shortwave infrared (1400-2500 nanometers)
SWIR-1	shortwave infrared-1 sensor in FS 3 (1000-1800 nanometers)
SWIR-2	shortwave infrared-2 sensor in FS 3 (1800-2500 nanometers)
T∑	temperature sum
TDM	tiller dry matter
TDMC	tiller dry matter content
TFM	tiller fresh matter
TWC	tiller water content
UV	ultraviolet light (300-379 nanometers)
VI	vegetation index
VIS	visible light (380-740 nm)
VNIR	visible and near infrared (380-1399 nanometers)

1 Introduction

Grasslands cover more than 30% of the earth's terrestrial surface (Blair et al., 2014). Consequently, they represent an important source of forage for livestock and contribute to the livelihoods of more than 800 million people worldwide (FAO, 2008; Psomas et al., 2011). In Central Europe, grasslands are further a major source of biodiversity and supply many important ecosystem services (Psomas et al., 2011). However, climate change and heavy exploitation threaten these ecosystems as well as the survival of many endemic species (EEA, 2001; Kemp et al., 2013; Theurillat and Guisan, 2001). Thus, several grasslands are now among the most threatened ecosystems (Blair et al., 2014). In order to conserve grassland ecosystems and to maintain their productivity and health, grassland management needs to be adjusted in accordance with changes in climate and intensities of use (Al Haj Khaled et al., 2005). Therefore, monitoring and mapping of variations in grassland properties have gained in scientific importance.

In the past decades, plant functional traits (FTs) have been identified as the most promising approach for assessing changes in the status of vegetation communities, from species-rich to species-poor, from intensive to extensive and across a wide range of agro-climatic regions. FTs are measurable morphological, physiological or phenological properties of plants, which determine how plants respond to or impact on the local environment (Violle et al., 2007). FTs are measured at plant level and are indicators of plant fitness within an ecosystem through their effects on growth, reproduction and survival (Schellberg et al., 1999; Weiher et al., 1999).

In Central Europe, various grassland communities exist that differ considerably in their floristic composition. Within these plant communities, plant species predominate that feature characteristic morphological, physiological and phenological properties, i.e. FTs. Using FTs it is possible to assess the functioning of ecosystems and to monitor their quality, productivity and health. Consequently, numerous studies have used this approach to assess the response of grassland communities to changes is land management (Cingolani et al., 2005; Craine et al., 2002; Lavorel et al., 2011). Thereby, FTs were mainly measured using costly and time-consuming field work as well as destructive sampling techniques (e.g. for estimating N-, C-, NDF- and dry matter content), for example according to the protocols given in Cornelissen et al., (2003). Even more men-power and financial input are required for deriving regional estimates of FTs or for monitoring their development over longer intervals in time. Thus, grassland scientists are looking for a cost-efficient, time-saving and non-destructive technique

in order to monitor responses of FTs to changes in management and climate on the local and regional scale.

Remote sensing (RS) has been identified as an effective solution for classifying vegetation cover and for describing the seasonal and interannual development of vegetation properties (Aragón and Oesterheld, 2008). RS is generally defined as "the practice of deriving information about the earth's land and water surfaces acquired from an overhead perspective, using electromagnetic radiation in one or more regions of the electromagnetic spectrum […]" (Campbell and Wynne, 2011, p. 6). Advantages of RS for vegetation studies include that it is a non-destructive technique (Jones and Vaughan, 2012) and that it provides the potential for estimating vegetation properties (such as FTs) in the spatial domain (Aragón and Oesterheld, 2008; He et al., 2006). Furthermore, RS data can easily be recorded iteratively over time (Loarie et al., 2007). Several authors have identified that FTs affect the spectral reflectance properties of leaves and entire plant canopies (Svoray et al., 2013; Ustin, 2013). This indicates that a RS-based detection of many FTs may be possible. Thus, RS may provide a universal solution allowing ecologists to collect data on FTs on demand for wide areas of the earth's surface.

1.1   From functional ecology to plant functional traits

Functional ecology investigates which roles (i.e. functions) plant species play within an ecosystem. It thereby pays particular attention to the morphological, physiological and phenological characteristics of plants, which determine their performance and survival. It thus provides insights into the true processes underlying ecosystem functioning and development. Within the 20th century, functional ecology has substantially gained in scientific importance and provides valuable information for related scientific disciplines such as agronomy and geography. Using functional approaches, numerous studies have investigated the response of ecosystems to variations in land-use, land-management and climate (Díaz et al., 2007a, 2007b; Lavorel et al., 2011; Pontes et al., 2010).

Among the most important concepts in functional ecology is the universal adaptive strategy theory, which was developed by John Philip Grime, (1977). He proposed to classify plant species according to the strategy they pursue to secure their existence within ecosystems. Using this method, a direct comparison of plant communities is possible, irrespective of their species composition. Thus, this approach can be used on a global, regional and local scale to assess ecosystem properties. Of central importance in this theory are three different strategy types, which feature also significant differences in their FTs. Competitive (C) strategists predominate

in nutrient-rich habitats and tend to feature an early start of growth, a rapid buildup of biomass and leaf area as well as a short leaf lifespan (Craine et al., 2001, 2005; Lavorel et al., 1997; Pontes et al., 2010). Furthermore, a high specific leaf area, forage value and leaf chlorophyll content are common properties of C strategists (Daughtry et al., 2000; Hejcman et al., 2007; Lavorel et al., 2007; Poorter and De Jong, 1999; Wright et al., 2005). In contrast, nutrient-limited environments host mainly species of the conservative strategy (S) type (Craine et al., 2002; Liancourt et al., 2005). S strategists feature a low plant height, specific leaf area, leaf nutrient concentration (particularly N) and nutritive value (Bryant et al., 1983; Cebrian et al., 1998; Coley et al., 1985; Díaz et al., 2004). On the other hand, characteristic for plants of this strategy type are a long leaf lifespan, a high tissue density and a later start of plant growth (Lavorel et al., 1997, 2007; Pontes et al., 2010). Plants belonging to the third, i.e. the ruderal (R), strategy type prevail in habitats with severely disturbed but potentially productive conditions (e.g. overgrazed sites). Ruderal strategists quickly complete their life cycles and produce a large number of seeds.

A related idea used for connecting the functional characteristics of plants to the prevailing site conditions (especially to climate and soil properties) is the concept of plant functional types (PFTs). In this approach, plants featuring similar morphological, physiological and phenological characteristics (i.e. FTs) can be assigned to a common class, i.e. a PFT (Lavorel et al., 2007). As PFTs can be defined independently of the species of a plant, it is possible to describe plant canopies, which feature little taxonomic overlap (i.e. have little similarity in their species composition), according to the predominant PFTs (Lavorel and Garnier, 2002). Using this approach, a worldwide uniform comparison of ecosystems as well as a monitoring of their reactions to changes in land management or climate are possible. Thus, this method can provide important information for scientists to diminish the impacts of variations in climate and intensities of agricultural use and to secure the survival of endangered grassland ecosystems.

1.1.1 A deeper look into the concept of plant functional traits

In order to identify a plant's PFT or changes in the site conditions using the C-S-R strategy, FTs are of uttermost importance. As the measurement of FTs does not require to determine the taxonomic identity of a plant, FTs also allow a comparison of ecosystems, irrespective of their species composition (Lavorel and Garnier, 2002; McGill et al., 2006). Thus, FTs are considered as more objective predictors of ecosystem dynamics and function than species (DeFries et al., 1995; McGill et al., 2006; Shaver et al., 2007).

FTs can be either categorical or numerical. Categorical FTs are characterized by qualitative or discrete variables (e.g. life-form, reproductive organs or photosynthetic pathway of a plant), whereas numerical FTs are given as quantitative, continuous variables (e.g. height, specific leaf area or water content of a plant). Many categorical FTs are easy to collect and are directly linked to plant function (Figure 1-1). However, measuring the values of many numerical FTs is more complex (e.g. measuring plant weight, leaf area index - LAI, seed mass, etc.).
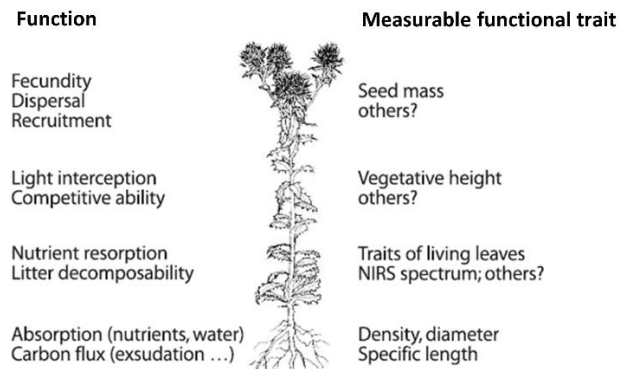
Figure 1-1. Examples of FTs and associated functions (Lavorel et al., 2007).

Both, categorical and numerical FTs can further be grouped into effect and response traits. Effect traits are related to an organism's impact on ecosystem processes or services, i.e. the goods provided by an ecosystem to its inhabitants, including humans (Lavorel et al., 2007). In contrast, response traits change as a result of variations in the environmental conditions acting upon plants in an ecosystem (Garnier et al., 2001). Thereby, response and effect traits are often interrelated to each other (Lavorel and Garnier, 2002). For example, effect traits impact soil fertility, which itself acts as environmental filter upon the persistence of species in an ecosystem and consequently upon response traits (Figure 1-2). Similarly, leaf nitrogen content, leaf dry matter content and specific leaf area are response traits to N supply (Al Haj Khaled et al., 2005; Pontes et al., 2010) and at the same time effect traits on soil fertility (De Bello et al., 2009). The response of ecosystems on changes in the environmental conditions is thus a complex process with impacts on many different effect and response traits.
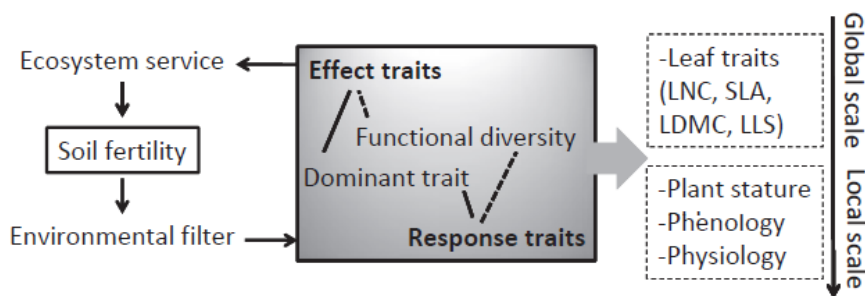
Figure 1-2. Simplification of the FT approach considering soil fertility as an environmental filter and its maintenance as an ecosystem service. LNC, leaf lamina N-content; SLA, specific leaf area; LDMC, leaf dry matter content; LLS, leaf lifespan (Schellberg and Pontes, 2012).

1.1.2 Plant functional traits and nutrient gradients

The FTs of grassland ecosystems vary considerably, depending on the availability of soil nutrients (Field et al., 1992; West et al., 1997; Wright et al., 2005). Through its impact on FTs, soil fertility also influences the community structure, the strategies of species competing for resources as well as the processes taking place in an ecosystem (Table 1-1). Grassland nutrient management can thus induce bottom-up changes in FTs and species interactions and alter the vegetation community structure. Consequently, nutrient supply is among the most important management tools for promoting the productivity, quality and health of managed grasslands and may be used to conserve the species diversity as well as related ecosystem functions and services (Pontes et al., 2010). Within the past decades, studies in grassland ecology have thus focused on the response of FTs to differences in nutrient management (Al Haj Khaled et al., 2005; Duru et al., 2004, 2010, Pontes et al., 2007, 2010).

Table 1-1. Summary of FTs associated with contrasting soil fertility and their effects on community structure and ecosystem processes in perennial grasslands (modified, Lavorel et al., 2007).

Level of organization	High fertility	Low fertility
Individual FTs	High specific leaf area, low leaf dry matter content, low C:N ratio, high FT plasticity, numerous small seeds with high dispersal	Long-lived species, low specific leaf area, low FT plasticity, few large seeds with low dispersal
Species interactions	Predominance of exploitative (C) species, rapid depletion of resources	Predominance of conservative (S) species, tolerance to low resource levels
Community	Abundance of forbs and some stoloniferous grasses	Abundance of cespituous grasses
Ecosystem processes	Fast rates of biogeochemical cycling, high net primary production	Slow rates of biochemical cycling, low net primary production

Intensive research in this domain has aimed at identifying the impact of soil nitrogen and phosphorus content on numerical traits (Cruz et al., 2002; Duru et al., 2004; Lavorel et al., 2007; Schellberg and Pontes, 2012). It was further shown that variations in the FTs of grassland communities can be seen as the result of a hierarchy of filters constraining their values. Thereby, the expressions of certain FTs along a nutrient gradient may either peak only within a small range (X, Y), feature gradual changes (V, W) or are relatively little affected (Z) (cf. Figure 1-3).
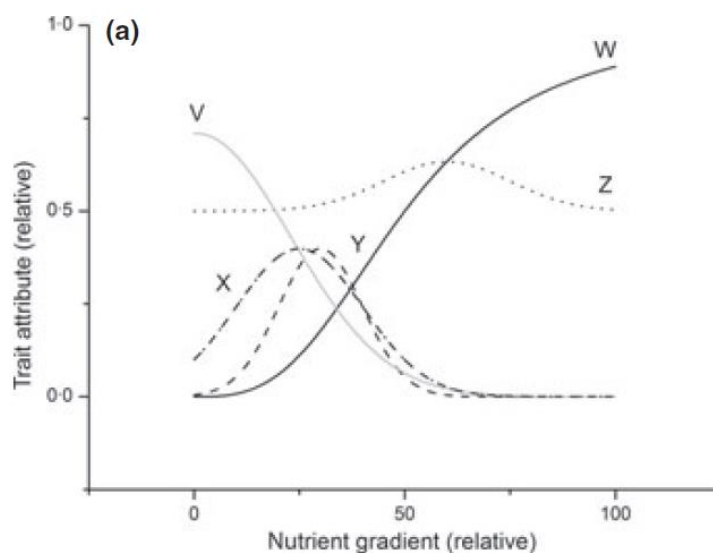
Figure 1-3. Theoretical response of numerical FTs to nutrient gradient in a grassland community. Temporal variation of FT attributes during growth is not considered (Schellberg and Pontes, 2012).

The structure of grassland communities as well as the values of the FTs may also vary over time. These temporal shifts exacerbate the establishment of explicit linkages between grassland FTs and ecosystem properties (McIntyre and Lavorel, 2001; Rusch et al., 2003; Westoby et al., 1999). Furthermore, spatial heterogeneity resulting from the interaction between various management factors (i.e. nutrient management and grazing or cutting regime) and site environmental conditions, increases the complexity of the relations between FTs and ecosystem status (Adler et al., 2001; Hirata, 1998; Janzen, 1984; Yasuda et al., 2003). Thus, changing the grassland management regime in order to conserve grassland ecosystems is a complex task, which requires a monitoring of the response of a grassland community to a set of management actions in the spatial domain. Nevertheless, FTs have been widely used to assess changes in grassland ecosystems due to their great potential for enhancing our understanding of ecosystem function (Schellberg and Pontes, 2012).

1.2 Remote sensing of vegetation - basic concepts

In the past decades, remotely sensed information has played a major role for monitoring and mapping vegetation at the local, regional and global scale. RS thereby relies on the principle that the properties of plants influence the amount of solar radiation reflected by a plant canopy in specific wavelengths or wavelength regions (Steiner et al., 2008; West et al., 2003). This reflected radiation is measured by the RS sensor in defined portions of the spectrum. Of special importance for vegetation studies are thereby the ultraviolet (UV), visible (VIS) and infrared (IR) wavelength regions, as given in Table 1-2. The spectral reflectance can be interpreted in a way that allows scientists to estimate specific vegetation properties.

Table 1-2. The range of the ultraviolet (UV), visible (VIS) and infrared (IR) regions of the electromagnetic spectrum.

Region name	Sub-region name	Wavelength range (nm)
Ultraviolet (UV)		300-379
Visible light (VIS)		380-739
	Blue	400-499
	Green	500-599
	Red	600-739
Near infrared (NIR)		740-1399
Shortwave infrared (SWIR)		1400-2500
	Near shortwave infrared (nSWIR)	1400-1799
	Far shortwave infrared (fSWIR)	1800-2500
Middle infrared		2501-4999
Thermal infrared		5000-15000

1.2.1 Multispectral and hyperspectral remote sensing

RS information in the VIS and IR regions of the spectrum can be recorded using different types of sensors, including multispectral and hyperspectral systems. These two sensor-types feature characteristic differences in their number of bands (i.e. sections of the electromagnetic spectrum measured in single channels of the RS sensor) and their bandwidths (i.e. the range of wavelengths a band is sensitive to). Multispectral systems measure radiation reflected by the earth's surface in approximately 3 to 15 bands, whereas hyperspectral systems provide spectral information in hundreds or even thousands of bands. Thereby, the bandwidths of multispectral systems are generally broader than those of hyperspectral systems. The spectral detail of a RS sensor has a large influence on the spectral signatures measured for the same plant canopy (Figure 1-4).
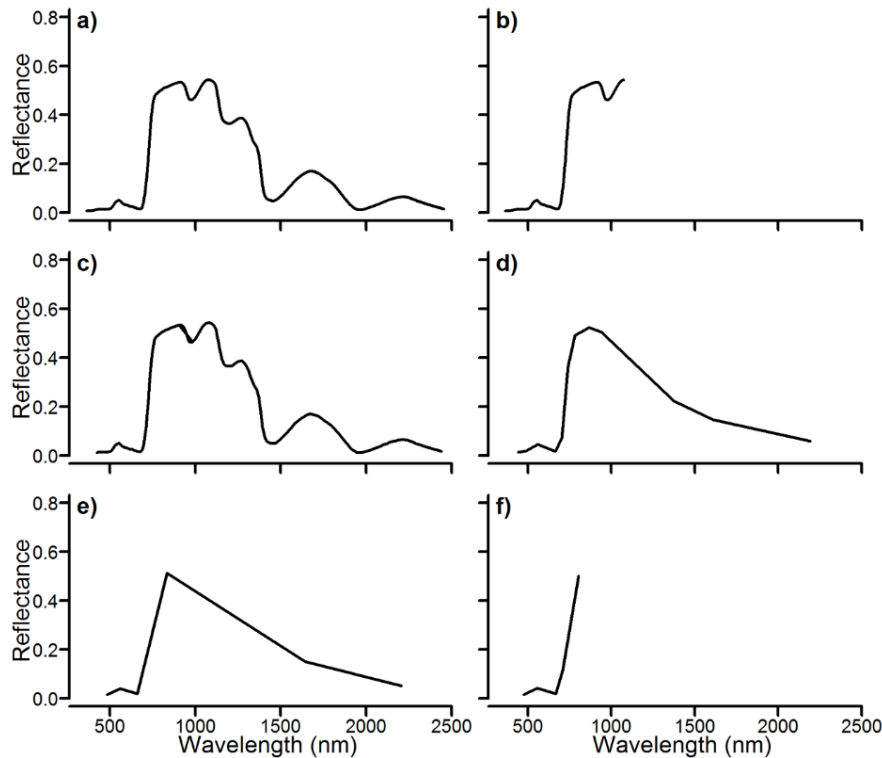
Figure 1-4. Spectral signatures of pasture derived from hyperspectral FS 3 (a), simulated HH 2 (b) and EnM (c) as well as from multispectral S-2 (d), L 7 (e) and RE (f) data. The number of spectral bands and spectral detail decreases from (a) to (f). Data were simulated using an average of 2689 spectra and the algorithm described in chapter 4.2.3.

Previous studies have shown that for distinguishing various types of grasslands as well as for monitoring changes in most of their FTs, broadband RS systems (i.e. most multispectral sensors) have significant limitations (Numata et al., 2008; Roberts et al., 1993; Thenkabail et al., 2012, 2004b, 2002; van Leeuwen and Huete, 1996). These limitations are caused as broadband sensors average spectral information over a wide range of wavelengths, resulting in a loss of critical spectral detail (Blackburn, 1998; Hansen and Schjoerring, 2003). Hyperspectral systems overcome this problem by measuring reflectance in a high number of narrow wavebands (Curran, 1989; Numata et al., 2008; Thenkabail et al., 2012). Thus, these sensors have successfully been used for detecting vegetation stress (Carter, 1994, 1998), plant biomass (Thenkabail, 2003), green vegetation cover (McGwire et al., 2000) as well as the chlorophyll content (Blackburn and Steele, 1999) and many chemical components of plants or leaves (Bauer et al., 1981; Blackburn and Steele, 1999; Curran, 1994; Peñuelas et al., 1993, 1995). Consequently, detecting many FTs of grasslands may be possible using hyperspectral RS systems (Homolová et al., 2013; Roelofsen et al., 2013; Ustin and Gamon, 2010).

1.2.2   Remote sensing sensors and platforms

RS sensors may be used as ground-based systems or may be mounted aboard different platforms, including satellites, manned aircrafts or unmanned aerial vehicles (UAVs). All of these platforms enable a collection of data with different properties regarding their areal coverage (the area viewed in one image or observation), their spatial resolution (the areal detail resolved) and their temporal resolution (the revisiting time of a sensor to the same area). Usually, an increase in one of these attributes (e.g. the spatial resolution) leads to the sacrifice of other attributes, such as temporal resolution or areal coverage (Rocchini et al., 2010). Thus, all RS systems have certain advantages and disadvantages and the selection of effective sensors depends upon the targeted application (e.g. the needed spatial or temporal resolution) as well as on the practical circumstances (e.g. the budget, the expertise of the analyzing team and the availability of data).

Until the early second millennium, satellite RS was constrained to the use of multispectral sensors (Psomas et al., 2011). However, with the launch of the Hyperion hyperspectral sensor (in 2000) as well as with the planned launches of Environmental Mapping and Analysis Program (EnMAP) and Hyperspectral Infrared Imager (HyspIRI) imaging spectrometers, a new era of hyperspectral RS has started (Göttlicher et al., 2011; Richter et al., 2012; Thenkabail et al., 2004b). Current research thus aims at exploring the opportunities of hyperspectral imaging systems for detecting a wider range of vegetation properties and to compare their performance to traditional multispectral sensors. However, difficulties in enabling meaningful comparisons between multispectral and hyperspectral systems are introduced by differences in their spatial resolution, viewing geometry and sensor calibration as well as by the atmospheric conditions at the times of sensor overpass (Geerken et al., 2005; Lu, 2006; Psomas et al., 2011).

To develop methods for detecting FTs using RS data, ground-based field spectroradiometers have been identified as good solution (Ferner et al., 2015; Mutanga et al., 2015; Sibanda et al., 2015, 2016; Thenkabail et al., 2000). Full-range field spectroradiometers can measure reflectance in thousands of narrow wavebands located in the spectral region between 350 and 2500 nm. These systems are lightweight and can be easily carried across fields to collect RS information at precisely defined locations. Thus, they allow a cost-efficient generation of multi-temporal datasets and provide hyperspectral data, in which spatial inaccuracies (e.g. due to failures in orthorectification) are minimized (Feilhauer and Schmidtlein, 2011). Furthermore, up-scaling of models developed based on field spectroradiometer data to satellite data is possible, when the spatial resolutions of both instruments are well above the size of individual

plants (Hansen and Schjoerring, 2003; Psomas et al., 2011; Verrelst et al., 2009; Xavier et al., 2006). Thus, field spectroradiometers have successfully been used as surrogate for air- and spaceborne RS systems to assess their potential for detecting vegetation properties of grasslands (Feilhauer and Schmidtlein, 2011; Hansen and Schjoerring, 2003; Rossini et al., 2012; Xavier et al., 2006; Anderson et al., 2004).

1.2.3   The spectral reflectance of grassland vegetation

Solar irradiation reaching a plant canopy may interact in different ways with the plant leaves, tillers or the underlying soil (Curran, 1989; Kumar et al., 2001). Figure 1-5 shows that the incident light may either be directly reflected back to the sky from the leaf, may be transmitted through the leaf, may be involved in multiple reflections within the canopy before being reflected back to the sky or may penetrate the canopy before being reflected back by the soil. Furthermore, parts of the incoming radiation are absorbed in different layers of the plant canopy and may be re-emitted by the plant leaves as fluorescence radiation.
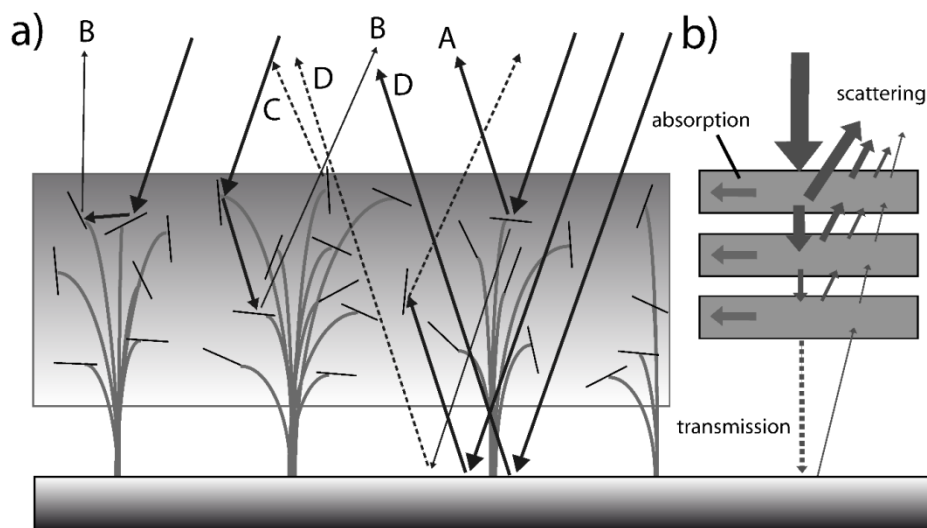
Figure 1-5. a) Illustration of interactions of radiation with a plant canopy with randomly oriented leaves, showing the multiple scattering events. The incident sunlight may either be directly reflected back to the sky from a leaf (A), with a small fraction being transmitted through the leaf, or else it may be involved in a secondary (B), or even tertiary (C) reflection before finally being reflected back to the sky. Similarly, some of the reflections may involve the soil (D). b) Simplification of the real canopy as layers, where the downward radiation is attenuated by absorption and scattering at each layer, while the upward radiation flux is the sum of all upwardly scattered radiation (modified, Jones and Vaughan, 2012).

The radiation exiting vegetation is further dependent upon canopy structural features, such as the distribution of leaf angles and the LAI as well as on plant biochemistry, phenology and physiology (Asner, 1998; Carter and Knapp, 2001; Gitelson and Merzlyak, 1996; Goel, 1988;

Numata et al., 2008). As these factors significantly vary between plant species, floristic composition of the vegetation community further influences the reflected spectral signal (Asner, 1998; Asner and Martin, 2009; Hill et al., 2004; Knyazikhin et al., 2012). Thus, a complex interaction between the radiation and the vegetation as well as the underlying soil determines the spectral signature of a plant canopy (Blackburn, 1998; Jackson and Pinter, 1986; Lorenzen and Jensen, 1988; Pinter et al., 1985; Schut et al., 2002).

In addition, canopy reflectance is influenced by diurnal, seasonal and inter-annual changes in the solar zenith- and azimuth-angles as well as by the viewing geometry, i.e. the sensor angle and height, of a RS system (Egbert and Ulaby, 1972; Gamon et al., 2006; Stagakis et al., 2010; Cochrane, 2000; Jackson and Pinter, 1986; Pinter et al., 1985). These can be mathematically expressed as the bidirectional reflectance distribution function (BRDF) (Barnsley et al., 1997; Diner et al., 1999; Verstraete et al., 1996). Although time series over longer intervals (i.e. several years) theoretically provide sufficient sampling of the range of illumination and viewing conditions to estimate the BRDF effects, these are confounded with seasonal variations in the properties of the vegetation (Los et al., 2005). Thus, BRDF effects are difficult to quantify.

Despite the uncertainties caused by BRDF effects and the complex interactions between radiation and plant canopies, differences in the spectral signatures of various vegetation types, such as grass monocultures, meadows and pasture or other materials, such as soil, exist (Figure 1-6). Especially the VIS- and IR-sections of the electromagnetic spectrum allow a detection of many different plant properties, including FTs (Curran, 1989; Thenkabail et al., 2000, 2004b, 2012). Therefore, RS may be suited to produce datasets of great value for agronomists and ecologists (Kawamura et al., 2008).
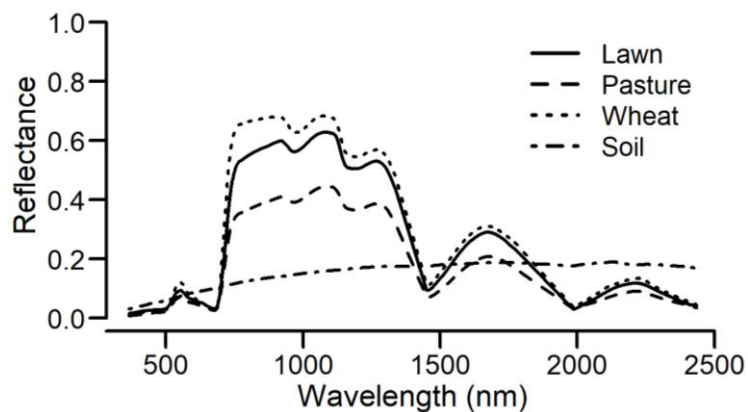
Figure 1-6. Reflectance of different vegetation types and bare soil. Spectra were collected using an ASD FieldSpec 3 (FS 3) spectroradiometer on June 23, 2016 in Bonn, Germany.

1.3 Classification of grassland vegetation using remote sensing

Grassland management strongly relies on accurate maps of the distribution of relevant vegetation communities and on information about changes in their properties throughout the growing season (Cingolani et al., 2004; Posse and Cingolani, 2004). Although it is relatively simple to classify broad vegetation types, such as different biomes, using multispectral RS sensors, difficulties occur when distinguishing the optically more similar grassland communities from each other (Numata et al., 2008; Thenkabail et al., 2004a; Ustin and Gamon, 2010). Thus, detailed maps of grassland community distribution and spatio-temporal information on their phenological status are up to date rarely available. However, such datasets would allow to monitor grassland production for large areas and to identify long-term changes in the spatial distribution of grassland ecosystems (Aragón and Oesterheld, 2008; Gianelle and Vescovo, 2007).

In recent years, the increasing availability of hyperspectral RS data has opened new perspectives for the characterization of grassland types across different spatial scales with comprehensive temporal coverage. Hyperspectral RS has successfully been used to classify vegetation canopies featuring different species compositions, Ellenberg indicator values, C-S-R strategy types, burned and unburned sites, grazed and ungrazed vegetation and management regimes (Fava et al., 2009; Harris et al., 2003; Magiera et al., 2013; Oldeland et al., 2010; Rahman and Gamon, 2004; Schmidtlein, 2005; Schmidtlein et al., 2012; Schmidtlein and Sassin, 2004; Sibanda et al., 2015, 2016; Trigg and Flasse, 2000). However, the availability of these datasets also provides the opportunity to distinguish plant functional types (PFTs) of grasslands (Field, 1991; Field et al., 1992). Thus, Ustin and Gamon, (2010) have proposed the concept of optical types, which allows to establish a direct link between reflected radiation, PFTs and the environmental conditions. Consequently, RS may allow a global characterization of grassland ecosystems based on their functioning.

However, the high dimensionality of hyperspectral remotely sensed information exacerbates the selection of the most effective wavebands for grassland classification. Thus, datamining techniques, including principal component analysis (PCA), lambda-lambda R^2 models and stepwise discriminant analysis have been applied to identify effective wavebands for differentiating vegetation (Aragón and Oesterheld, 2008; Thenkabail et al., 2004b). These studies showed that the best few narrow wavebands, located within the most relevant regions of the electromagnetic spectrum, enable RS scientists to effectively distinguish vegetation types. Adding more bands only marginally increases the classification accuracy. For this reason,

normalized VIs incorporating the most relevant bands for differentiating grasslands perform similarly well compared to complex datamining algorithms. Furthermore, the use of ratios in VI-calculation, diminishes BRDF effects and emphasizes relevant spectral information (Jensen, 2007).

On the other hand, classification accuracies achieved using a single VI substantially vary over time (Aragón and Oesterheld, 2008; Poças et al., 2012; Sánchez-Azofeifa et al., 2009; Zutta, 2003). Thus, successfully distinguishing grasslands is not possible using solely one VI at all phenological stages. However, other regions of the spectrum provide additional spectral information, which may be suited to classify grassland communities at these points in time (Asner and Heidebrecht, 2003). Finding a method, which identifies the ideal VIs for distinguishing different grassland communities over a growing season is thus of great importance.

1.4   Remote sensing of grassland plant functional traits

In previous studies, RS data have successfully been related to morphological (Numata et al., 2008), phenological and biochemical properties of vegetation relevant to plant function (Daughtry et al., 2000; Field, 1991; Inoue and Penuelas, 2001; Yoder and Pettigrew-Crosby, 1995; Numata et al., 2008; Xavier et al., 2006; Thenkabail et al., 2012). This suggests that FTs affect the spectral reflectance of leaves and canopies (Svoray et al., 2013; Ustin, 2013). As the expressions (numerical or categorical values) of FTs are strongly linked to environmental resource constraints (i.e. to a lack of nutrients limiting plant growth), RS may provide data that help to optimize the fertilization of grasslands, support agricultural production and, at the same time, maintain ecosystem functioning (Magiera et al., 2013; Ustin and Gamon, 2010).

However, FTs fluctuate throughout the entire growing season. Thus, acquiring multitemporal data for relating spectral measurements to FTs is important in order to capture the entire range of FT expressions (Karnieli et al., 2002; Psomas et al., 2011; Xavier et al., 2006). A study by Ling et al., (2014) showed that a model developed using information from a sufficiently large timeframe (in the order of several years) can be used to estimate plant biochemical properties, such as N-content, irrespective of the vegetation phenological state. These results indicate that detecting many other FTs may be possible over entire growing seasons and years using RS measurements. Thus, RS of FTs has a vast potential for providing spatio-temporal information on grassland functioning and enable scientists to create valuable datasets for agricultural and

ecological research as well as for ecosystem management (Aragón and Oesterheld, 2008; Cingolani et al., 2004; Paruelo et al., 2004).

Up to date, only few scientists have tried to estimate the FTs of species-rich grassland-stands using RS technology (Homolová et al., 2013; Roelofsen et al., 2013). In these studies, field spectroradiometers were the most widely used instruments because they allow a clear registration between the measured field of view (FOV, i.e. the size of the area a detector is sensitive to reflected radiation) and the manually sampled vegetation. They further provide a wide spectral range and a high spectral resolution. Models including such high spectral detail provided promising results for estimating a number of FTs (Roelofsen et al., 2013).

Thereby, the detection of FTs is complex as changes in one FT (e.g. plant biomass) are strongly related to changes in others (e.g. to leaf area or plant dry matter) and vice versa (Figure 1-7; Göttlicher et al., 2011). This makes it difficult to disentangle the interactions between spectral reflectance and a set of mutually changing FTs and to identify wavelengths that are sensitive solely to single functional properties.
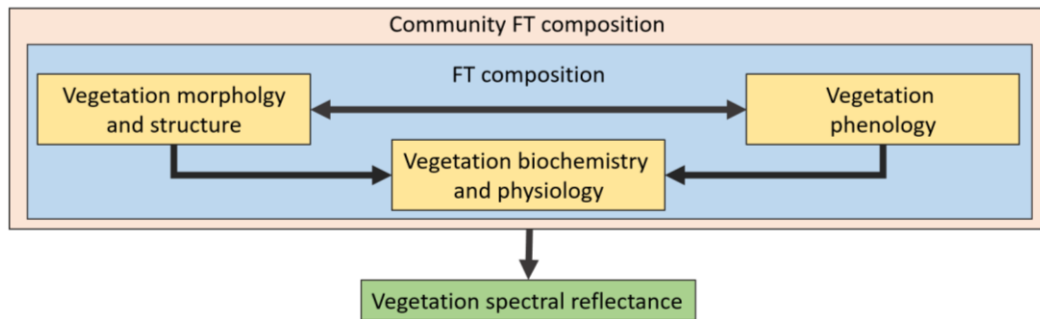
Figure 1-7. Vegetation morphology and structure, vegetation biochemistry and physiology as well as vegetation phenology are interrelated to each other (double arrows) and determine values of single FTs. These single FT values are expressed as the FT composition of a plant. FT composition can be aggregated to the plant community. This community FT composition finally influences the spectral reflectance.

Additionally, the spatial resolution of most RS sensors is above the size of an individual plant. This implies that the spectral signal is composed of radiation reflected by a number of plants, featuring individual sets of FT expressions. For this reason, FTs need to be aggregated to the community in order to allow a correct registration of the studied plant canopy and the measured spectral signal (Roelofsen et al., 2013). Thereby, establishment of a community trait value is not straight-forward because FTs vary greatly among individual plants, even over short distances both, horizontally as well as vertically within the canopy (De Bello et al., 2009). Previous research showed that FTs related to nutrient availability are best estimated when

expressed on a mass-base (mg g^{-1} dry matter), compared to a canopy-surface- (g m^{-2} canopy surface) or a leaf-surface-base (mg m^{-2} leaf surface) (Roelofsen et al., 2013). These findings suggest that sampling the entire vertical dimension of the canopy (or extracting entire plants) enable creating the strongest relations between canopy reflectance and FTs (cf. Figure 1-5 b).

1.4.1   Relevant spectral regions for estimating plant functional traits

To support grassland scientists in adapting the management according to the local reactions of ecosystems to changes in the environmental conditions, several key-FTs exist that are the most relevant for maintaining grassland quality, species diversity and agricultural production (Starks et al., 2006; Zhao et al., 2007). Among these are plant height (PH), fresh matter, LAI, the fraction of photosynthetically active radiation absorbed (fPAR$_{abs}$), chlorophyll content, the concentrations of nitrogen (N) and carbon (C) as well as the contents of water in leaves and canopies (Bacour et al., 2006; Hansen and Schjoerring, 2003; Huber et al., 2008; Richter et al., 2012; Thenkabail et al., 2000, 2012; Vallentine, 1990). Of further importance for grazing animals is forage quality, as determined by the nutrient detergent fiber (NDF) content (Bailey et al., 1996; Kawamura et al., 2008; Reid et al., 1992; Schauer et al., 2005).

Due to their large importance in agriculture and ecology, many previous studies have addressed plant biophysical variables related to plant function. The results of these investigations are summarized in Table 1-3. As many substances feature mutual relationships (i.e. high correlations between FTs; e.g. if water content increases, frequently also chlorophyll content increases), band regions relevant for their detection overlap (Knyazikhin et al., 2012; Numata et al., 2008; Psomas et al., 2011; Stagakis et al., 2010).

Variations in PH, chlorophyll content (expressed as SPAD), plant fresh matter (PFM) and C-content have been observed to be strongly related to the spectral reflectance in the red-edge (720-760 nm) and NIR regions. Changes in the expressions of other FTs, including plant-, tiller- and leaf water content (PWC, TWC and LWC) as well as of leaf fresh matter (LFM), N-and NDF-content were mostly related to bands in the NIR and SWIR-regions of the spectrum. For estimating plant, tiller and leaf dry matter (PDM, TDM and LDM), wavelengths in the SWIR appeared to contain the most valuable information. To derive fPAR$_{abs}$ based on spectral reflectance, the visible domain was the most important. Other FTs, such as leaf area (LA), specific leaf area (SLA), plant, tiller and leaf dry matter content (PDMC, TDMC and LDMC) as well as leaf-stem-ratio (LS), tiller fresh matter (TFM) and C/N-ratio were less intensively studied.

Table 1-3. Bands relevant for detecting FTs as well as the model accuracies reached in previous studies.

FT	Bands	R²	Source
PH	763, 793, 872, 882, 905, 915, 946, 956, 966, 1124	0.68	Xavier et al., (2006)
SPAD	430-600, 620-750, 750-1000	>0.74, <0.86	Rossini et al., (2012); Stagakis et al., (2010); Thenkabail et al., (2004b)
LA	-	-	-
PWC	950-1250, 1390-1800, 2000-2350	-	Clevers et al., (2008); Elvidge, (1990); Numata et al., (2008)
TWC	970, 1200, 1400, 1940	-	Kumar et al., (2001)
LWC	970, 1200, 1400, 1700, 1940, 2005, 2035, 2235, 2280, 2295, 2345	0.4	Hunt Jr., (1991); Kumar et al., (2001); Ripple, (1986); Roelofsen et al., (2013)
SLA	-	-	-
PDMC	-	-	-
TDMC	-	-	-
LDMC	-	-	-
LS	-	-	-
PFM	600-700, 740-1000	0.3970; 0.5730	Tucker, (1977); Wang et al., (2008)
TFM	-	0.3546	Wang et al., (2008)
LFM	1205, 1710	-0.4649; 0.6378	Psomas et al., (2011); Wang et al., (2008)
PDM	1672, 2045, 2218; 2000-2400	0.3747, 0.5231	Asner, (1998); Elvidge, (1990); Numata et al., (2008); Roberts et al., (1993); Wang et al., (2008)
TDM	1672; 2000-2400	0.2767, 0.4328	Asner, (1998); Elvidge, (1990); Roberts et al., (1993); Wang et al., (2008)
LDM	1672; 2000-2400	-0.4657, 0.5950	Asner, (1998); Elvidge, (1990); Roberts et al., (1993); Wang et al., (2005)
N	480, 550-750, 840, 1230-1350, 1400-1680, 2050-2350	>0.72; <0.9	Kumar et al., (2001); Ling et al., (2014); Thenkabail et al., (2012); Shibayama and Akiyama, (1986)
C	550, 780-1400	-	Roelofsen et al., (2013)
C/N	-	-	-
NDF, lignin	514, 580, 700, 955, 1120, 1160, 1200, 1420, 1540, 1690, 1736, 1780, 1820; 1300-1900, 1900-2500	< 0.74; 0.15-0.39	Elvidge, (1990); Numata et al., (2008); Roelofsen et al., (2013)
CSH, biomass	400-750, 780-1000, 1100 - 1250, 1540-1650, 2045- 2218	>0.69, <0.96; <-0.52, >-0.93	Fava et al., (2010); Lorenzen and Jensen, (1988); Numata et al., (2008); Tucker, (1977); Wang et al., (2008)
LAI, fPAR$_{abs}$	500-550, 620-750, 680, 2280	>0.57, < 0.95	Asner, (1998); Broge and Leblanc, (2000); Hunt Jr., (1991); Rossini et al., (2012); Darvishzadeh et al., (2011); Wang et al., (2008)

Furthermore, Table 1-3 shows that the model accuracies reached (expressed as the coefficient of determination, R^2) for detecting the same FT vary considerably between studies. Thereby, the strength of the relations between reflectance data and FTs were heavily influenced by the spectral and spatial resolutions of the sensors used as well as by the architecture and the phenological stage of the vegetation communities (Feilhauer and Schmidtlein, 2011; Ling et

al., 2014; Poças et al., 2012; Sánchez-Azofeifa et al., 2009; Zutta, 2003; Numata et al., 2008). Additionally, for deriving biophysical information on mixed species canopies, lower accuracies were achieved than for grass monocultures (Kawamura et al., 2008). Generally, high accuracies ($R^2 > 0.6$) were reached for detecting PH, SPAD, N-content and CSH, whereas it was shown that LWC, PFM, PDM, TDM and LDM of vegetation canopies are relatively difficult to estimate using RS.

1.4.2   Estimating plant functional traits based on hyperspectral reflectance data

To relate the biophysical and biochemical properties of vegetation to remotely sensed data, statistical models have found wider application than their physically-based counterparts (e.g. radiative transfer models, RTMs) (Thenkabail et al., 2012). For developing statistical models, data on specific vegetation properties are first measured using manual sampling methods and subsequently related to the spectral reflectance by means of statistical mathematics. Although these models are difficult to transfer between regions or even between different times at the same location, high model fits can be achieved for defined areas at a known phenology (Feilhauer and Schmidtlein, 2011).

A widely used approach based on statistical modelling for deriving plant properties are VIs (Fava et al., 2009; Hansen and Schjoerring, 2003; Tucker, 1977; Rouse Jr. et al., 1974). For calculating a VI, a small set of bands (frequently two) is combined mostly as a normalized ratio and related to a plant variable, i.e. a plant morphological or biochemical property. Advantages of utilizing VIs for estimating plant properties are that they require a low number of spectral bands and little computational effort. On the other hand, this approach has its limitations in assessing subtle variations in specific plant properties because it makes use only of a small part of the spectral information available in hyperspectral data (Psomas et al., 2011). Models based on multiple linear regression exploit more detail in spectral information and frequently produce better accuracies for estimating plant properties than VIs (Darvishzadeh et al., 2008b; Psomas et al., 2011). These models create a mathematical function describing the relations between a plant property and the information contained in the spectral signatures of the studied vegetation. However, multiple linear regression models may be subject to overfitting (i.e. an overestimation of model accuracy) when dealing with high numbers of independent variables (Lindberg et al., 1983; Lorber et al., 1987; Næs and Martens, 1984). Thus, VIs and regression models are not suited when a high number of spectral bands (as available in hyperspectral data) is used to estimate plant properties, such as FTs.

Hence, more sophisticated datamining methods, such as partial least squares regression (PLSR) or principal component regression (PCR) have gained in attention within the RS community. Specifically PLSR approaches using a selection of predictor variables were identified as valuable techniques for relating vegetation properties to hyperspectral reflectance (Darvishzadeh et al., 2008a; Feilhauer and Schmidtlein, 2011; Kawamura et al., 2008; Martens and Martens, 2000). As a first step in these algorithms, a subset of spectral reflectance data containing relevant but uncorrelated spectral bands is created. This subset is then summarized as a few latent vectors (similar to principal components) and used for prediction of a dependent variable (i.e. a plant property) in linear statistic models, such as regression. Thus, PLSR in combination with band selection procedures provides an effective solution for coping with multicollinearity (i.e. with mutual information of adjacent spectral bands) while preserving relevant components of hyperspectral RS data for detecting vegetation properties (Chen et al., 2009; Darvishzadeh et al., 2008b; Feilhauer et al., 2010; van der Heijden et al., 2007). Consequently, PLSR was intensively used within the past decades to estimate the quality, biomass and LAI of vegetation, the chlorophyll-, N-, phosphorus- and NDF-content of vegetation or single plants and most recently to detect the FTs of grassland communities (Darvishzadeh et al., 2008b; Ferner et al., 2015; Kawamura et al., 2008; Ramoelo et al., 2013; Roelofsen et al., 2013; Schut et al., 2005, 2006; Zhao et al., 2007). These results show that PLSR is a good choice for detecting the expressions of FTs of grassland along nutrient gradients throughout several growing seasons and years.

1.5   Research aims and objectives

To reliably monitor the changes in ecosystem properties and functions, data availability on FTs in the spatial and temporal (i.e. seasonal and annual) domain is of large importance (Aragón and Oesterheld, 2008; Lavorel et al., 2007). Providing the opportunity to collect spatially contiguous data using novel hyperspectral imaging systems, RS may be a suitable technique for identifying the extent and the spatial variation of FTs according to changing environmental conditions at all possible scales (Schellberg and Pontes, 2012). Thus, RS may add to improvements in precision agriculture, where time-critical information on crop growth, water status and changes in community structure allow more timely management interactions (Jones and Vaughan, 2012). In addition, research identifying specific spectral regions relevant for estimating key FTs can support decisions concerning the design of future RS sensors or allow an improved utilization of available sensors for mapping FTs.

Up to date, few authors have tried to assess the FTs of species-rich grassland communities dominated by different PFTs using their spectral reflectance (Homolová et al., 2013; Roelofsen et al., 2013). None of these studies have thereby observed the relations between FTs and reflectance properties over several growing seasons. The main aims of this research were

(1) to investigate how grassland communities dominated by different PFTs can be distinguished over a growing season and several years using VIs,

(2) to detect the response of grassland FTs to variations in nutrient management using spectral reflectance measurements,

(3) to study which current or planned multispectral and hyperspectral ground-based or spaceborne RS systems are suitable for detecting these FTs and

(4) to test whether RS can provide information to grassland managers, which allows to adapt management strategies in order to support a sustainable agricultural use of grassland under changing climate conditions and intensities of use.

1.6   Thesis structure and outline

As shown in Figure 1-8, this dissertation is separated into five main parts. Chapter 1 is a general introduction and provides an overview on functional ecology, the concept of FTs and the operating principles of RS of vegetation. It further lists ideas on how field-based estimates of the status of grassland FTs can be complemented or even replaced using remotely sensed information. Additionally, the general aims of this thesis are listed and the study area is presented.

Chapter two is published as peer reviewed article in the journal "Remote Sensing" (Hollberg and Schellberg, 2017). It shows how five intensity levels of grassland can be best distinguished at several points in time using 15 different remotely sensed VIs. These VIs were selected because they are sensitive to the most important plant properties affecting the spectral reflectance (i.e. the biomass, LAI, chlorophyll content, water content and chemical composition of plants) and include bands from a wide range of wavelength regions. Spectral reflectance was measured on 38 dates throughout the growing seasons 2012-2014 using a ground-based ASD FieldSpec 3 (FS 3) spectroradiometer. Subsequently, the VIs were calculated and their potential for distinguishing the different grassland canopies at different phenological stages and in several years was assessed. Additionally, a multiple VI approach was developed, which adds to a more stable classification of grassland communities over time.

```
┌─────────────────────────────────────────────────────────────────────────┐
│                           1 Introduction                                  │
│          - What are FTs and why should we use RS to detect them           │
│     - Principles, applications and theory of RS to detect vegetation      │
│                        properties and FTs                                  │
│          - The Rengen Grassland Experiment – climate, soil and            │
│                            vegetation                                      │
└─────────────────────────────────────────────────────────────────────────┘
```

```
┌───────────────────────────┐  ┌───────────────────────────┐  ┌───────────────────────────┐
│ 2 Distinguishing Intensity│  │ 3 Can we detect grassland │  │ 4 The potential of remote │
│ Levels of Grassland       │  │ plant functional traits   │  │ sensing sensors featuring │
│ Fertilization Using       │  │ based on canopy           │  │ different spectral        │
│ Vegetation Indices        │  │ reflectance?              │  │ resolution and range for  │
│ - Temporal variation in   │  │ - FTs vary over time and  │  │ detecting FTs of grassland│
│ grassland spectral        │  │ differ between vegetation │  │ - Creating PLSR models to │
│ reflectance over time     │  │ communities               │  │ estimate FTs using six    │
│ - Classifying grasslands  │  │ - How to detect these     │  │ different RS sensors      │
│ using VIs: identification │  │ variations in different   │  │ - Assessing the potential │
│ of efficient VIs          │  │ grassland canopies using  │  │ of these existing and     │
│ - Variations in           │  │ RS                        │  │ planned multispectral     │
│ classification accuracy   │  │ - Relating spectral       │  │ and hyperspectral RS      │
│ - Temporally stable       │  │ reflectance to FTs        │  │ sensors for the detection │
│ grassland classification: │  │ using PLSR                │  │ of FTs                    │
│ the multi-VI approach     │  │ - Evaluation of model     │  │                           │
│                           │  │ performances              │  │                           │
└───────────────────────────┘  └───────────────────────────┘  └───────────────────────────┘
```

```
┌─────────────────────────────────────────────────────────────────────────┐
│                           5 Conclusions                                   │
│ - How to distinguish different grassland communities using remotely       │
│                        sensed information                                  │
│ - Estimating FTs using remote sensing measurements: efficient data        │
│                 processing and analysis techniques                        │
│ - Which remote sensing sensors are suited for detecting grassland FTs     │
│                - Recommendations for future studies                       │
└─────────────────────────────────────────────────────────────────────────┘
```

Figure 1-8. Structure of this thesis and content of the five chapters.

Chapter three is internally reviewed, revised and ready for submission as research article to the journal "Remote Sensing of Environment" (Hollberg et al., 2017a). The study describes how spectral reflectance needs to be acquired, processed and analyzed to estimate the expressions of numerical FTs. Therefore, manual measurements of twenty-three different FTs and the associated spectral reflectance were recorded in five different grassland canopies. The dataset was collected on 29 dates throughout the growing seasons 2012-2014. A PLSR model was developed for estimating each single FT based on canopy reflectance and subsequently assessed for its accuracy. Finally, the most relevant spectral regions for studying each FT were identified.

The following (fourth) chapter is an article that is internally reviewed, revised and dedicated for submission to the journal "International Journal of Applied Earth Observation and Geoinformation" (Hollberg et al., 2017b). In this study, it is examined which current and planned satellite sensors can be used to detect the FTs of different grassland communities. FS 3 derived reflectance data were resampled to the resolutions of the ASD Handheld 2 (HH 2), Environmental Mapping and Analysis Program (EnM), Sentinel-2 (S-2), Landsat 7 Enhanced Thematic Mapper + (L 7) and RapidEye (RE) sensors. Subsequently, PLSR models were created for the 23 FTs using the raw FS 3 data and the resampled spectral bands. In the next step, the accuracies for deriving the FTs achieved by each sensor were evaluated. Finally, it was shown which sensors are suitable for detecting single FTs of grassland vegetation and what influences spectral range and resolution have on the model performances.

The fifth chapter is a general conclusion. It points out if and how hyperspectral RS may support grassland ecologists in assessing the response of grassland communities to changes in nutrient management or climate. Furthermore, perspectives for future research are presented.

1.7 The Rengen Grassland Experiment

To test the strengths of the relations between FTs and spectral reflectance, it was necessary to select a study site, which features a wide range of different agriculturally used grassland communities along a gradient in management intensity level. Ideally, this study site should be well-documented in terms of its vegetation composition and its soil properties. Furthermore, floristic composition of the investigated communities should not substantially change throughout the time of the study. Our choice was the Rengen Grassland Experiment (RGE), which is located in Rhineland Palatinate, Germany (Figure 1-9).
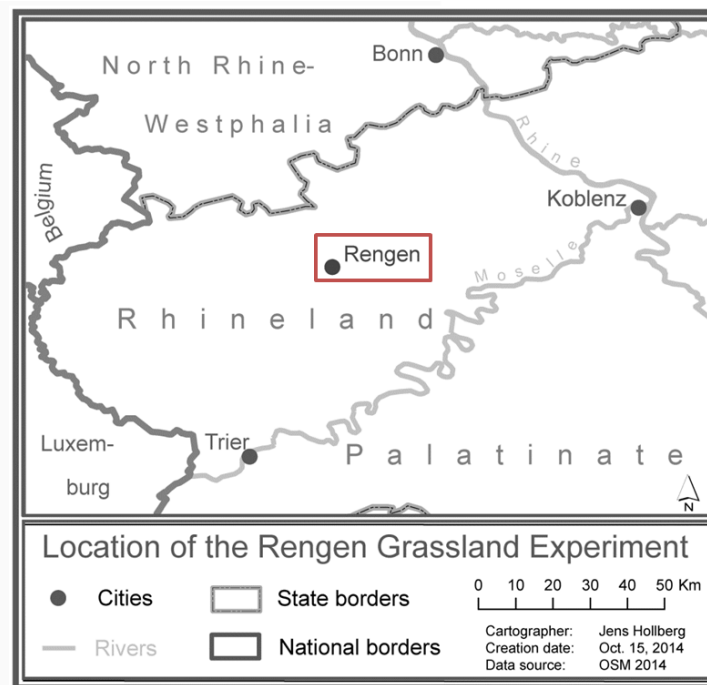
Figure 1-9. Location of the RGE (data: OSM, 2014; map: Hollberg, J.L., 2014).

The experiment was established in 1941 and comprises five fertilization levels, including lime only (Ca), lime and nitrogen (CaN), lime, nitrogen and phosphorus (CaNP) and lime, nitrogen, phosphorus and potassium as CaNPKCl and CaNPK$_2$SO$_4$, respectively. The experiment consists of 50 single fertilized plots (i.e. ten replicates per treatment) and five unfertilized control plots (Table 1-4, Figure 1-10).

Table 1-4. Amounts of nutrients (kg ha^{-1}) supplied annually to the treatments since 1941 (modified, Schellberg et al., 1999).

Nutrient	Treatment				
	Ca	CaN	CaNP	CaNPKCl	CaNPK$_2$SO$_4$
CaO	1000	1309	1309	1309	1309
N	0	100	100	100	100
P$_2$O$_5$	0	0	0	80	80
K$_2$O	0	0	0	160	160
Mg	67	67	75	90	75
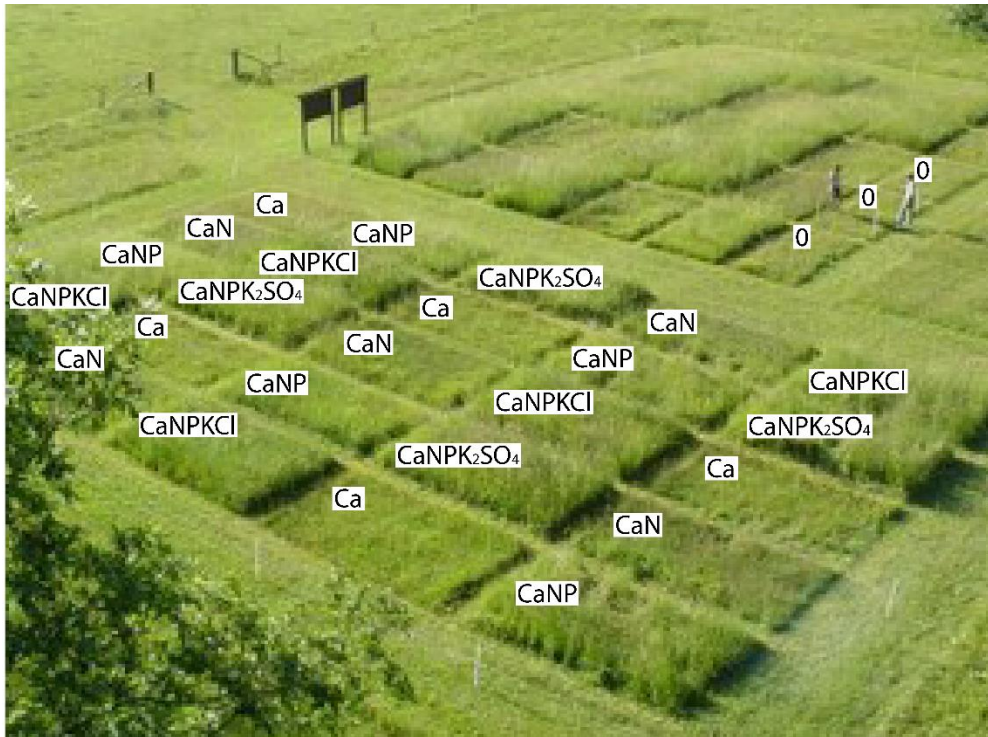
Figure 1-10. Image of the Rengen Grassland Experiment. Annotations indicate fertilization.0 represents unfertilized control plots (modified, Hejcman et al., 2010a).

All plots are managed as a two-cut system. Due to differences in fertilization, grassland communities have developed that feature significantly different species compositions (Hejcman et al., 2010a). Consequently, plants in these communities vary in their pace of phenological development, their morphology as well as in their chemical composition and physiology (Figure 1-11; Chytrý et al., 2009; Hejcman et al., 2007). Plant communities in the Ca- and CaN-treatments develop slower in green leaf area than those in the NP(K)-treatments and produce relatively low amounts of biomass (Hejcman et al., 2010b; Schellberg et al., 1999). However, these communities maintain green leaf area over long periods in time, whereas senescence starts in the NP(K) treated communities in June (growth one, cf. Figure 1-11) and September (growth two). More details on the vegetation composition and the biophysical properties of the single

plots of the experiment can be found in chapters 2.2.1; 3.2.1 and 4.2.1 as well as in Chytrý et al., (2009); Hejcman et al., (2007) and Schellberg et al., (1999). Details on the soil properties existing at the site can be found in Hejcman et al., (2010a).
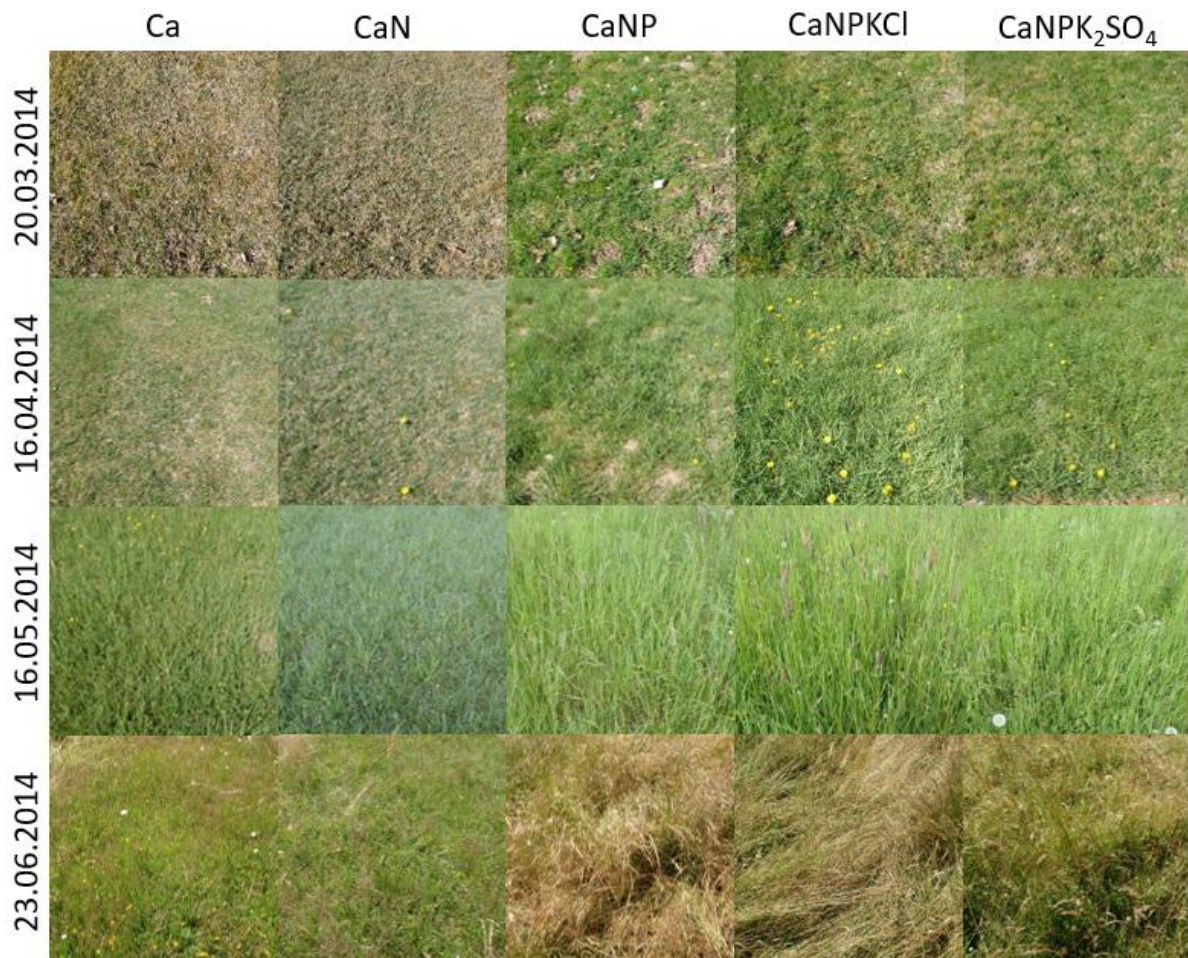
Figure 1-11. Optical characteristics of the grassland communities in the Rengen Grassland Experiment over a growing season (Photo: Hollberg, J.L., 2014).

2 Distinguishing intensity levels of grassland fertilization using vegetation indices

Abstract

Monitoring the reaction of grassland canopies on fertilizer application is of major importance to enable a well-adjusted management supporting a sustainable production of the grass crop. Up to date, grassland managers estimate the nutrient status and growth dynamics of grasslands by costly and time-consuming field surveys, which only provide low temporal and spatial data density. Grassland mapping using remotely-sensed VIs has the potential to contribute to solving these problems. In this study, the potential of VIs for distinguishing five differently-fertilized grassland communities was explored. Therefore, we collected the spectral signatures of these communities in a long-term fertilization experiment (since 1941) in Germany throughout the growing seasons 2012-2014. Fifteen VIs were calculated and their seasonal developments investigated. Welch tests revealed that the accuracy of VIs for distinguishing these grassland communities varies throughout the growing season. Thus, the selection of the most promising single VI for grassland mapping was dependent on the date of the spectra acquisition. A random forests classification using all calculated VIs reduced variations in classification accuracy within the growing season and provided a higher overall precision of classification. Thus, we recommend a careful selection of VIs for grassland mapping or the utilization of temporally-stable methods, i.e., including a set of VIs in the random forests algorithm.

2.1 Introduction

Grasslands are the largest of the earth's four major vegetation types and belong to the world's most productive agricultural lands (Price et al., 2001). Grass swards are known for their high spatial and temporal variability (Schut et al., 2002) and therefore require intensive monitoring to enable a management that is well adjusted to the prevailing environmental conditions. Maps displaying the phenological status of grassland allow creating a spatio-temporal model of grassland production (Gianelle and Vescovo, 2007). Such information is crucial for adjusting the nutrient management in order to mitigate water pollution (through leaching of soil nutrients) and to conserve the flora and fauna of grassland ecosystems. Commonly, grassland agronomists evaluate the phenological status, the quality and the spatial distribution of grasslands in costly and time-consuming field surveys, as described in Cornelissen et al., (2003). The methods defined in this handbook require destructive sampling and allow only a low spatial and temporal data density. Research developing non-destructive, cost-effective and time-saving methods for

grassland mapping and monitoring is urgently needed. These goals can be reached using a combination of minor field sampling efforts and RS (Aragón and Oesterheld, 2008).

Among the available RS methods, VIs are frequently used for assessing different grasslands types (e.g. Hill, 2013; Wardlow et al., 2007). Classification of these types based on VIs requires consideration of the timing of data acquisition in relation to growth stage, as well as of type, wavelength and bandwidth of the VI used. Aragón and Oesterheld, (2008) have shown that classification accuracy of grasslands depends on the date of the spectral observation. The reason for these changes in classification accuracy is that the optical properties of grassland vegetation are underlying permanent variations (Psomas et al., 2011). These variations in the individual VIs throughout a growing season are caused by changes in the vegetation's biophysical properties as a result of weather conditions in interaction with management actions (Poças et al., 2012). VIs composed of NIR and VIS light strongly correlate with biomass (Fava et al., 2009), LAI and chlorophyll content (Daughtry et al., 2000; He et al., 2006). Thus, VIs based on these wavelengths are capable of distinguishing vegetation canopies, as long as they differ significantly in these variables. In contrast, spectral reflectance at longer wavelengths (between 1300 and 2500 nm) is highly influenced by water absorption of plants (Asner, 1998; Kumar et al., 2001). This relation between plant water content and absorption of incoming radiation affects the spectral reflectance of plants. Thus, selecting VIs sensitive to the vegetation's water content may enable a successful classification at times when those VIs appear relatively similar, which are sensitive to other crop variables, such as biomass, LAI or chlorophyll content. Further, VIs more sensitive to nitrogen and lignin content, as well as to morphological and physiological properties indicating plant stress may improve classifications at times when grasslands differ in these variables.

Furthermore, bandwidth and spectral resolution have a major impact on the ability of VIs to distinguish grassland communities. Although several efforts have been made to classify grasslands using broadband data (Adams et al., 1995; Lucas et al., 1993; Roberts et al., 2002), it was found that they are not spectrally distinct in the broadband system throughout all times of a growing season (Numata et al., 2008). It was also shown that the utilization of hyperspectral data may significantly improve the quality of maps displaying the distribution of different grassland communities. Novel or planned hyperspectral satellite missions (such as Hyperion, EM and HyspIRI) may open new perspectives for mapping grasslands using narrowband VIs and are of special importance for distinguishing grassland types and management characteristics as well as for monitoring these plant communities (Price et al., 2001).

Hyperspectral RS can provide a cost-effective, time-saving and non-destructive method for mapping differences in growth dynamics as induced by fertilizer application as well as the spatial distribution of grassland communities at high spatial and temporal resolution. However, multitemporal studies investigating the performance of hyperspectral and broadband VIs for mapping Central-European grasslands are still missing. Basic research into this direction necessitates not only a high temporal, but also a high spatial and spectral resolution of RS data across clearly-defined grassland communities. These requirements are not met using satellite data only, because frequent cloud cover and low spatial coverage of hyperspectral satellite systems prevents acquiring dense time series in Central Europe. The solution lies in utilizing field spectroradiometers, which can acquire hyperspectral data on demand for dates when cloud cover is low. To collect spectra of clearly separable grassland communities, we identified a fertilizer experiment on grassland as the ideal setting.

The above-mentioned deficits in the classification of grassland types make clear that studies are required where the criteria growth stage, bandwidth and type of VI are rigorously tested. Therefore, the aim of this study was to identify single VIs providing the most valuable information at specific points in time that enable grassland scientists to distinguish between differently-managed grassland communities. Furthermore, we introduce a novel approach in grassland research, which uses multiple VIs sensitive to changes in different plant properties for classifying grasslands. Accordingly, our key hypotheses were:

1. Each plant community on grassland is characterized by a unique VI development throughout the growing season.
2. The performance of each VI for distinguishing such plant communities varies throughout the growing season.
3. VIs sensitive to a certain plant property (e.g., chlorophyll content) may allow a successful classification at times when VIs sensitive to other plant properties (e.g., water content, biomass, etc.) fail to classify correctly.
4. Combining several VIs for grassland classification allows a temporally more stable classification of communities than using one single VI because for distinguishing communities at a point in time, a set of optimal VIs is selected.

To test these hypotheses, we collected a series of spectral signatures of five species-rich grassland communities in a long-term fertilization experiment for 38 dates during the growing seasons of 2012–2014. Subsequently, we calculated 15 broadband and narrowband VIs and tested the performance of each single VI for distinguishing these five communities using the

Welch test (Welch, 1938). In addition, multiple VIs for classifying the same grassland communities using the random forests algorithm were tested (Breiman, 2001). Finally, we compared the classification accuracy achieved using single VIs and the Welch test to the performance reached by the random forests algorithm.

2.2   Materials and methods

2.2.1   Study area

The RGE is a long-term fertilization experiment, which was set up in 1941. It is located near the village of Rengen (Rhineland-Palatinate, Germany) in the Eifel Mountains, approximately 60 km west of Koblenz. The experiment is located at the position 50°14′21.6″N, 6°49′34.6″E at an elevation of 475 m asl. The temperate, maritime climate at the site features an annual mean precipitation of 811 mm and a mean annual temperature of 6.9 °C (Rengen Experiment Meteorological Station). A detailed description of the experiment is given in Schellberg et al., (1999). In brief, the experiment was set up on a formerly wet heathland site in randomized block design. In 1941, the area was grubbed, and a mixture of grasses and herbs was sown. Five fertilizer treatments have been applied annually: lime only as calcium oxide (CaO, Ca), lime and nitrogen (CaO/N, CaN), lime, nitrogen and phosphorus (CaO/N/P_2O_5, CaNP) and lime, nitrogen, phosphorus and potassium (CaO/N/P_2O_5/KCl, CaNPKCl and CaO/N/P_2O_5/K_2SO_4, CaNPK_2SO_4, respectively). The plots in this experiment are representative of grassland fields on farms under different management intensities and stand for fields of a similar type spread all across European grassland areas. Treating the plots with different types of fertilizer resulted in significant differences in plant and soil nutrient content (for more details, see Hejcman et al., 2010b).

This work was conducted on five plots of the RGE with a size of 3 m × 5 m (Figure 2-1). The plots were harvested twice annually, i.e., once at the beginning of July and once in the middle of October. Previously-published data from this experiment (Hejcman et al., 2007; Schellberg et al., 1999) indicate that dry matter production increased gradually from Ca, CaN, CaNP, CaNPK_2SO_4 to the CaNPKCl treatment and that biomass production in the first cut is higher than in the second cut. Furthermore, long-term fertilization resulted in significant differences in the floristic compositions of the communities. The vegetation in the Ca and CaN treatments mostly resemble the montane meadow of Geranio-Trisetetum (Polygono-Trisetion), whereas the CaNP plot features a transitional type between Poo-Trisetetum and Arrhenateretum (both

from the Arrhenatherion alliance) (Chytrý et al., 2009). In the NPK treatments, vegetation corresponded to the mesotrophic Arrhenateretum meadows (Chytrý et al., 2009).

All of these differences in the properties of plant canopies have strong effects on their optical characteristics. Generally, a more rapid change in visual appearance at the beginning of the growing seasons is observed in the NPK-treated plots each year. These plots develop rapidly in green biomass and reach high LAIs and a bright green canopy. Later, in June, senescence of plants commences, which leads to higher contributions of senesced yellow plant material. In contrast, development in green biomass in the Ca and CaN treatment is usually much slower, but the color of these canopies remains green, even later in the growing season.

2.2.2   Spectral measurements

Field spectroradiometers have successfully been used for discriminating differences in grassland types caused by management practices or climatic variability (Price et al., 2001; Psomas et al., 2005). In addition, there is evidence in the literature that field spectroradiometer data are highly correlated with satellite data (Poças et al., 2012) and relatively free of atmospheric effects (Thenkabail et al., 2000). Thus, we collected spectral measurements in the RGE during the growing seasons of 2012–2014 (Table 2-1) using an FS 3 spectroradiometer (Analytical Spectral Devices Inc., Boulder, CO, USA). This instrument covers a spectral range between 350 nm and 2500 nm in 1-nm steps, with a 3-nm full width at half maximum (FWHM) at a wavelength of 700 nm and 10 nm at 1400 nm and 2100 nm (ASD Inc. (ed.), 2010).

Table 2-1. Number of data collection days between 2012 and 2014 by growth.

	No. of Acquisition Days		
	2012	2013	2014
Growth one	4	7	8
Growth two	7	6	6

The spectroradiometer was mounted on a motor-driven rail-crane that automatically moved along a rail track next to the five plots. It was equipped with a photoelectric guard (light barrier) to ensure a systematic sampling of spectral properties at the same position (Figure 2-1; cf. Gamon et al., 2006). From this vehicle, spectra of the vegetation were measured on three circular spots within each plot from a height of 2 m above ground at nadir position, resulting in a field of view (FOV) of 90 cm in diameter per spot (Figure 2-1). On each measuring day, between twelve and thirty-three spectra per plot were acquired between 10:00 a.m. and 4:00 p.m., i.e., between 210 minutes before and 150 minutes after solar noon. Spectra were recorded

under clear (sunny) conditions, which ensured that influences of clouds were minimal. The spectral reflectance of the plant canopies was calculated based on a Spectralon® 400 cm² white-reference zenith polymer target (95% reflectance, Labsphere Inc., North Hutton, NH, USA) always after three measurements were taken.
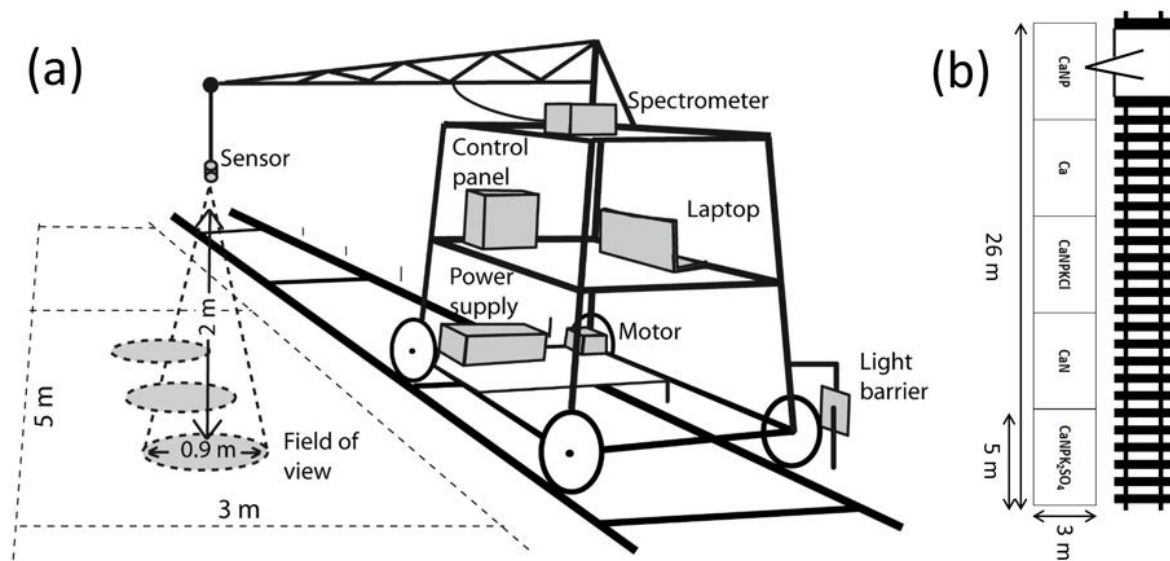
Figure 2-1. Setup of the automated field observation system with its components (a) and arrangement of fertilizer treatments and monitored plots (b).

2.2.3 Calculation of the temperature sum

It is well known that changes in plant development are closely related to changes in weather variables, such as precipitation and accumulated temperature (Poças et al., 2012; Ritchie and NeSmith, 1991), and not to the date or day of year. Thus, we decided to use the temperature sum (T$\sum$) as the temporal variable. T$\sum$ was calculated for the years 2012-2014 based on the average daily temperatures given in the 1×1 km mosaic, provided by Deutscher Wetterdienst (DWD, 2015) according to the method by Ernst and Loeper, (1976). Daily mean temperatures above 0°C were added up. To correct for low solar irradiation during the winter months, a weight factor of 0.5 was assigned to January, 0.75 to February and 1 to the remaining months (Ernst and Loeper, 1976). As a starting point of the growing season, a value of 200 °C d was assumed. At this point and before the onset of the second growth in July, T$\sum$ was set to zero to provide equal scales for the first and the second growth.

2.2.4 Calculation of the vegetation indices

Based on the spectral measurements, 12 narrowband and 3 broadband VIs were calculated (Table 2-2). Therefore, five bands of the multispectral RE satellites were simulated using their spectral response function (BlackBridge (ed.), 2012):

$$\gamma_x = \frac{\int_{n0}^{n} \gamma_n * \rho_n}{\rho_t} \tag{2.1}$$

where γ_x is the reflectance of the simulated RE band, n is the band number of the spectral measurement, γ_n is the reflectance of band n, ρ_n is the response of band n, given in the spectral response function, and ρ_t is the sum of values given in the response function of band x. RE appeared to us as an interesting broadband sensor because its spatial resolution (6.5 m) is higher than spatial resolution of other broadband systems (e.g., Landsat 7, 8 or S-2) and was thus better comparable to the high spatial resolution of field spectroradiometer data. We selected these VIs because they are sensitive to different plant properties, contained different spectral information and are commonly used in grassland science. The VIs that were used can be grouped into three categories according to Table 2-2:

1. VIs sensitive to green vegetation, biomass and leaf area,
2. VIs sensitive to plant chlorophyll content,
3. VIs sensitive to the plants' content in lignin, N, water, pigments or to plant physiological performance and phaeophytization (environmental stress).

To display the temporal development of the VIs as smoothed curves, first daily averages for each VI were calculated. Subsequently, the local polynomial smoothing algorithm (loess) (Cleveland et al., 1992), which is implemented in the ggplot2 (Wickham and Chang, 2016) package for R (R Development Core Team, 2015), was used to create smoothed VI curves.

Table 2-2. Selected VIs for discriminating differently fertilized grassland plots.

VI	VI Full Name	Formula	Sensitivity	Source
GNDVI	Green normalized difference vegetation index	$\dfrac{(NIR - GREEN)}{(NIR + GREEN)}$	Green vegetation/biomass, LAI	Gitelson et al., (1996)
nGNDVI	Narrowband green normalized difference vegetation index	$\dfrac{(780\ nm - 550\ nm)}{(780\ nm + 550\ nm)}$	Green vegetation/biomass, LAI	Gitelson et al., (1996)
NDVI	Normalized difference vegetation index	$\dfrac{(NIR - RED)}{(NIR + RED)}$	Green vegetation/biomass, LAI	Rouse Jr. et al., (1974)
nNDVI	Narrowband normalized difference vegetation Index	$\dfrac{(800\ nm - 670\ nm)}{(800\ nm + 670\ nm)}$	Green vegetation/biomass, LAI	Rouse Jr. et al., (1974)
nREP	Narrowband red edge position	$700 + \dfrac{40 \times \frac{670\ nm + 780\ nm}{2} - 700\ nm}{740\ nm - 700\ nm}$	Chlorophyll	Guyot et al., (1988)
LCI	Leaf chlorophyll index	$\dfrac{(NIR - RE)}{(NIR - Red)}$	Chlorophyll	Datt, (1999)
nLCI	Narrowband leaf chlorophyll index	$\dfrac{(850\ nm - 710\ nm)}{(850\ nm + 680\ nm)}$	Chlorophyll	Datt, (1999)
nNPCI	Narrowband normalized pigment chlorophyll index	$\dfrac{(680\ nm - 430\ nm)}{(680\ nm + 430\ nm)}$	Chlorophyll	Peñuelas et al., (1994)
nNDLI	Narrowband normalized difference lignin index	$\dfrac{\log \frac{1}{1754\ nm} - \log \frac{1}{1680\ nm}}{\log \frac{1}{1754\ nm} + \log \frac{1}{1680\ nm}}$	Lignin content	Serrano et al., (2002)
nNDNI	Narrowband normalized difference nitrogen index	$\dfrac{\log \frac{1}{1510\ nm} - \log \frac{1}{1680\ nm}}{\log \frac{1}{1510\ nm} + \log \frac{1}{1680\ nm}}$	Nitrogen content	Serrano et al., (2002)
nPRI	Narrowband photochemical reflectance index	$\dfrac{(550\ nm - 530\ nm)}{(550\ nm + 530\ nm)}$	Physiology (photosynthesis, pigments)	Peñuelas et al., (1994)
nWC	Narrowband water content	$\dfrac{1193\ nm}{1126\ nm}$	Water content/water stress	Underwood et al., (2003)
nWI	Narrowband water index	$\dfrac{900\ nm}{970\ nm}$	Water content	Peñuelas et al., (1997)
nSIPI	Narrowband structure intensive pigment index	$\dfrac{(800\ nm - 450\ nm)}{(800\ nm + 650\ nm)}$	Pigments	Peñuelas et al., (1995)
nNPQI	Narrowband normalized phaeophytization index	$\dfrac{(415\ nm - 435\ nm)}{(415\ nm + 435\ nm)}$	Phaeophytization	Barnes et al., (1992)

2.2.5   Welch test

Using Welch's t-test (Welch, 1938), we determined how well the different grassland communities can be distinguished at different points in time using certain VIs. The Welch test essentially delivers similar results as a two-sample t-test, but does not assume a normal distribution and equal variances of the samples, which were not given in our dataset. The Welch test was calculated for each VI for a given T$\sum$ by testing the VI value measured in one plot against the VI value measured in all other plots. The VI value of a certain plot at a certain T$\sum$ was assumed to be different from the remaining plots if p was estimated <0.01. The results of the five plots were summarized, and the classification accuracy was calculated for each T$\sum$. The overall accuracies for the two growths were calculated by averaging each VI's accuracy at each T$\sum$. Subsequently, the Welch test accuracies were plotted using local polynomial smoothing (loess) (Cleveland et al., 1992) in the ggplot 2 package (Wickham and Chang, 2016) in R (R Development Core Team, 2015).

2.2.6   Random forests classification

Random forests (Breiman, 2001) is a classification method based on classification and regression trees. To classify data, in the first step, a random sample with known output classes is extracted from the dataset. Based on this random sample, a number of binary decisions (splits) are made, which at the end, achieves the highest possible purity of the output classes. At each split, a number of variables is tested as the splitting variables. More splits are performed until the highest possible purity of the output classes is reached. This network consisting of a few to some hundreds of splits is called a tree. Subsequently, a number of additional trees is grown based on other random samples. The sum of trees grown by this principle is called a random forest. Usually, approximately 63% of the samples of the complete dataset are used for growing the trees, and the remaining 37% of the samples are left for model validation. Finally, the decision of an observation belonging to a class is made based on the number of trees within a forest assigning the value of the observation to that class.

In this study, all 15 VIs were tested as split variables at each node. A number of n = 200 trees for creating the forest was identified to be sufficient. To investigate the classification accuracy, the Out-Of-Bag (OOB) error was calculated. This error indicates the accuracy reached by the forest by testing the decisions created by the forest against the validation dataset. Subsequently, OOB errors for each T$\sum$ were plotted using lines created by the smooth.spline function in R (Chambers and Hastie, 1992). Furthermore, the variable importance indicating the probability

of a VI being used in the classification at a split was calculated by dividing the number of splits based on one VI by the total number of splits in a tree. The average importance of the VIs of each growth revealed their overall importance and was further tested for significance using a two-paired t-test. Furthermore, variable importance by $T\sum$ was plotted for five selected VIs using the local polynomial smoothing algorithm (loess) (Cleveland et al., 1992) in the ggplot 2 package (Wickham and Chang, 2016) in R (R Development Core Team, 2015).

2.3 Results

The results of this multi-temporal study are presented in the following sections separately for pooled data on growth one and growth two. Treating the two growths individually was necessary because they varied significantly in their development. This implies important consequences for the classification of the grassland communities.

2.3.1 Seasonal curves of the vegetation indices

In Figure 2-2, the developments of narrowband red edge position (nREP), leaf chlorophyll index (LCI), NDVI, narrowband water index (nWI) and narrowband water content (nWC) by $T\sum$ within the five plant communities are shown. These VIs were selected for visual presentation because they represent the best performing VIs for each group averaged over both growths according to Section 2.4, as well as the best performing VIs of each growth. The shape of the curves of all VIs measured in the Ca, CaN and CaNP treatment were more similar in growth two than in growth one. This was mostly related to the lower amplitude of changes in VIs that we observed in growth two.

The curves of nREP, LCI, NDVI and nWI increased at the beginning of both growths in all plots. Thereby, the slopes of the curves derived for the NP(K)-treated plots were steeper than those in the Ca and CaN plot, but the CaNP treatment did not reach as high VI values as the NPK treatments. The $T\sum$ at which peaks of these four VIs in the NP(K)-treated plots were reached differed between the VIs and between the two growths. The highest values in these four VIs were found at higher $T\sum$s in growth one than in growth two. Furthermore, the chlorophyll- and biomass-related VIs (nREP, LCI and NDVI) reached their peaks earlier than the water-related nWI. Towards the end of both growths, values of the four VIs decreased steeply in the NPK treatments. In contrast, VIs in the Ca and CaN plots remained relatively stable. Opposed to the four previously-mentioned VIs, the curve of nWC decreased at the beginning of both growths. Thereby, the highest decline rates were observed in the NP(K)

treatments, which reached their minimum later in growth one than in growth two. Afterwards, nWC in the NP(K) treatments began to rise. nWC in the Ca and CaN treatments decreased slower than in the NP(K) treatments at the beginning of both growths, but remained relatively stable towards their end.
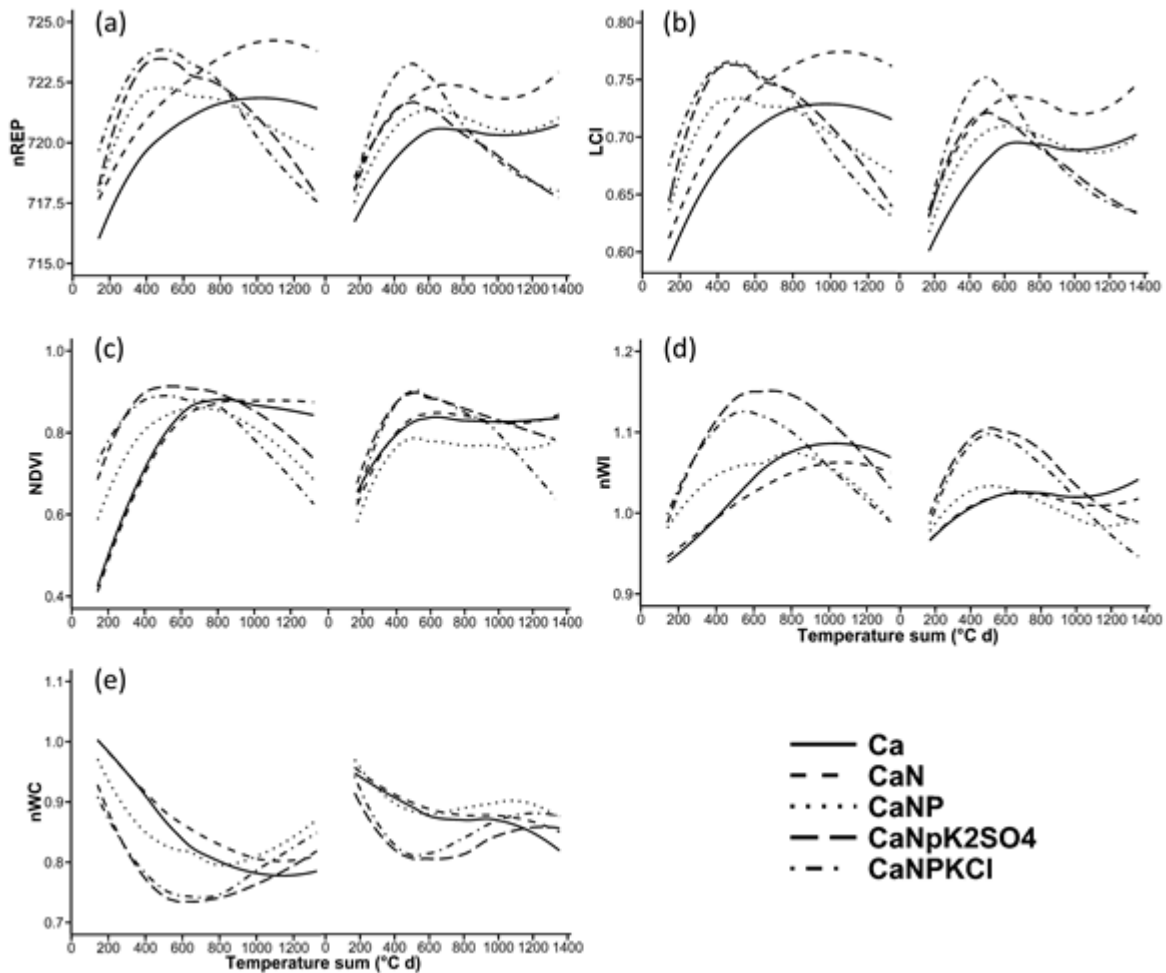
Figure 2-2. Smoothed curves of temporal development of (a) nREP, (b) LCI, (c) NDVI, (d) nWI and (e) nWC in growing seasons one and two.

In growth one, curves in the Ca, CaN and CaNP treatments featured differences in their values of nREP, LCI and nWC throughout most phases of the growing season. However, the curves measured in the CaNPKCl and CaNPK$_2$SO$_4$ treatments were similar in these three VIs. At the same time, these treatments differed considerably in nWI, particularly at the end of growth one. At the beginning of growth one, NDVI values were different between the plots. At later stages, NDVI values in the five plots became relatively similar. In growth two, larger differences between the CaNPKCl and the CaNPK$_2$SO$_4$ treatment were identified for nREP, LCI and NDVI

than in growth one. In contrast, both NPK treatments showed similar courses of their curves for nWI and nWC.

2.3.2 Distinguishing the grassland communities using the Welch test

Although time courses of many VIs tested in this study followed similar patterns, uncertainty remained for how the identified differences have influenced the accuracy for classifying the grassland plots using one VI at a time. Table 2-3 displays the overall accuracies of the single VIs achieved using the Welch test. In the first growth, nWC significantly differed between the five plots in 91% of the cases and provided the highest rates of discrimination, followed by nWI, nLCI, narrowband structure intensive pigment index (nSIPI) and LCI. The weakest accuracy was achieved by narrowband normalized phaeophytization index (nNPQI), followed by narrowband photochemical reflectance index (nPRI), narrowband normalized pigment chlorophyll index (nNPCI) and narrowband green normalized difference vegetation index (nGNDVI). In the second growth, significant differences in the VIs between the plots were most frequently found using LCI, nWI, nREP, nSIPI and nWC. As in growth one, the lowest classification rates in the second growth were reached with nPRI, nNPQI and NPCI.

Regarding the differences in classification accuracy reached by the broadband and narrowband versions of VIs, results between the two growths differed. In growth one, broadband NDVI and GNDVI outperformed their narrowband versions, whereas the opposite was found in growth two.

Table 2-3. Ranks and overall accuracies of the 15 VIs for the first and the second growth, as determined by the Welch test (12 < n < 33, p = 0.01, α = 0.99).

	Index	nWC	nWI	nLCI	nSIPI	LCI	nNDLI	NDVI	nNDNI	
Growth one	Accuracy	0.91	0.85	0.84	0.84	0.83	0.83	0.80	0.80	
	Index	nNDVI	nREP	GNDVI	nGNDVI	nNPCI	nPRI	nNPQI		Average
	Accuracy	0.79	0.79	0.76	0.75	0.73	0.68	0.41		0.77
Growth two	Index	LCI	nWI	nREP	nSIPI	nWC	nLCI	nNDLI	nNDNI	
	Accuracy	0.76	0.75	0.72	0.71	0.71	0.67	0.64	0.64	
	Index	nGNDVI	nNDVI	NDVI	GNDVI	nNPCI	nNPQI	nPRI		Average
	Accuracy	0.62	0.62	0.61	0.61	0.46	0.46	0.44		0.63

The probability for nREP, LCI, NDVI, nWC and nWI to distinguish plots at different T∑s correctly is shown in Figure 2-3. At the beginning of the first growth, accuracies of LCI, NDVI, nWI and nWC were above 80% and further increased to more than 95%. The accuracy of nREP was about 50% at the onset of growth, but drastically increased during the initial stages of

growth one and successfully separated more than 95% of the plots at a T∑ of 450 °C d. Afterwards, the accuracies of nREP, LCI and NDVI dropped to levels between 65% and 70%. Accuracies of nWC and nWI remained more stable, making them the strongest and second strongest VI, respectively. At the end of growth one, the accuracy of the chlorophyll-related VIs started to increase earlier than the accuracy of the water-related VIs. Thus, they achieved similar accuracies, like the water-related VIs.
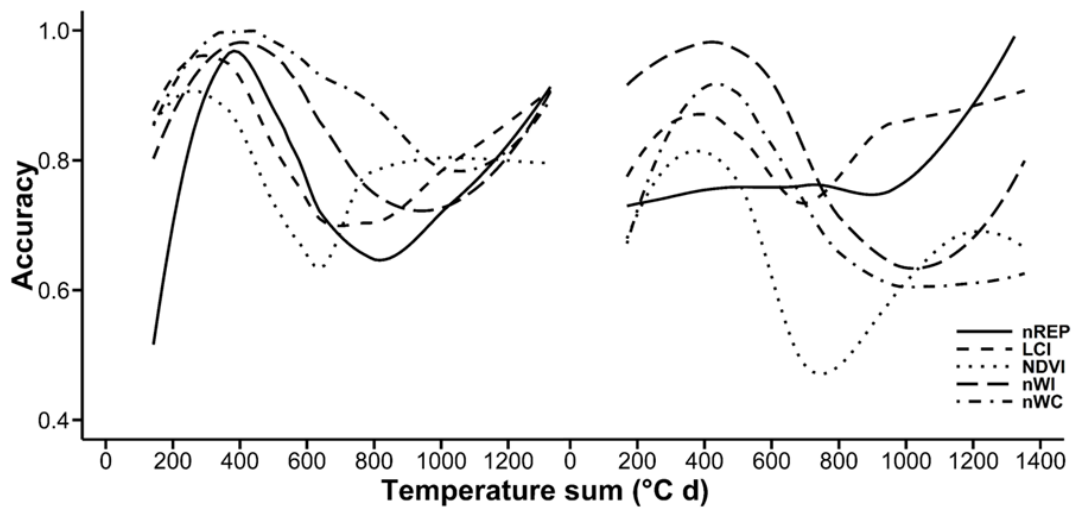
Figure 2-3. Accuracies of nREP, LCI, NDVI, nWI and nWC to distinguish plots at different T∑s.

During the onset of the second growth, the highest classification accuracies were reached using nWI (above 90%). Similar to the previous growth, the accuracies of all VIs (except for nREP) increased until T∑s of 400–450 °C d were reached. Afterwards, all VIs' accuracies dropped, except for nREP, which remained constant at this time. As LCI recovered as the first VI, it was the best performing VI between 800 and 1150 °C d. The water-related VIs recovered in their accuracies the latest. At the end of growth two, nREP steeply increased and outperformed the other four VIs.

2.3.3   Random forests classification

The random forests classification was performed to investigate how the utilization of several VIs improves the classification accuracies, compared to single VIs. The error rate of the classification was expressed as OOB error, which is shown as a function of T∑ in Figure 2-4. It was observed that OOB errors in the second growth (12%) were higher than in the first growth (5%). Furthermore, the classification error in growth one remained relatively stable (between

2.5% and 6%). In contrast, OOB errors in growth two varied significantly with the T$\sum$ ranging between 2.5% and 17.5%.
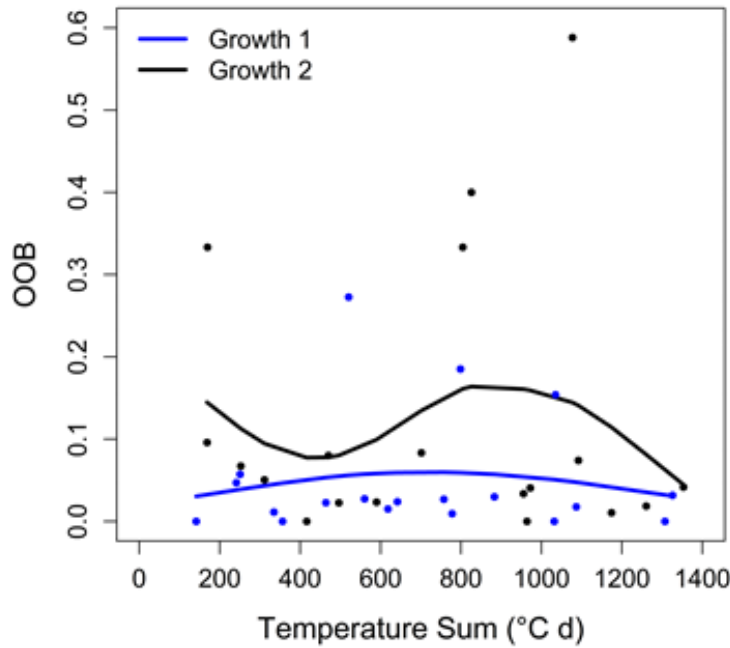
Figure 2-4. Random forests: Out-Of-Bag (OOB) errors of growths one and two.

To identify the probability of a VI for being selected as a split variable in random forests, the variable importance was calculated and averaged for each growth (Figure 2-5). The results of the t-test (cf. Table A 1) indicate significant differences in the VIs' importance. In the first growth, nWI reached the highest importance (16% of the decisions made) and was selected significantly more frequently than all other VIs, except for nREP, which ranked second. LCI, nSIPI, nWC and narrowband normalized difference lignin index (nNDLI) outperformed NDVI, nGNDVI, nNDVI, GNDVI, PRI, nNPCI and nNPQI significantly. Medium to low importance (between 6% and 4%) was found for nNDNI, nLCI, NDVI, nGNDVI, nNDVI and GNDVI. These VIs have been of significantly higher importance than nNPCI and nNPQI. During the second growth, the differences in importance between the VIs were lower than in the first growth. However, similar VIs influenced the classification the strongest: nREP, nWI, LCI, nSIPI and nWC were of significantly higher importance than nLCI, nNDVI, GNDVI, NDVI, nPRI and nNPQI. Of medium to low importance were nNDNI, nNPCI, nGNDVI, nNDLI, nLCI, nNDVI, GNDVI and NDVI. nNPQI and nPRI were of significantly lower importance (2.9% and 3.5%, respectively) than all other VIs.
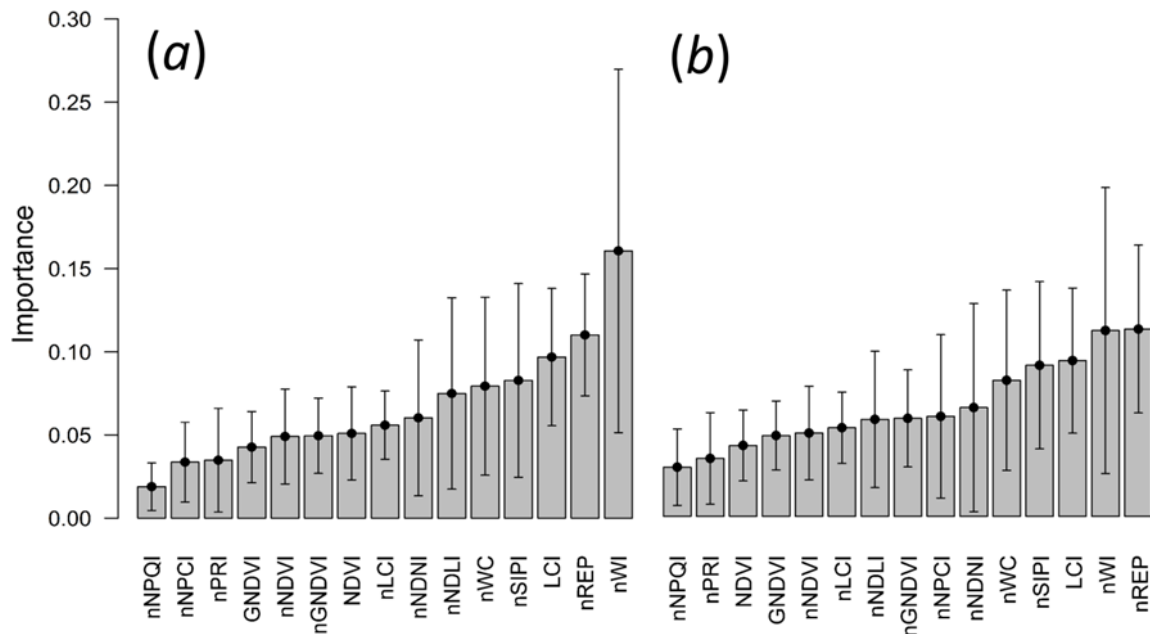
Figure 2-5. Overall importance of the VIs in the random forests classification for growth one (a) and growth two (b). The error bars indicate the standard deviation in overall importance calculated from the importance derived for the single T∑s.

Figure 2-6 shows the variations in importance of nREP, LCI, NDVI, nWI and nWC throughout the growing season. At the beginning of growth one, nREP was most important for the classification. However, at T∑s above 400 °C d, the importance of all biomass and chlorophyll-related VIs (nREP, LCI and NDVI) decreased, whereas the importance of the water-related VIs (nWI and nWC) increased. Thus, at T∑s larger than 600 °C d, nWI was of the highest importance, followed by nWC or nREP. After a T∑ of 900 °C d was reached, the importance of nWI and nWC decreased. Consequently, the classification was more influenced by chlorophyll-related VIs (particularly LCI and nREP) at T∑s larger than 1150 °C d. During the entire first growth, NDVI was among the VIs with the lowest importance.

At the onset of the second growth, nREP was the most important VI. However, over time, the importance of LCI and nWI increased and exceeded nREP at T∑s larger than 650 °C d. Similar to nWI, nWC increased in importance at the beginning of the second growth, but did not reach the high levels of nREP, LCI and nWI. At T∑s larger than 950 °C d, the importance of nWI decreased. Thus, during the remaining period of growth two, LCI or nREP featured the highest importance. Similar to growth one, NDVI had a minor impact on the classifications throughout the entire growth.
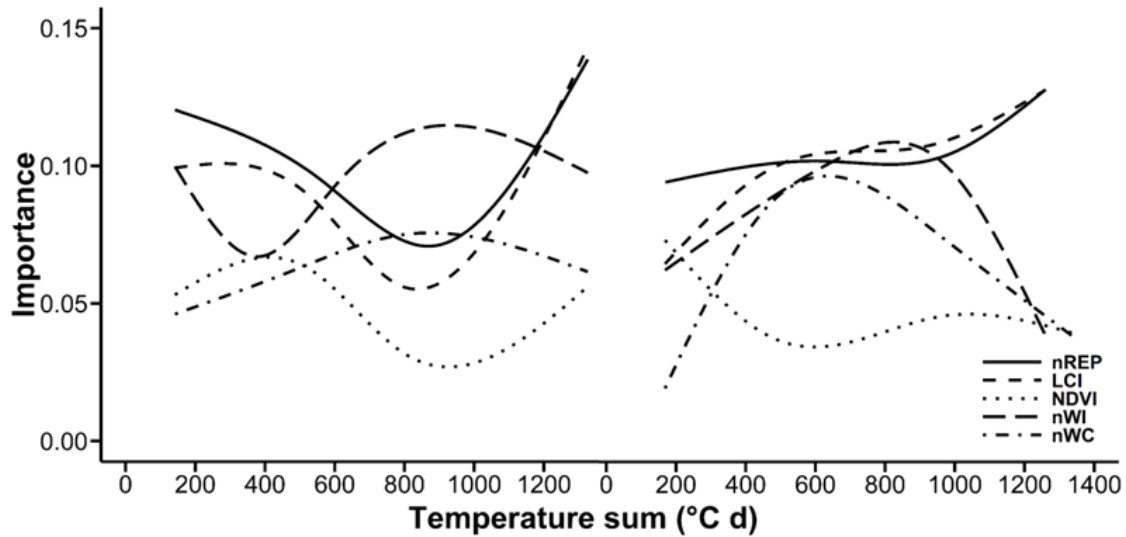
Figure 2-6. Importance of nREP, LCI, NDVI, nWI and nWC in growth one and growth two.

2.4 Discussion

2.4.1 Critical reflection on the experimental settings

In this work, the performance of 15 different VIs for distinguishing five differently-fertilized grassland communities (Ca, CaN, CaNP, CaNPKCl and CaNPK$_2$SO$_4$) was tested. Constant fertilization lead to a characteristic plant species composition in each plot, which differed between treatments and changed only marginally between years (Hejcman et al., 2007). Similarly, biomass production varied between the plots; the lowest biomass was produced in the Ca treatment, followed by CaN, CaNP and the NPK treatments (Hejcman et al., 2010b; Schellberg et al., 1999).

Because observations were made in three years, it was assured that annual fluctuations in precipitation or radiation were captured in the dataset. This setup, as well as the utilization of T$\sum$ as the temporal variable secured that no climatic or management factors influenced the species composition and the biomass development. Minor disturbances such as lodging of plants (especially at the end of the first growth in the NPK-treated plots) and the naturally-occurring variability of the plant canopies was diminished by acquiring measurements at three different locations within each plot. Stagakis et al., (2010) identified significant effects of the sensor viewing angle and the sensor height on the spectral reflectance measured over plant communities. In this study, the utilization of the crane system allowed systematic measurements from a 2-m height and nadir position, which widely eliminated these effects. Changing cloud cover (Gamon et al., 2006; Roelofsen et al., 2013), as well as changes in solar elevation angle (Stagakis et al., 2010) are often considered as additional confounding factors of the spectral

39

measurements. Diurnal changes in solar elevation were adapted by acquiring spectra between 10:00 a.m. and 4:00 p.m. and averaging this information for an entire day. Visual inspection of VI values recorded on the single days revealed that they were relatively stable. Furthermore, acquiring data in a large interval in time covered the daily occurring variance in spectral signal and further stabilized VI values. However, seasonal changes in solar elevation may have altered the irradiation conditions. However, we assume that these effects were minimized by utilizing VIs because their use significantly lowers the impact of illumination conditions and cloud cover (Jensen, 2007). Additionally, frequent measurements of the white reference panel ensured that reflectance was adapted for changes in solar irradiance.

2.4.2   Seasonal curves of the vegetation indices

Based on multitemporal measurements of five different VIs (nREP, LCI, NDVI, nWI and nWC) sensitive to different biophysical parameters, differences in the VI development over time were investigated. Comparing both growths, similar developments were observed. However, lower maxima of positively-developing VIs (nREP, LCI, NDVI and nWI), as well as higher minima for negatively-developing VIs (nWC) were observed in growth two. The reason behind this is that growth rates were lower in the second growth, resulting in lower intensities of green vegetation reflectance and lower amounts of water stored in plants. As observed by other scientists (Psomas et al., 2005; Rossini et al., 2012), VIs followed strong seasonal dynamics throughout the growing season. In the NPK-fertilized plots, VIs related to biomass, as well as to chlorophyll and water content, such as nREP, LCI, NDVI and nWI, passed through a rapid increase at the beginning of both growths. At later stages, nREP, LCI and NDVI decreased as a result of starting senescence in the NPK-treated plots. This was supported by Asner, (1998), who found significant effects of senescent grass components on the NIR reflectance, which has been used for the calculation of these VIs. In contrast, nWI remained at a high level for a longer time, indicating that water content remained stable at the onset of senescence. At the time, NP(K) fertilized plots started senescing, all four VIs in the Ca and CaN plots increased because these plots host slow-growing species (Chytrý et al., 2009; Hejcman et al., 2007). Such species not only increase in their biomass over a longer time-span, but also remain relatively constant in their water and chlorophyll content. nWC developed contrary to the four other VIs due to its negative response to water content.

2.4.3 <u>Testing the classification accuracy of the fifteen vegetation indices using the Welch test</u>

To test the ability of every single VI for distinguishing the five different vegetation communities, a Welch test was performed for each $T\sum$. The average of the Welch tests' results allowed an estimation of the overall classification accuracy of each VI in the individual growths. It was shown that classification performance of all VIs (except nNPQI) was lower in growth two than in growth one. The explanation for this is that VI curves in the second growth featured lower amplitudes and were less distinct from each other. These relatively low amplitudes were caused by a lower and more similar sward height and biomass production in growth two (Table A 2).

At the beginning of both growths, classification accuracies were relatively low. We assume that this was caused by small differences in canopy biomass occurring at this stage. This is supported by measurements of Compressed Sward Height (CSH), which are highly correlated to canopy biomass (Harmoney et al., 1997). CSH featured a standard deviation between the five communities of 2.93 cm in the initial stage (464 °C d, 2014) and 18.21 cm in the final stage (464 °C d, 2014) of growth one (Table A 2). Similarly, a standard deviation of 1.18 cm was shown at the beginning (210 °C d, 2014) and 4.57 cm at the end (1353 °C d, 2014) of growth two (Table A 2). Furthermore, it is likely that subtle differences in the reflectance of the plant canopies in the early stages of both growths have been concealed by the influence of soil on the reflectance signal (Numata et al., 2008). At later stages of the two growths, biomass increased steadily, which mitigated the contribution of soils to the spectral reflectance (Norman et al., 1985; Schut et al., 2002). Combined with increasing differences in biomass occurring between the different fertilizer treatments, an increase in the classification accuracies was achieved. However, as soon as biomass production in the NPK-treated plots languished, classification accuracies dropped, as canopies were optically more similar.

Due to the onset of senescence in the NPK-treated plots, on the one hand, and the constant abundance of green biomass in the Ca and CaN plots, on the other hand, classification rates at the ends of both growths increased. This contradicts with results published by Fava et al., (2009), who stated that the senescence of vegetation lowers the differences between VIs. We assume that the postponed onset of senescence in the Ca and CaN plots led to increased classification accuracies in this study. This is supported by Sánchez-Azofeifa et al., (2009), who demonstrated that the ability to distinguish plant types based on spectral information is strongly dependent on their phenological stage.

During the first growth, the most successful separation in this experiment was achieved using nWC and nWI, which are known to respond to plant water content. The high overall classification rates of nWI and nWC were caused by the relatively stable classification accuracy in the middle of the growth. This stability was caused by differences in water holding capacity of the canopies because canopies featuring low biomass production (Ca and CaN treatments) desiccate earlier after rain events than the canopies of highly productive communities (NPK treatments). VIs coined for detecting changes in biomass, such as NDVI as well as nNDVI, GNDVI and nGNDVI, achieved lower classification accuracies. The reason for the poor performance of these VIs is the strongly decreasing classification accuracy in the middle of the growths. An explanation for this decrease in classification accuracy are the saturation effects of these VIs, which were observed under high LAIs (Cho et al., 2007; Lorenzen and Jensen, 1988; Wang et al., 2005). Interestingly, LCI, which is related to chlorophyll content, was less affected by saturation in the middle of the growth and seems to be more suitable for mapping grasslands featuring high LAIs than the previously-mentioned VIs. In the final stage of growth one, the classification accuracies of nREP and LCI increased and reached the accuracy level of nWI and nWC. This behavior is explained by the good performance of these VIs for distinguishing the senescing NPK treatments from the Ca and CaN treatments. nNPQI (related to phaeophytization), nPRI (indicating plant vitality) and nNPCI (related to chlorophyll content) achieved the lowest accuracies.

During the second growth, the highest classification accuracies were achieved by LCI, followed by nWI and nREP, which confirms the strong performances of these VIs, which was already found in growth one. The relatively good performances of LCI and nREP compared to the water content-related VIs in growth two leads to the assumption that the lower LAIs support the utilization of chlorophyll- or biomass-related VIs. Again, our results indicate that nNPQI, nPRI and nNPCI, as well as the nGNDVI, nNDVI, NDVI and GNDVI are not well-suited for classifying the studied grassland communities. Finally, nWI and nSIPI, provided high classification accuracies for both growths, which suggests that these VIs are relatively stable for the classification of grasslands along nutrient gradients.

No clear result was obtained whether broadband or narrowband VIs provide the highest accuracies for classifying the studied grassland communities. In growth one, broadband NDVI and GNDVI outperformed the narrowband versions, whereas in growth two, the narrowband versions provided higher classification accuracies. These results contradict the findings made by Thenkabail et al., (2004b), who found an increased classification accuracy using exclusively

narrowbands to separate weeds, shrubs, crops and grasses in Africa compared to a classification using exclusively broadbands. This suggests that the selection of broadband or narrowband VIs for achieving optimal classification is also dependent upon the timing of spectral data acquisition.

2.4.4 Random forests classification

We applied a random forests classification to investigate how much the inclusion of all 15 VIs improved the classification of the five plots compared to single VIs. Our results show that classification accuracy increased by 4% in growth one and 12% in growth two in comparison to the strongest VI using the Welch test. Furthermore, the classification accuracy achieved by random forests was more stable (remaining always above 82%) than the best performing VIs identified using the Welch test. In growth one, classification rates varied marginally over time, whereas OOB errors in growth two fluctuated between 2.5% and 17.5%. These variations in growth two and the resulting lower overall accuracy were most likely caused by larger influences of soil reflectance on the signal (Schut et al., 2002) at the beginning of growth two, as well as by smaller differences in between the plots' canopy biomass in the green-up phase (Table A 2). The increasing classification accuracy at the end of growth two was caused by the onset of senescence in the NPK-treated plots, whereas the other plots remained stable in their amount of green leaf area (Idso et al., 1980).

Variable importance indicates the frequency a VI is selected inside a random forest. In growth one, nWI was the most important VI, followed by nREP and LCI. Our results show that other VIs, such as nSIPI, nNDLI, nNDNI and nLCI, carry additional important information for improving the classification. Interestingly, other biomass-related VIs (i.e., NDVI, nGNDVI, nNDVI and GNDVI), as well as water-related VIs (i.e., nWC) were of relatively low importance compared to the Welch test. We assume that nWI as a water-related VI, as well as nREP and LCI as chlorophyll-related VIs carried similar information and lead to the low importance of these VIs. Of minor importance were nPRI, nNPCI and nNPQI, which indicates that these VIs marginally support the classification. In the second growth, the ranking in importance of the VIs was similar, but the weight of the VIs was more evenly distributed. This even distribution supports the assumption that especially if classification accuracy was low using single VIs, the addition of VIs sensitive to other biophysical variables increased the classification accuracy. Therefore, nREP as the most important VI was closely followed by nWI, LCI, nSIPI and nNDNI. As biomass-related VIs were less influenced by the high LAIs in growth two, nGNDVI

and nNPCI increased in importance compared to growth one. As these two VIs included similar information as nNDVI, GNDVI and NDVI, the latter VIs were of lower importance. As observed in the first growth, nPRI and nNPQI were rarely selected by random forests.

Using nREP, LCI, NDVI, nWI and nWC, the importance of the VIs under changing T$\sum$s was investigated. In growth one, the results of variable importance widely confirmed our findings made using the Welch test. It was shown that the importance of water-related VIs was relatively stable at times when biomass- and chlorophyll-related VIs saturated due to high LAIs of the grass canopies (Cho et al., 2007; Lorenzen and Jensen, 1988; Wang et al., 2005). NDVI was of low importance throughout the entire first growth, which confirms its low classification accuracy identified using the Welch test. Throughout the entire second growth, the chlorophyll-related VIs, nREP and LCI, were relatively stable in their importance. However, nWI and nWC added valuable information especially at T$\sum$s between 400 and 1000 °C d, indicating that these VIs are particularly important when LAIs in the canopies are high and obscure differences in biomass or chlorophyll content. Again, NDVI was of minor importance.

2.5 Conclusions

This study presents an approach for classifying grassland communities along a gradient from intensive to extensive fertilizer management in a two-cut-system using a set of 15 remotely-sensed VIs. It was shown that VIs are useful to identify differences between the grassland communities at different times throughout a growing season. Each VI featured characteristic fluctuations over time in the individual plots. It is well documented for this particular experiment that plots differ significantly in their biophysical properties, such as biomass production, LAI and chlorophyll content. Hence, we conclude that the tested VIs were sensitive to these properties.

The different time courses of VI development have far-reaching consequences for the use and interpretation of VIs when classifying grassland. None of the VIs was able to feature constantly high classification accuracies throughout the entire growing season. However, while classification accuracies of VIs sensitive to one biophysical variable decreased, the accuracies of other VIs remained more stable allowing higher classification accuracies. Biomass- or chlorophyll-related VIs, such as nREP, NDVI or LCI, provided good results when plants had further developed in the intensively-managed plots than in the extensively-managed plots. However, at later stages when the extensively-managed plots caught up in development, water content-related VIs, such as nWI or nWC, were the better alternative for a classification because

biomass-related VIs were affected by saturation effects. Further, classification in the second growth was more difficult than in the first growth, due to less distinct differences in biophysical characteristics in between the plant communities. Thereby, the classification performed particularly weak when slow-growing canopies had fully developed and fast-growing canopies had not yet entered senescence. At this stage, nWI and nWC did not reach the high classification accuracies of growth one, so that none of the VIs separated the communities reliably.

This problem was solved by applying all 15 VIs in the random forests algorithm. A time series of random forest models using the best VIs for classifying the plant communities was created. As spectral information in this procedure was used more effectively, classification accuracies increased in both growths, but most considerably in the second growth. Furthermore, our multitemporal analysis has shown that classification accuracies using this approach remained relatively stable throughout the entire first growth. Although classification rates in the second growth varied to some degree, significant improvements were made compared to the utilization of single VIs. These results suggest that the selection of an appropriate VI (depending on the plant development) is essential for classifying grasslands using single VIs. However, an alternative using random forests was promising, because it yielded a more robust grassland classification.

The utilization of this multi-VI approach for grassland mapping at larger spatial extent could improve the separation of designated plant communities in respect to their floristic composition and plant properties. Future research should be guided towards testing random forests classifiers using VIs for grassland mapping with aerial or satellite imagery for other grassland communities featuring higher or lower temporal variability in biomass production and spectral reflectance. Results of such studies may significantly improve existing monitoring techniques (e.g., using single VIs), allow a more detailed grassland mapping and contribute to a sustainable management of grassland ecosystems.

3   Can we detect grassland plant functional traits based on canopy reflectance?

Abstract

This study presents an approach to detect variations in FTs of different grassland communities under field conditions using hyperspectral reflectance measurements. FTs are phenological, morphological or physiological properties of plants, which are measured on the single individual. In order to assess the response of grassland communities to changes in management or environmental conditions, ecologists measure the FTs of grasslands using destructive sampling techniques in time-consuming and expensive field surveys. Hyperspectral RS may offer an efficient alternative to these approaches.

The presented study was conducted in a long-term fertilization trial (since 1941), in which different levels of fertilization from limed only to full NPK-fertilization were applied. In the five different investigated treatments, grassland communities differing considerably in their FTs have developed. Spectral data and plant samples were collected from these communities throughout the growing seasons of 2012-2014. Subsequently, the strengths of the relations between spectral data and 23 different FTs were tested using PLSR. The accuracy (R^2_{val}) for detecting the FTs ranged between 0.1 and 0.8. PH, $fPAR_{abs}$, C/N-ratio, TFM, N-content, CSH, SPAD, NDF-content and LA were estimated with $R^2_{val} \geq 0.6$. Models for PFM, LFM, LDM and LDMC reached moderate accuracies ($0.4 \leq R^2_{val} < 0.6$). $R^2_{val} < 0.4$ (i.e. low accuracies) were calculated for TDMC, PDMC, PDM, TDM, PWC, TWC, LWC, C-content, L-S-ratio and SLA. These results show that 13 of the 23 FTs can be detected with moderate or high accuracy from hyperspectral reflectance data. This underlines the potential of RS to support ecologists in assessing the response of grassland communities to changes in management regime and climate.

3.1   Introduction

Grasslands cover the largest share among all agriculturally used areas in Europe, represent a major source of forage for livestock and are thus of particular importance for the production of meat and milk (Eurostat (ed.), 2017; O`Mara, 2012; Price et al., 2001). Furthermore, grasslands are home to a large number of endemic species (Hopkins and Holz, 2006). However, non-adjusted management of grassland ecosystems may have negative impacts on the environment. These include the pollution of water bodies due to an inaccurate fertilizer application, the emission of greenhouse gasses into the atmosphere, the reduction of plant species diversity and the enhancement of soil erosion due to overgrazing (Bai et al., 2001; Pimentel, 2006; Tilman et al., 2002; Velthof and Oenema, 1995). Thus, grassland science is looking for methods, which

support land managers in enabling a cost-effective and sustainable milk and meat production and, at the same time, help to conserve these ecosystems. To understand the response of grassland communities to management actions, ecologists monitor the vegetation's phenological, morphological, biochemical or physiological properties, referred to as FTs. FTs are usually measured for individual plants, can be up-scaled to the canopy (community traits) and be used comparatively across species (Violle et al., 2007). Thus, FTs help us understanding how single plants or entire grassland ecosystems respond to changes in the environmental conditions and management (Díaz et al., 2004; Kleyer et al., 2008; Lavorel and Garnier, 2002).

This study investigates exclusively numerical FTs, which are measured as continuous variables (e.g. plant height, leaf area, biomass, etc.). The response of these FTs to differences in nutrient supply has previously been extensively studied (Al Haj Khaled et al., 2005; Cruz et al., 2002; Duru et al., 2004; Pontes et al., 2010). It was shown that nutrient supply has a large impact on the expressions of FTs and that they vary over time (Al Haj Khaled et al., 2005; Schellberg and Pontes, 2012). Consequently, FTs can be used as indicators for successional changes of grasslands in response to management actions or changes in climate (Cousins et al., 2003; Kahmen et al., 2002).

Currently, data on FTs is obtained by field surveys, which are referenced only to a certain point in time and require destructive as well as time-consuming and costly sampling methods (Cornelissen et al., 2003; Homolová et al., 2013). RS has the potential to complement, extend or even replace these manual measurements of many FTs, providing spatially contiguous data of large areas at a high temporal resolution and at low costs (Homolová et al., 2013). Thus, RS may provide an efficient solution to map and monitor FTs.

Historically, the application of satellite RS to detect FTs was limited by the low spectral resolution of sensors (Schaepman et al., 2009). However, the development of satellite-borne hyperspectral sensors, such as Hyperion (operated between 2001 and 2017), HISUI (launch planned in 2017), EnM (launch planned in 2019) and HyspIRI (launch planned around 2022) has opened new perspectives for satellite RS of FTs. Thus, Ustin and Gamon, (2010) stated in their review that many FTs sensitive to nutrient gradients may be detected by hyperspectral RS measurements. Thereby, the main challenge is to relate the spectral reflectance in particular bands of the electromagnetic spectrum to FTs, which are of importance for ecologists to assess ecosystem function (Schaepman et al., 2009).

Many studies have shown that plant morphology, plant phenological status and species composition are related to the spectral reflectance of vegetation (Danson et al., 1992; Goel,

1988; Myneni et al., 1989; Psomas et al., 2005; Sánchez-Azofeifa et al., 2009; Schmidt et al., 2004; Verrelst et al., 2009). Furthermore, several functionally important compounds such as pigments, water content and canopy N-content can be detected using RS (Feret et al., 2008; Fuentes et al., 2001; Gitelson et al., 2005; Inoue and Penuelas, 2001; Serrano et al., 2000; Sims and Gamon, 2002; Trombetti et al., 2008; Zhang et al., 2013). To obtain insights into which spectral regions are valuable to detect specific FTs and to enable optimal sensor designs, ground-based field spectrometry has proven to be indispensable (Houborg et al., 2015). These systems were successfully used to collect RS data with a high spectral resolution and a broad spectral range and link these measurements to chemical, morphological and structural properties of grassland vegetation (Asner, 1998; Ferner et al., 2015; Kumar et al., 2001).

Up to date, no study has tested RS technology to detect the FTs of mixed grasslands along a fertilizer gradient during all phenological stages of vegetation development over several years. However, differences in phenology and vegetation composition (as induced by nutrient supply) significantly affect the spectrum-trait-relations and represent a substantial complication for utilizing RS in studies of FT detection (Houborg et al., 2015). Developing a method for estimating FTs using spectral reflectance measurements, which is stable for the phenological development and the floristic composition of grasslands, will allow a systematic monitoring of grassland ecosystems using RS. Such information will provide data for ecologists to adapt management strategies throughout the entire growing season and support an adjusted fertilization as well as an ecologically and economically sustainable use of grasslands.

The objective of this study was to examine the overall capability of hyperspectral RS for estimating different FTs of species-rich grassland communities. For this purpose, we aimed to (1) identify the response of the spectral reflectance to differences in FT expressions of grassland communities as induced by nutrient status, (2) calibrate and validate models for estimating these FTs based on their spectral reflectance and (3) test these relations over several growing seasons and years.

Therefore, we collected data on numerical FTs and measured the spectral signatures of grassland vegetation during three growing seasons. All FTs were related to reflectance using statistical modelling techniques such as PLSR. Finally, FTs detectable by RS measurements as well as the most important spectral regions for estimating these FTs were identified.

3.2 Materials and methods

3.2.1 Study area

The RGE has been selected as study site. It exists since 1941 and is located in the Eifel Mountains (Rhineland-Palatinate, Germany, 50°13`N, 6°51`E) at an elevation of 475 m. The site features a temperate, maritime climate with a mean annual precipitation of 811 mm and a mean annual temperature of 6.9 °C (RGE Meteorological Station). In 1941, the formerly wet heathland site has been grubbed and a mixture of grasses and herbs was sown thereafter. The experiment was established in a randomized block design and consists of 55 plots. This study was conducted on a subset of five plots, i.e. a series of the five fertilizer treatments next to each other as shown in Figure 3-1. The limitation of the experiment to five plots was necessary due to the high demand of labor for processing plant samples. However, previous experiments have shown that FTs within the same treatment do not significantly vary (data not shown). Since 1941, five different fertilizers have been applied annually in these 15 m² plots arranged along a transect of 26 m in length (Figure 3-1)**.** Yearly cutting of grass swards was performed in early July and in late October. All other management factors were held constant.
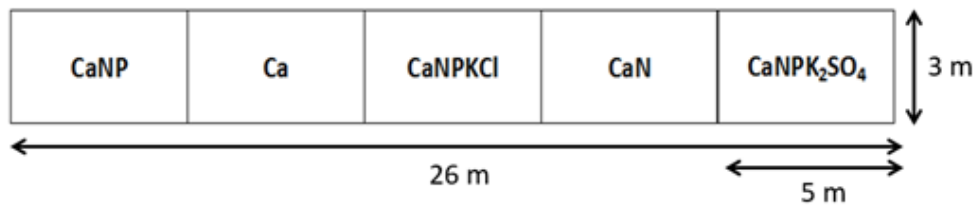
Figure 3-1. Setup of the five fertilizer treatments used in this study: lime as calcium oxide (Ca), lime and nitrogen (CaN), lime, nitrogen and phosphorus (CaNP) and lime, nitrogen, phosphorus and potassium (CaNPKCl and CaNPK$_2$SO$_4$).

The long-term application of different fertilizers has led to changes in the soil nutrient contents of the treatments, including P (significantly higher in P treated plots) and K (significantly higher in NPK-treated plots), while N- and C-contents were similar in all plots (Hejcman et al., 2010b). The differences in soil nutrient content have caused significant shifts in the floristic compositions of the plant communities (Chytrý et al., 2009; Hejcman et al., 2007, 2010a). Today's plant communities are stable between years but vary from montane meadows of *Geranio-Trisetetum* (*Polygono-Trisetion* alliance) in the Ca and CaN treatments, transitional types between *Poo-Trisetetum* and *Arrhenateretum* (both from the *Arrhenatherion* alliance) in the CaNP treatment to mesotrophic *Arrhenateretum* meadows in the CaNPKCl and the CaNPK$_2$SO$_4$ treatments (Chytrý et al., 2009). These differences in floristic composition in interaction with differences in the nutrient management between plots have caused a gradient

49

of dry matter production, with the Ca treatment having the lowest dry matter production, followed by CaN, CaNP and both NPK treatments (Schellberg et al., 1999). Differences in the floristic composition and dry matter production have far-reaching impacts on the expressions of FTs within the plant communities, which are expected to be strong enough to cause significant alterations in the spectral reflectance signals

3.2.2 Spectral measurements

We selected a FS 3 spectroradiometer (Analytical Spectral Devices Inc., Boulder, CO, USA) for measuring spectral reflectance. This instrument was used successfully in a previous study for linking FTs to reflectance (Roelofsen et al., 2013) and provides the opportunity to collect spectral data at a high temporal resolution. The instrument covers a spectral range between 350 and 2500 nm with a resolution of 3 nm FWHM at a wavelength of 700 nm and 10 nm FWHM at wavelengths of 1400 and 2100 nm (ASD Inc. (ed.), 2010). The sampling interval is 1.4 nm between 350 and 1000 nm and 2 nm between 1000 and 2500 nm. All bands are interpolated to 1 nm steps leading to in total 2150 spectral bands (ASD Inc. (ed.), 2010).

To prevent confounding effects caused by differences in observation height and angle, as well as to ensure that spectral measurements are repeatedly taken at the same position, the spectroradiometer was mounted aboard a motor-driven vehicle equipped with a light barrier (Figure 3-2 a; cf. Gebhardt et al., 2006). This vehicle was operated on a 30 m rail-track along the five plots. The sensor-head was affixed at the end of a boom to measure canopy radiance at nadir position at 2 m height above ground, which yields a FOV of 0.64 m² (Figure 3-2 b). Plots were measured in three single subplots (a, b, c) to account for plot-internal variability.

Data were recorded on sunny days (to minimize influences of clouds and atmospheric water vapor) in approximately biweekly intervals in both growths during the growing seasons 2012-2014. This resulted in a total of 29 days of spectral measurements (Table 3-1), which was sufficient for detecting major changes in vegetation development and variations in FTs. On each measurement day, 12 to 39 single measurements within each plot were recorded between 10 am and 4 pm. Spectral reflectance was calculated using the collected radiance of the dark current (collected approx. every 15 minutes), the white reference (collected for each plot) as well as the radiance of the plant canopies. White reference radiance was acquired at 30 cm above a Spectralon® zenith polymer target (95% reflectance; Labsphere Inc., North Hutton, NH, USA).

Table 3-1. Number of days, on which spectra, FTs, fraction of photosynthetically active radiation absorbed (fPARabs) and compressed sward height (CSH) were sampled per growth.

Year	Growth	Spectra	FTs	fPAR$_{abs}$	CSH
2012	1	4	4	4	
2012	2	5	4	5	
2013	1	4	4	3	1
2013	2	4	4	3	2
2014	1	6	6	6	6
2014	2	6	6	6	5
total	1, 2	29	28	27	14

To enhance spectral information, splice correction (Stevens and Ramirez-Lopez, 2013) at 1000 and 1800 nm (filter size=25 bands) and a smoothing filter using second order polynomial transformation (Savitzky and Golay, 1964) with a filter size of 31 bands between 350 and 1350 nm, 51 bands between 1350 and 1800 nm and 101 bands between 1800 and 2500 nm were applied. After preprocessing, spectra were averaged for each day and plot (reducing 2689 single measurements to 189 averaged spectra) to account for small-scale variations in grass canopies and for bidirectional reflectance effects. Since the sensitivity of hyperspectral reflectance towards variations in FTs can be further enhanced using spectral transformations (Knox et al., 2011; Schlerf et al., 2010), such as continuum removal (Mutanga et al., 2004; Schmidt and Skidmore, 2003) and derivative spectra (Ferner et al., 2015; Roelofsen et al., 2013; Rollin and Milton, 1998), we tested these preprocessing techniques using the continuum removal function (Stevens and Ramirez-Lopez, 2013) and the *diff()* function in R statistical software (R Development Core Team, 2015).
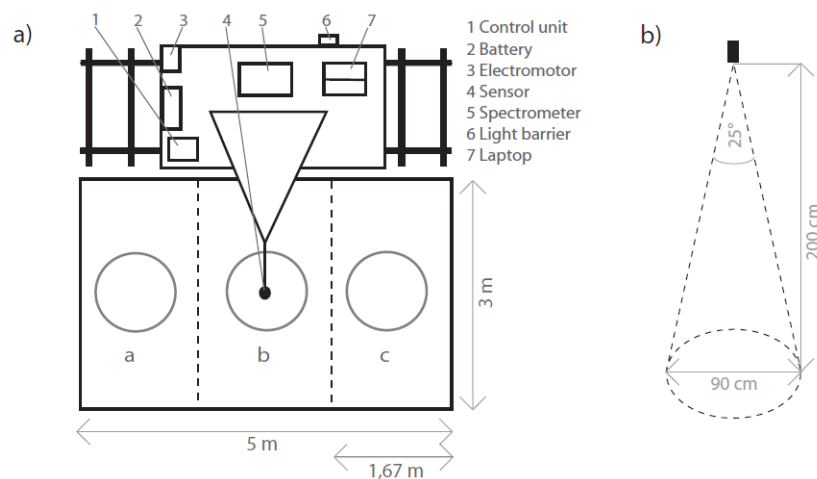
Figure 3-2. a) Setup of the measuring system and one plot with respective subplots (a, b, c). b) Viewing geometry (angle of view, field of view and height) of the sensor.

3.2.3 Manual measurements of plant functional traits

FTs (Table 3-2) were recorded on 28 days throughout the growing seasons 2012-2014 (cf. Table 3-1) on the same (± one) day of spectral data acquisition to ensure that canopies were measured at the same development stage. In each subplot (cf. Figure 3-2 a, 5 m²), ten individual plants were randomly selected taxon-free for subsequent analysis in the laboratory. In preliminary tests, a sample size of ten plants per subplot (i.e. 30 per plot) has shown to be sufficient to cover the heterogeneity within plots and provide a stable mean.

Table 3-2. FTs acquired based on manual measurements, including definition, unit, and measuring instrument (I= incoming solar radiation below ($_s$) and above ($_i$) canopy).

FT	Definition	Unit	Instrument	Formula
PH	Plant height	cm	yardstick	-
SPAD	SPAD value	-	SPAD meter (Minolta 502, Marunouchi, Japan)	-
LA	Overall area of plant leaves	cm²	Scanner (Epson Expression 1100, Suwa, Japan)	-
PWC	Plant water content	%	-	((PFM-PDM)/PFM)*100
TWC	Tiller water content	%	-	((TFM-TDM)/TFM)*100
LWC	Leaf water content	%	-	((LFM-LDM)/LFM)*100
SLA	Specific leaf area	cm² g^{-1}	-	LA/LDM
PDMC	Plant dry matter content	%	-	PDM/PFM*100
TDMC	Tiller dry matter content	%	-	TDM/TFM*100
LDMC	Leaf dry matter content	%	-	LDM/LFM*100
LS	Leaf-tiller ratio	-	-	LDM/SDM
PFM	Plant fresh matter	%	Scale (Sartorius BP 110 S, Göttingen, Germany)	-
TFM	Tiller fresh matter	g	-	PFM-LFM
LFM	Leaf fresh matter	g	Scale (Sartorius BP 110 S, Göttingen, Germany)	-
PDM	Plant dry matter	g	Scale (Sartorius BP 110 S, Göttingen, Germany)	-
TDM	Tiller dry matter	g	-	PDM-LDM
LDM	Leaf dry matter	g	Scale (Sartorius BP 110 S, Göttingen, Germany)	-
N	N (g) per g dry matter	%	Elemental analyzer (Euro EA 3000, Redavalle, Italy)	-
C	C (g) per g dry matter	%	Elemental analyzer (Euro EA 3000, Redavalle, Italy)	-
C/N	C (g) per N (g)	-	-	C/N
NDF	Fiber content per unit dry matter	%	Scale (Sartorius BP 110 S, Göttingen, Germany)	-
CSH	Compressed sward height	cm	Rising plate meter	-
fPAR$_{abs}$	Fraction of photosynthetically active radiation absorbed	µmol s^{-1} m^{-2}	Ceptometer (Delta-T Devices Sun Scan SS1, Cambridge, UK)	I_s/I_i

Sampling of plants was conducted in the entire plots (not solely in the spectroradiometer FOV) to maintain plant density within the plots. Furthermore, we assumed that FT values are

relatively homogenous throughout the entire vertical dimension of the plant canopy and that even lowermost layers of vegetation influence the spectral signal due to persistent gaps in the upper canopy layers (cf. Roelofsen et al., 2013). Thus, it was decided to extract complete plants for subsequent analysis.

In the laboratory, PH, SPAD, LA, PFM, TFM, LFM, PDM, TDM and LDM were measured. Subsequently, the remaining FTs were calculated according to the formulas given in Table 3-2. To estimate dry matter products, samples were dried for 48 hours at 60°C. For C-, N- and NDF-analysis, plants collected within each subplot were combined to one sample. Afterwards, the plant material was grinded for 120 seconds at a frequency of 30 tilts per second in a ball mill (Retsch MM 400, Haan, Germany). For analysis of C- and N- content, aliquots of 0.2 g $\pm$ 0.005 g were weighed, wrapped in zinc capsules (5 x 9 mm, IVA Analysetechnik GmbH & Co KG, Meerbusch, Germany) and analyzed in an elemental analyzer (Euro EA 3000, Redavalle, Italy). NDF analysis was performed using the grinded plant material according to van Soest et al., (1991).

Ten measurements of CSH were taken within each plot using a rising plate meter (30 cm diameter, 238 g, pressure of 3.4 kg m^{-2}). To estimate fPAR$_{abs}$, ten measurements of incoming radiation above canopy and ten measurements at the bottom of the canopy were recorded using a Sun Scan SS1 ceptometer. To enable comparison with spectral data, the measurements of FTs taken at each date were averaged for each plot (later used to develop one model per FT for all plots, i.e. a general model) or subplot (later used to develop one model per FT for each single plot, i.e. a specific model), respectively. According to the mass-ratio hypothesis (Grime, 1998), up-scaling of plant properties to the community level is possible if sufficiently large sample sizes are acquired. This was given in this study, as preliminary tests have shown. To evaluate temporal variability of FTs on the plot level, coefficients of variation (CV) were calculated.

3.2.4   Relating plant functional traits to spectral reflectance

Among the statistical approaches for modelling single dependent variables based on a high number of independent variables, PLSR has been identified as an effective approach (Wold et al., 2001). First, this method is less prone to problems related to correlated predictor variables (multicollinearity) than multiple regression analysis or constraint ordination (Schmidtlein et al., 2012). Second, PLSR is able to summarize data effectively because it takes account of only those variations in predictors that are related to the target variable (Homolová et al., 2013). Third, it performs particularly well when the number of explanatory variables is large compared

to the number of observations (Wold et al., 2001). Thus, PLSR has been successfully applied to relate biophysical information (such as FTs) to hyperspectral datasets (Ferner et al., 2015; Hansen and Schjoerring, 2003; Ramoelo et al., 2013; Roelofsen et al., 2013; Schmidtlein et al., 2012).

PLSR was performed in *R* (R Development Core Team, 2015) using backward selection of predictors implemented in the *autopls* package (Schmidtlein et al., 2015). For mitigating effects of shadows and bidirectional reflectance, brightness normalization according to Feilhauer et al., (2010) was used. Logarithmic transformation was applied to PH, LA, PWC, TWC, TDMC, PFM, TFM, LFM, PDM, TDM, C/N-ratio, NDF-content and CSH to reach normal distribution of data. Afterwards, reflectance measured at wavelengths highly influenced by water absorption between 1336 and 1550 nm and 1776 and 1999 nm (Clevers et al., 2008; Curran, 1989) and regions distorted by sensor noise between 350 and 364 nm and 2361 and 2500 nm were excluded from further analysis, leaving 1557 bands.

The resulting spectral reflectance curves, its derivatives and the continuum removed spectra were tested individually as independent variables and the expressions of each single FT as dependent variables. Based on the independent variables, PLSR creates LVs comparable to principal components having a good representation of predictors as far as correlated to the dependent variable (Schmidtlein, 2005). It thereby reduces the dimensionality of spectral data by applying a linear transformation (Vinzi et al., 2010). Backward selection of bands was performed using the automated iterative search criterion with filters based on significance in jackknifing, thereby removing 25% of predictors per iteration. Further, important wavelengths for predicting the dependent variables were identified using weighted regression coefficients. Model validation was based on leave-one-out cross validation (LOO CV). Using LOO CV, N (total number of observations) iterative calibrations and validations of the model were performed, thereby retaining one observation in each iteration to validate the model.

3.3 Results

3.3.1 Manual measurements of plant functional traits

Among the 23 measured FTs, large differences were observed regarding their CV (Table 3-3). This variability documents changes in FTs, which occurred due to differences in plant development and species composition, which in turn were determined by the given levels in fertilization. Highly variable FTs (CV > 0.5) were PH, LA, LS, PFM, TFM, LFM, PDM, TDM, LDM and CSH. Moderate variability ($0.2 \leq CV \leq 0.5$) was observed for $fPAR_{abs}$, C/N-ratio, N-

content, TDMC, PDMC and SLA, whereas SPAD, NDF-content, LDMC, PWC, TWC, LWC and C-content were relatively stable (CV <0.2). Concerning the effect of fertilization on FTs, the largest variability over time was observed in the NPK fertilized plots, whereas the Ca- and CaN treatment featured lower variations in most of the FTs (data not shown).

Table 3-3. Mean, minimum (Min), maximum (Max), standard deviation (SD), coefficient of variation (CV) and number of observations (N) of FTs measured during the growing seasons 2012-2014.

	Mean	Min	Max	SD	CV	N
PH	34.95	6.89	101.11	23.13	0.66	138
SPAD	36.10	23.67	49.12	5.46	0.15	138
LA	17.67	1.51	89.52	14.30	0.81	139
PWC	0.72	0.39	0.93	0.12	0.16	126
TWC	0.70	0.48	0.92	0.09	0.13	126
LWC	0.65	0.26	0.78	0.10	0.15	136
SLA	204.19	59.80	619.39	90.29	0.44	137
PDMC	0.31	0.13	0.51	0.08	0.25	126
TDMC	0.31	0.14	0.52	0.07	0.24	126
LDMC	0.34	0.22	0.53	0.06	0.18	136
LS	0.93	0.16	2.37	0.55	0.60	126
PFM	0.73	0.12	2.86	0.57	0.78	138
TFM	0.53	0.05	2.64	0.54	1.03	138
LFM	0.20	0.03	0.85	0.13	0.67	138
PDM	0.19	0.03	0.75	0.14	0.73	126
TDM	0.12	0.01	0.68	0.11	0.98	126
LDM	0.07	0.01	0.25	0.04	0.67	137
N	1.65	0.75	3.32	0.55	0.33	134
C	44.80	41.36	47.04	0.99	0.02	134
C/N	30.65	13.35	59.25	10.23	0.33	134
NDF	0.55	0.39	0.73	0.07	0.13	134
CSH	11.65	2.30	28.11	7.16	0.61	69
$fPAR_{abs}$	0.73	0.05	1.00	0.27	0.37	130

3.3.2 Spectral reflectance of the different fertilizer treatments

In Figure 3-3, spectral signatures that were measured in 2014 are displayed. No data collected in 2012 and 2013 is presented in this illustration because it was observed that development in reflectance over time showed the same characteristics with only slight shifts due to variations in annual phenological development (data not shown). Spectral reflectance differed between the five grassland communities (Figure 3-3). At the beginning of both growths, Ca and CaN treatments featured low reflectance in the NIR region (750-1400 nm), whereas reflectance in the red region (620-720 nm) was relatively high. In the NP(K)-fertilized communities, the opposite was observed. With advancing time, red reflectance in the Ca and CaN treatments dropped and NIR reflectance increased. NIR reflectance peaked between 45% and 60% in the

NP(K) treatments and values between 40% and 50% in the Ca and CaN treatments. In the final stages of both growths, red reflectance in the NP(K) treated plots increased and NIR reflectance decreased, whereas these spectral regions remained stable in the Ca and CaN-plots. Relatively high reflectance in the near shortwave infrared (nSWIR; 1400-1800 nm) and far short wave infrared (fSWIR; 1800-2500 nm) was measured in the Ca and CaN treatment at the beginning of both growths. In these plots, SWIR reflectance dropped over time whereas it remained stable or even increased in the NP(K) treated plots.

Differences in reflectance between the two growths were observed in the initial growth stage. In the second growth, NIR reflectance increased more quickly than in growth one and reached its peak three to four weeks after cutting the grass (July 31). In contrast, in growth one an increasing NIR reflectance was observed for about six weeks after the onset of the growing season. More time elapsed after this peak in growth two, and so a distinctly larger drop in NIR reflectance in the NPK-fertilized plots was observed.
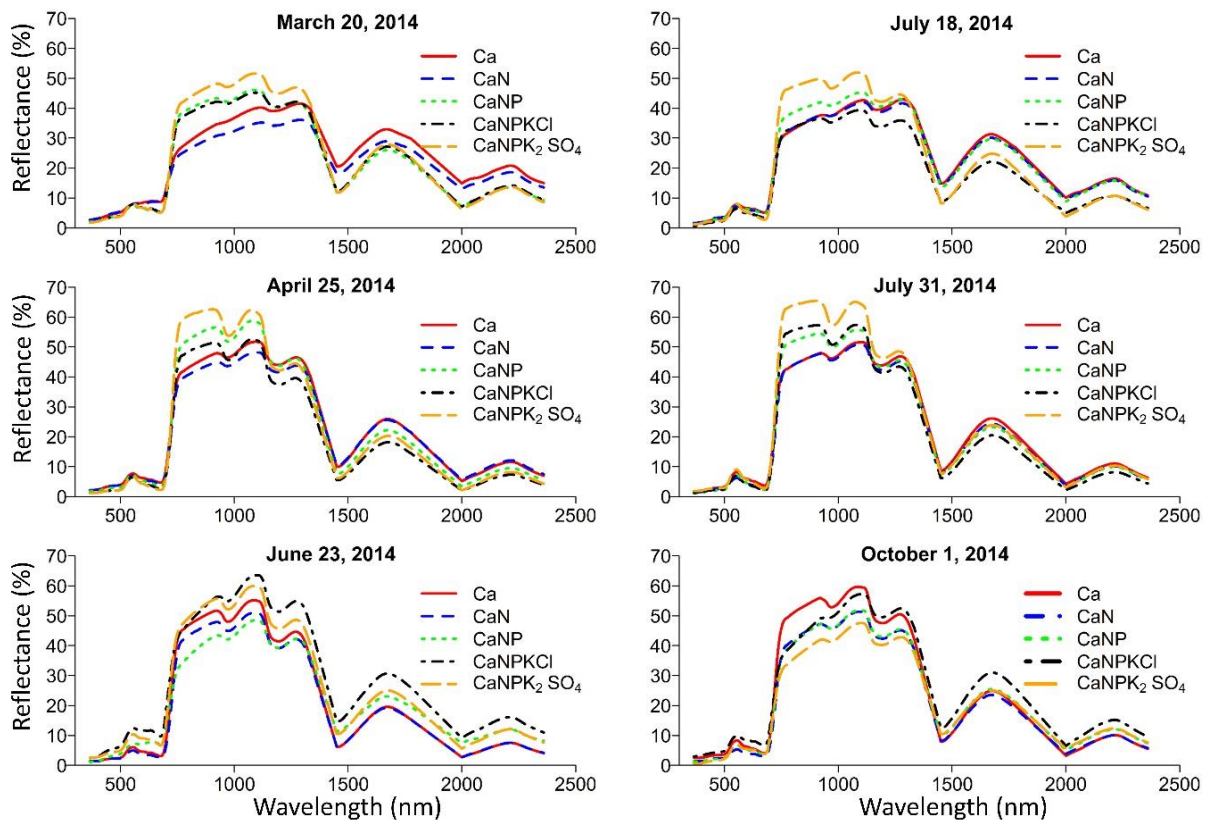
Figure 3-3. Spectral reflectance of grassland canopies in 2014 in growth one (left) and growth two (right).

3.3.3 Detecting plant functional traits using spectral reflectance measurements – model results

To test the relations between spectra and FTs, PLSR models for each FT were created for the raw, first derivation and continuum removed spectra using data collected from all treatments and years. The average R^2_{cal} and R^2_{val} show that the FTs were estimated with the highest accuracy using first derivation spectra, followed by raw spectra and continuum removed spectra (Table 3-4).

Table 3-4. Averaged model fits as R^2 in calibration (R^2_{cal}) and validation (R^2_{val}) using raw spectra, first derivation spectra and continuum removed spectra for predicting all 23 FTs.

Spectral preprocessing	R^2_{cal}	R^2_{val}
Raw spectra	0.50 [b]	0.42 [b]
first derivation	0.56 [a]	0.49 [a]
Continuum removal	0.40 [c]	0.35 [c]

[a, b, c] significantly different groups according to two-tailed t-test (n=23, p=0.05)

To test whether specific PLSR models (i.e. models stratified by plant community) outperform the general model (i.e. a model using data from all treatments), specific models were calculated using first derivation spectra. As sample sizes for the specific models were low, FTs and spectra were calculated for each subplot individually to ensure a more robust statistical analysis. Model accuracies of the specific models are shown in Table 3-5. The results indicate that no significant difference in the model accuracy between the specific models and the general model exists *(n=21, p=0.05, data not shown)*. Considering these findings, we decided to focus on general models created using first derivation spectra in the following parts of this study.

Table 3-5. Averaged model fits as R^2 in calibration (R^2_{cal}) and validation (R^2_{val}) for predicting all 23 FTs using first derivation spectra, calculated for every treatment individually (specific models).

Treatment/model type	R^2_{cal}	R^2_{val}
Ca	0.57	0.45
CaN	0.52	0.42
CaNP	0.58	0.49
CaNPKCl	0.57	0.49
CaNPK$_2$SO$_4$	0.55	0.46
Average fit (specific models)	0.56	0.46

Of the 23 models, 17 used data from the full range of wavelengths (VIS, NIR, nSWIR and fSWIR), whereas five (TFM, CSH, PFM, LDM, TWC and SLA) models did not include fSWIR data. nSWIR data was not used in three models (LDM, TWC and LWC). Wavelengths from the VIS portion of the spectrum were used in 22 of the 23 models while NIR reflectance was

used in all models. The important role of VNIR for modeling the majority of FTs from RS data is underlined when looking at the frequency of waveband selection (Figure 3-4). Most often selected were the VIS and NIR region in the 23 models – especially bands around 1130 nm, the regions around 390, 980, 1370 nm as well as the regions between 500 and 570 nm and 680 and 700 nm. However, also bands in the nSWIR region around 1580 nm were selected for 13 models while fSWIR reflectance was less frequently used.
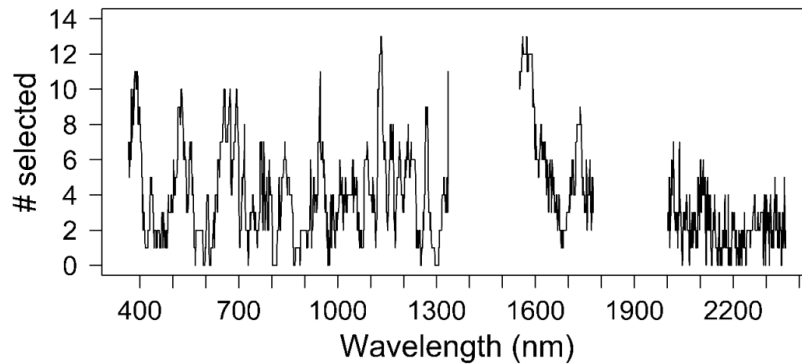
Figure 3-4. Number of times (# selected) a band was used in PLSR models for detecting the 23 FTs.

Thereby models of single FTs featured differences in their complexity regarding the number of LVs and the number of selected bands (Table 3-6). This complexity was not related to model performance, i.e. complex models were not necessarily the best performing ones and vice versa. However, FTs showing high variability (cf. Table 3-3) were modeled with higher accuracy (average R^2_{val} 0.54) than intermediately variable FTs (average R^2_{val} 0.51) and FTs featuring low variability (average R^2_{val} 0.43).

Models predicting PH, fPAR$_{abs}$, C/N-ratio, TFM, N-content, CSH, SPAD, NDF-content and LA performed well ($R^2_{val} \geq 0.6$, Table 3-6). Models for TFM and CSH thereby only included bands from the visible region (350-700 nm), the red-edge position (around 740 nm) as well as from the NIR and nSWIR regions (Figure 3-5). For estimating PH, fPAR$_{abs}$, C/N-ratio, SPAD, NDF-content and LA, all regions of the measured spectrum were used.

Moderately high fits ($R^2_{val} \geq 0.4$, < 0.6) were achieved for PFM, LFM, LDM and LDMC. Models relating LFM and LDMC to first spectral derivation incorporated bands from all spectral regions (VNIR, nSWIR, fSWIR), while PFM and LDM models were mainly based on bands from the VNIR.

Model fits for estimating PDM, TDMC, PWC, TWC, PDMC, TDM, LWC, C-content, LS-ratio and SLA were poor ($R^2_{val} < 0.4$). For modelling PDM, TDMC, PDMC, TDM, LS, PWC and C-

content, bands distributed across the entire range of the recorded spectrum were used. To relate spectral data to LWC, bands from VNIR and fSWIR were of importance. TWC estimation was based on bands in the VNIR region. The model for estimating SLA reached the lowest accuracy and incorporated bands from the red edge region, NIR and nSWIR.

Table 3-6. PLSR model results on plot level, including number of predictors (# pred.), number of observations (N), number of latent vectors (# LV), R^2 in calibration (R^2_{cal}) and validation (R^2_{val}) as well as normalized root mean square error in calibration ($nRMSE_{cal}$) and validation ($nRMSE_{val}$).

	# pred.	N	# LV	R^2_{cal}	R^2_{val}	nRMSE$_{cal}$ [%]	nRMSE$_{val}$ [%]
PH	149	138	4	0.82	0.80	11.57	11.85
fPAR$_{abs}$	590	130	7	0.85	0.79	9.63	10.71
C/N	97	134	3	0.76	0.75	10.98	11.27
TFM	140	138	4	0.74	0.71	13.47	14.14
N	331	134	4	0.74	0.71	10.45	11.09
CSH	442	69	3	0.74	0.70	16.50	17.38
SPAD	398	138	2	0.66	0.67	12.84	12.83
NDF	93	134	7	0.72	0.65	15.47	17.13
LA	223	139	9	0.77	0.65	10.56	12.67
PFM	787	138	3	0.61	0.56	16.41	17.16
LFM	297	138	8	0.65	0.53	13.05	15.03
LDM	42	137	7	0.59	0.52	15.02	15.08
LDMC	331	136	5	0.58	0.49	16.45	17.00
PDM	60	126	4	0.45	0.38	20.79	23.44
TDMC	347	126	2	0.42	0.38	23.78	24.61
PWC	135	126	5	0.45	0.35	19.33	20.40
TWC	24	126	2	0.40	0.34	29.06	28.49
PDMC	117	126	2	0.39	0.34	30.1	31.14
TDM	11	126	6	0.41	0.32	29.23	31.39
LWC	397	136	5	0.34	0.22	22.48	25.42
C	1050	134	5	0.39	0.21	26.87	31.56
LS	11	126	2	0.24	0.20	32.26	32.62
SLA	126	137	2	0.15	0.10	56.62	53.57
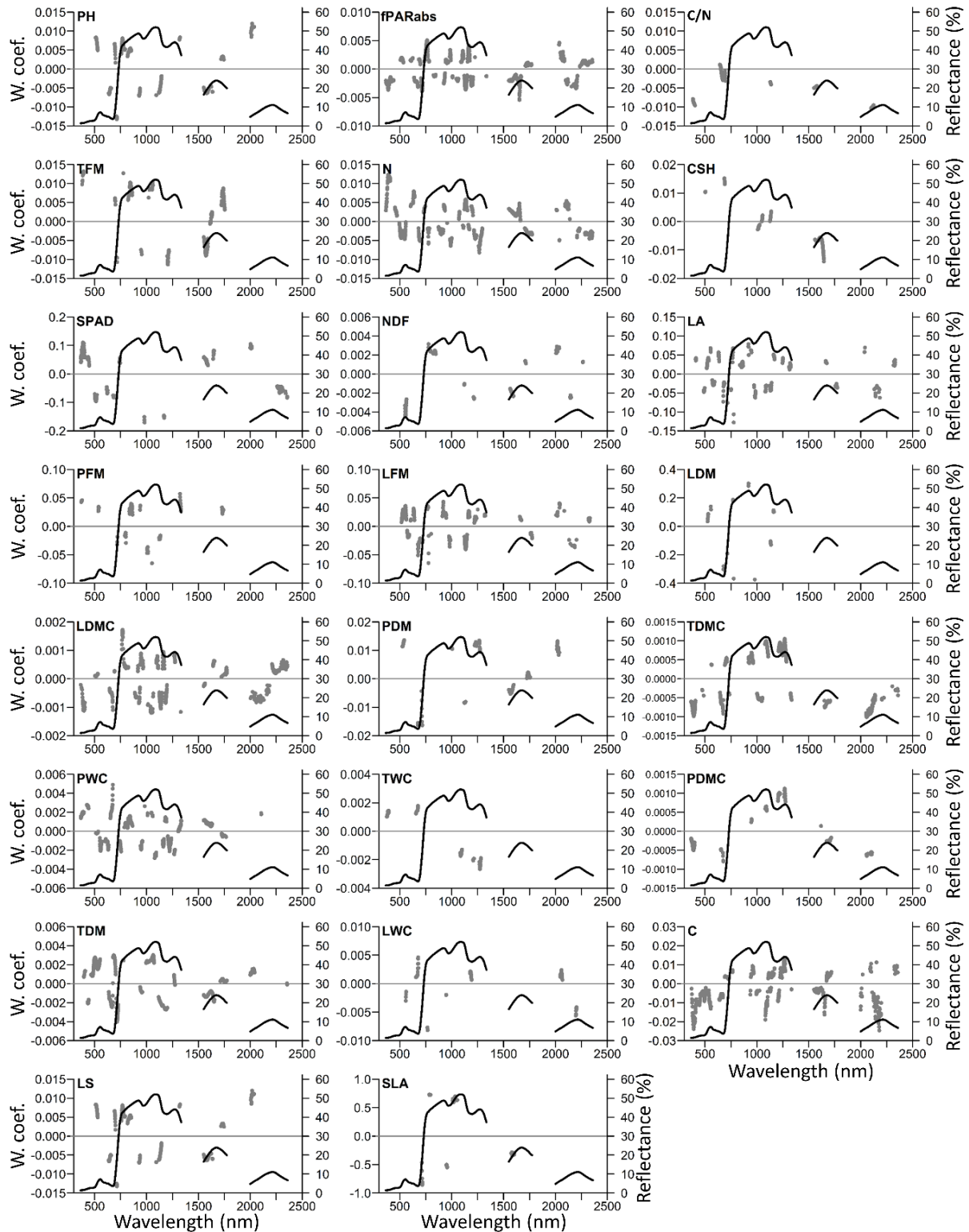
Figure 3-5. Weighted regression coefficients (W. coef.) for all 23 FT models (grey), indicating the influence of a band in the regression model. The spectrum shown in all figures is the average of all spectra collected (black).

3.4   Discussion

In this study, the relations between spectral reflectance and 23 different FTs of five Central-European grassland canopies were analyzed. Measurements of reflectance and FTs were recorded along a gradient in fertilization from limed only to full (NPK) application on 29 dates throughout the growing seasons 2012-2014.

Previous studies have shown that spectral reflectance is influenced by a variety of factors, including solar irradiation intensity and direction as well as by the sensor viewing geometry (Disney et al., 2006; Lobell et al., 2002; Ross, 1981; Stagakis et al., 2010; Widlowski et al., 2004). To cope with diurnal variations in the angle of solar irradiation, we sampled each plot at different times throughout each sampling day. Furthermore, fluctuations in irradiation intensity caused by changing atmospheric conditions were assumed to be low because field spectroradiometer data is relatively free of atmospheric effects (Thenkabail et al., 2002). Differences in observation geometry influencing reflectance, including sensor height and observation angle, were minimized by using a crane system providing a fixed sensor detent. In addition, the high number of measurements from different years ensured that variability in climatic factors (i.e. precipitation, temperature as well as the sum of incoming solar irradiation) and all phenological stages of plants were covered. We found the largest variations in FTs in the NPK-treatments. In these treatments, nutrient limitation was low and plant species pursuing intense and rapid development in biomass and LAI (i.e. C-strategists in CSR strategy scheme; Grime, 1977) predominated. In contrast, stress strategists (S-type; Grime, 1977) were more abundant in the Ca- and CaN-treatments. Plants of this type are limited in growth and thus feature lower FT variability (Aerts and Chapin III, 2000; Ryser, 1996; Westoby et al., 2002).

Sampling of plants from areas outside of the sensor's FOV was necessary to prevent thinning of vegetation during this multitemporal study. However, as a sample size of ten individual plants per subplot provided a stable mean, we assume that the spatial heterogeneity of FTs occurring within the plots was covered. Thus, we are confident that, although the sampled area of reflectance (recorded in 0.64 m² of each subplot) and FT data (sampled in the entire subplots) did not match, the calculation of means in reflectance and FTs were representative for the entire canopies.

We identified PH, TFM, CSH, LA, PFM, LFM, LDM, PDM, TDM and LS-ratio as highly variable FTs. These FTs were mostly related to plant height, LAI and biomass and exhibited distinct changes over the growing season. These differences in the seasonal variations depended upon soil nutrient supply, with the NPK-treatments showing the largest variations. Intermediate

variabilities caused by soil nutrient status and seasonal development were observed for fPAR$_{abs}$, C/N-ratio, N-content, TDMC, PDMC and SLA. Low variations were characteristic for SPAD, NDF-content, LDMC, PWC, TWC, LWC and C-content.

A comparison of the plots' mean spectral reflectance highlighted differences in the optical properties induced by different fertilization levels and phenological developments. It is usually assumed that changes in VIS and NIR reflectance are mainly caused by variations in green LAI, green biomass and chlorophyll content, whereas longer wavelengths respond to other parameters, such as the proportion of senescent plant material (Asner, 1998; Homolová et al., 2013; Lorenzen and Jensen, 1988; Stagakis et al., 2010). At the beginning of the two investigated growths, in each year NIR reflectance in the NPK-treatments significantly increased, whereas reflectance in the SWIR and the red region remained relatively low. The increase in NIR reflectance at the beginning of both growths was related to the presence of fast growing plants, which dominated in these plots. At the same time, a slow development of NIR reflectance as well as a relatively high red and SWIR reflectance were measured in the Ca- and CaN-treatments, in which plants pursuing a more conservative strategy type predominated (C-type in CSR strategy scheme; Grime, 1977). The slow development of green biomass, LAI and chlorophyll content caused low rates of increase in NIR as well as a slow decrease in red and SWIR reflectance in these plots. At the end of each growth, in the NPK-treatments senescence commenced, and so reduced the fraction of green material in the canopy. As a result, reflectance decreased especially in the region between 900 and 1000 nm, increased in the red and fSWIR-range and remained relatively stable between 1000 and 1400 nm. These results confirm the findings of previous studies (Asner, 1998; Elvidge, 1990; Roberts et al., 1993). In contrast, reflectance in Ca- and CaN-treatments remained relatively stable until the end of both growths. This was caused by the dominance of slow growing species, which start late in their growth but feature a long leaf life span (Lavorel et al., 2007; Pontes et al., 2010).

3.4.1   Overall model performance and important spectral regions

The average fits of PLSR models obtained using raw, continuum removed and first derivation spectra revealed that the latter mentioned spectral data worked best for estimating the majority of FTs. This good performance of first derivation spectra has also been observed in other studies using band selection techniques for detecting biochemical plant properties (Smith et al., 2003; Yoder and Pettigrew-Crosby, 1995). We assume that derivation calculation suppresses other factors interfering with the spectral response to changes in plant properties such as soil reflectance, diurnal and seasonal changes in solar irradiance as well as shadow effects within

the canopy (Cho et al., 2010; Huang et al., 2004; Laba et al., 2005; Ramoelo et al., 2011; Rollin and Milton, 1998; Schlerf et al., 2010).

The comparison between models created using data stratified by treatment (specific models) and models using pooled data for all treatments (general models) revealed that there were no significant differences in model performances. This was surprising because we expected that stratified models may enable higher model accuracies. We assume that stratification of models in this study did not enable improved accuracies because data were collected in all phenological stages of the vegetation. This multitemporal sampling scheme had the effect that a large range in FT expressions occurred in each plot, which caused the stratification to be non-effective. We further conclude that the *autopls* band selection process is able to identify bands that are robust against confounding factors (e.g. to different canopy structures, biomass and species compositions).

Our analysis further revealed that spectral reflectance from all regions of the measured spectrum was useful for detecting most (13) of the 23 estimated FTs. Thereby, NIR was used in all 23, VIS in 22, nSWIR in 20 and fSWIR in 17 models. Similarly, Thenkabail et al., (2004a) observed that the entire range of wavelengths is important for estimating many plant properties. As most frequently selected regions, we identified 365 to 394 nm, 515 to 544 nm, 635 to 664 nm, 665 to 694 nm, 935 to 964 nm, 1115 to 1144 nm, 1205 to 1234 nm, 1551 to 1580 nm, 1581 to 1610 nm and 1611 to 1640 nm. This again underlines the high importance of the VIS and NIR portions of the spectrum for deriving plant properties such as FTs (Wang et al., 2008).

Accuracies for estimating single FTs were highly variable, ranging from R^2_{val} 0.1 for SLA to R^2_{val} 0.8 for PH. This wide span in accuracy shows that hyperspectral RS is not a suitable solution to detect all FTs. A comparison between the coefficients of determination reached by the PLSR-models and the measured variability of FTs using CV suggests that highly variable FTs are frequently detected with higher accuracies than less variable FTs. Thus, RS may be a good choice for estimating especially highly variable FTs of grassland with high temporal resolution and so support ecologists in monitoring changes in ecosystem functioning.

Using RS for FT monitoring was successful for 13 of our models ($R^2_{val} \geq 0.4$), which suggests that these FTs can be estimated throughout entire growing seasons. Such temporally stable models were also produced by Ling et al., (2014) for N-content of different species-rich grassland communities. Our results further suggest that, although different growth rates, levels of stress and site attributes exist for mixed grassland canopies (Jacquemoud et al., 2009; Schmidt et al., 2004; Verrelst et al., 2009), the flexible PLSR algorithm is able to disentangle

multiple relations within datasets and select single bands mostly related to one FT. However, for models performing with low and moderate accuracies, no bands were found within the measured spectrum that were highly correlated to the respective FT, or else these were confounded by other canopy characteristics (e.g. canopy structure or changes in other FTs).

Although previous studies have shown that the underlying soil may have strong effects on canopy reflectance (Asner, 1998; Feilhauer and Schmidtlein, 2011; Lorenzen and Jensen, 1988), we assume that soil reflectance had only minor effects on our spectral dataset because LAI and fractions of canopy cover were relatively high. However, senescent material may have exacerbated estimation of FTs at the end of both growths, particularly in the NPK-treatments. Nevertheless, it was shown that PLSR was able to select band combinations that were only marginally affected by senescent material and litter and thus modelled more than 50% of the recorded FTs with moderate to high accuracy.

However, PLSR model validation by LOO-CV is not entirely free from effects of over-fitting, i.e. increasing the model fit by including additional bands without actually improving prediction accuracy (Allen, 1974). Thus, it should be noted that model accuracies tend to be optimistic. However, by using the entire dataset for model calibration and validation, this approach minimizes randomness in the observations used for training and evaluation and provides balanced estimates of model errors (Darvishzadeh et al., 2008a; Efron and Gong, 1983; Schlerf et al., 2005).

3.4.2 Accuracies of individual models for detecting plant functional traits

Model accuracies were high ($R^2_{val} > 0.6$) for nine of the 23 measured FTs. PH was estimated with the highest precision ($R^2_{val} = 0.8$), which is particularly important as it is frequently used as a proxy for plant competitive ability (Duru et al., 2010; Homolová et al., 2013). This good model performance for estimating PH was expected because other authors, such as Ollinger, (2011), state that morphological FTs, such as PH, show persistent and stable relations to canopy reflectance. As found in previous studies, models for estimating $fPAR_{abs}$, N-content, TFM and SPAD also featured relatively good performances (Ling et al., 2014; Roelofsen et al., 2013; Rossini et al., 2012; Wang et al., 2008). Furthermore, C/N-ratio, CSH, NDF-content and LA were modelled precisely using PLSR. This gives strong evidence that these nine FTs can be derived throughout the entire growing season for different species-rich plant communities and thus effectively be mapped and monitored using RS data.

Moderate model accuracies ($0.4 \leq R^2_{val} < 0.6$) were achieved for four FTs, including LDM, LDMC, PFM and LFM. This was comprehensible because these FTs have been influenced by adhesive water brought by precipitation events, which occurred prior to sampling. These rain events strongly influenced sample weight, which made it difficult to identify spectral bands reacting to water content in plant tissue, irrespective of the amount of adhesive water.

Low accuracies ($R^2_{val} < 0.4$) were found for ten FTs. Estimation of PDM and TDM reached lower accuracies than those obtained by Wang et al., (2008). The main reason might be that both FTs were recorded for single plants of species-rich canopies in the presented study, whereas Wang et al., (2008) studied rice monocultures. Furthermore, as stated already above, a number of FTs, including PDMC, TDMC, PWC, LWC and TWC, may have been difficult to estimate due to the influences of adhesive water on sample weight. Additionally, accuracies for detecting these FTs may have decreased due to interferences in their effects on the spectral signatures with other plant variables, such as biomass and canopy structure. A low accuracy for detecting C-content was expected, because this FT is difficult to detect on canopy levels using optical RS data (Patenaude et al., 2005). As LDM was measured with moderate and TDM with low accuracy, poor performance for estimating LS-ratio using our spectral dataset was expected. In addition, model accuracy for deriving SLA was low. This observation is confirmed by Homolová et al., (2013), who state that detecting SLA using spectral is more difficult than detection of most other FTs.

3.5 Conclusions

In this study, the relations between spectral reflectance and 23 FTs of five different species-rich grassland communities were examined throughout three years. Using PLSR, it was possible to detect 13 FTs based on hyperspectral reflectance data with high or moderate accuracy ($R^2_{val} > 0.4$). These results underline the large potential of RS as non-destructive technique to provide information on selected FTs with high temporal resolution and at low costs.

It was further demonstrated that one PLSR model can be fitted to estimate a FT of different plant communities when data from all phenological stages are included. This makes a prior stratification of vegetation into single subsets unnecessary. Among the spectral regions used in the models, NIR and VIS were the most important. However, spectral data from the nSWIR- and fSWIR-range provided additional information for estimating the majority of the tested FTs. Thus, for this purpose, the entire spectral region between 350 and 2500 nm has proven to be valuable.

It is concluded that RS can support grassland ecologists in deriving detailed information on plant responses to changes in the environmental conditions and to monitor the development of grassland ecosystems. Such information may allow grassland scientists to adapt nutrient management to variations in climate as well as to changes in the intensities of use. Future research should be guided towards the development of operational RS-based estimates of FTs on regional, local and global scales. Such attempts may include assessments of the ability of modern imaging spectrometers aboard novel RS satellites to provide information on FTs.

4 The potential of remote sensing sensors featuring different spectral resolutions and ranges for detecting the plant functional traits of grassland vegetation

Abstract

Recent studies have revealed the vast potential of hyperspectral RS data for detecting FTs. However, it remains unanswered, which particular ground-based and spaceborne RS sensors are suitable for this purpose. The objective of this study was to assess the potential of six different RS systems featuring different spectral ranges and resolutions for estimating FTs.

Therefore, ground-based FS 3 spectroradiometer data was collected throughout the growing seasons 2012-2014. This dataset was used to simulate the reflectance of the hyperspectral HH 2, EnM as well as of the multispectral S-2, L 7 and RE sensors. Within one day distance in time to the acquisition of RS data, FTs were measured manually. Finally, PLSR was used to relate single FTs to each sensor's spectral reflectance.

Using hyperspectral systems it was possible to estimate 13 (FS 3), 11 (EnM) and ten (HH 2) FTs with acceptable precision ($R^2_{val} > 0.4$). Among the multispectral sensors, S-2 reached the highest average accuracy providing R^2_{val} larger than 0.4 for nine FTs. Only four FTs were successfully detected using L 7 and none using RE data. These results show that hyperspectral systems perform better than multispectral systems for estimating the majority of tested FTs. Although most important information was located in the VIS and NIR regions of the spectrum, including longer wavelengths (i.e. SWIR) led to an increased accuracy for estimating many FTs. For improving the detection of FTs it was thus more efficient to cover a broad spectral range than to include a high band number within a limited spectral range. Large differences in the model accuracies were found between the single FTs. FTs related to green biomass or LAI as well as to chlorophyll and NDF-content were detected with high accuracies using hyperspectral systems ($R^2_{val} > 0.6$). In contrast FTs related to plant water-, dry matter- and C-content as well as to leaf area or LS-ratio were more difficult to detect ($R^2_{val} \leq 0.6$).

4.1 Introduction

Grassland scientists commonly evaluate the development and state of grassland ecosystems based on their FTs. FTs are defined as morphological, physiological and phenological plant properties, which indicate the performance of plants in an ecosystem under given environmental

67

conditions (Violle et al., 2007). However, FTs are currently recorded using field-methods (e.g. as described in Cornelissen et al., (2003)), which often require labor-intensive, costly and destructive sampling procedures. Thus, grassland agronomists and ecologists are looking for non-destructive methods that can provide cost-effective estimates of FTs. Such methods would facilitate information collection for ecological research and add to an improved grassland management under changing environmental conditions and intensities of use, for instance through a more precise application of fertilizer. As contactless technique, RS is a powerful and versatile tool for estimating plant properties, such as FTs, because it can reduce the amount of labor and costs associated with sampling and analysis and enable researchers to collect data at different spatial scales (Hansen and Schjoerring, 2003; Kawamura et al., 2008; Peñuelas and Filella, 1998).

For deriving biophysical variables of vegetation using remotely sensed information, multispectral (i.e. broadband) VIs have been used the most frequently (e.g. Brantley et al., 2011; Elvidge and Chen, 1995; Shen et al., 2008). Although selected plant properties and FTs (e.g. biomass and chlorophyll content) can successfully be derived using these systems, multispectral sensors have limitations to detect many other FTs due to a lack in spectral detail (Atzberger et al., 2011; Glenn et al., 2008; Gong et al., 2003; Govaerts et al., 1999; Haboudane et al., 2004; Hansen and Schjoerring, 2003; Hunt Jr. et al., 2013; Sampson et al., 2001; Steininger, 2000). Hyperspectral RS sensors paired with suited algorithms to extract important information from these high-dimensional datasets have been observed to enable increased estimation accuracies compared to multispectral systems (Broge and Leblanc, 2000; Elvidge and Chen, 1995; Thenkabail, 2001). Thus, hyperspectral RS has gained in importance in science in the past decades and may enable scientists to derive FTs with high accuracy (Homolová et al., 2013; Ustin and Gamon, 2010). First attempts for assessing key FTs based on hyperspectral reflectance data were undertaken in chapter 3 and in Roelofsen et al., (2013). In these studies, PLSR was identified as an effective algorithm for relating FTs to vegetation spectral properties. However, it remains unclear how spectral range and resolution influence the accuracy for estimating FTs using RS data and which planned or operational sensors may be suitable for this purpose.

To answer this question, we used FS 3 data to simulate the reflectance of five different RS systems, including the hyperspectral HH 2- and EnM-sensors as well as the multispectral S-2-, L 7- and RE-sensors. Although the spectral properties of field spectroradiometer data differ from actual satellite data due to the position of field spectroradiometers close to the canopy and

different sensor geometries (Feilhauer and Schmidtlein, 2011), these devices have been identified as valuable data-source for investigating the potential of different RS sensors for detecting vegetation properties (Feilhauer et al., 2013; Feilhauer and Schmidtlein, 2011; Mutanga et al., 2015; Rossini et al., 2012). Using simulated data further provides the advantages to minimize spatial inaccuracies between RS and plant data and to deliver information collected with the same viewing geometry (spatial resolution and angle). Furthermore, field spectroradiometer datasets can be acquired with high temporal resolution and directly on demand.

The objective of this study was to test the model performances for the prediction of twenty-three FTs based on reflectance data measured with a FS 3 spectroradiometer as well as on simulated HH 2, EnM, S-2, L 7 and RE data. The results will support decisions regarding the selection of suitable RS sensors to estimate FTs and allow an assessment of the impact of spectral range and resolution on the detection accuracies. Additionally, valuable information for the design of future RS sensors dedicated to monitor vegetation is provided. This research is thus an important step to enable RS scientists to produce spatiotemporal datasets on FTs and support ecologists in adjusting grassland management under changing climate conditions and intensities of use. Therefore, we have focused on the following hypotheses:

1. FTs related to biomass, LAI or chlorophyll content can be detected with high accuracies using RS systems, whereas FTs related to dry matter, dry matter content or water content are more difficult to estimate.
2. The performance of a sensor for predicting FTs depends on its number of spectral bands, its bandwidth and its spectral range.
3. Hyperspectral RS systems (i.e. FS 3, HH 2 and EnM) provide higher accuracies for detecting FTs than multispectral systems (i.e. S-2, L 7 and RE).

To answer these questions, field spectroradiometer data and manual samples of FTs were collected in different intensity levels of grassland throughout the growing seasons of 2012-2014. In the next step, spectral reflectance of five different RS systems was simulated based on the measured spectral signatures. Subsequently, PLSR models relating the spectral reflectance to FTs were developed for each sensor. Finally, the performances of the different RS systems for detecting FTs were assessed and suggestions for the selection of efficient sensor systems for an application in grassland ecology are given.

4.2 Materials and methods

4.2.1 Study area

Data were collected in the RGE. This experiment was identified as ideal study site because it features a broad range of plant communities differing in their FTs. Furthermore, the fertilization experiment allows a systematic sampling of spectral signatures and plant samples in clearly defined and well-documented vegetation communities. The experiment is located at 50°13`N and 6°51`E at an elevation of 475 m in Rhineland Palatinate, Germany. A temperate-maritime climate with an annual precipitation of 811 mm and a mean annual temperature of 6.9 °C prevails at the site (RGE meteorological Station).

The experiment was established in 1941 in randomized block design and has been managed constantly since then. The site today consists of 55 plots, which are treated with different fertilizers, including Ca, CaN, CaNP, CaNPKCl and $CaNPK_2SO_4$ in ten replicates as well as of five unfertilized control plots. Each plot has a size of 3×5 m² (Figure 4-1). Grass swards in all plots were cut in July and in October, which leads to two subsequent growths. Thereby, more biomass is produced in growth one than in growth two (Schellberg et al., 1999).

As a result of differences in fertilizer application, grassland communities have developed, which vary in their floristic composition as well as in their biophysical and chemical properties (Chytrý et al., 2009; Hejcman et al., 2007, 2010a; Schellberg et al., 1999; Šmarda et al., 2013). The communities in the Ca- and CaN-treatments were assigned to the montane meadows of *Geranio-Trisetetum* (*Polygono- Trisetion* alliance) (Chytrý et al., 2009). Communities in the CaNP-fertilized plots belong to a transitional type between *Poo-Trisetetum* and *Arrhenateretum* (both from the *Arrhenatherion* alliance). The CaNPKCl and $CaNPK_2SO_4$ treatments are characterized by communities belonging to the mesotrophic *Arrhenateretum* meadows (Chytrý et al., 2009).

Due to high labor demand for collecting and processing of *in-situ* data, we had to limit our study to one replicate of each treatment. However, the variation in plot floristic composition and biomass development among replicates of the same treatment was observed to be small (Chytrý et al., 2009; data not shown). Hence, we assume that the five selected plots are sufficient to reliably represent the FTs and the spectral signatures of the other replicates.

4.2.2 Collection of reflectance spectra

Field spectroradiometers have been successfully used in various studies for investigating the relations between spectral reflectance and grassland biophysical parameters (Ferner et al., 2015; Roelofsen et al., 2013). Furthermore, these systems can be used to simulate other sensors and compare their performance in establishing relations between spectral data and plant properties, such as FTs (Inoue et al., 2012; Mutanga et al., 2015; Ustin et al., 2009). In this experiment, hyperspectral RS data were collected using a FS 3 spectroradiometer (Analytical Spectral Devices Inc., Boulder, CO, USA). The device measures reflected radiance in a spectral range between 350 and 2500 nm and has a spectral resolution of 3 nm FWHM at a wavelength of 700 nm and 10 nm at wavelengths of 1400 and 2100 nm (ASD Inc. (ed.), 2010). However, measured spectral data are interpolated to 1 nm intervals yielding 2150 single bands. Spectral signatures of the five grassland communities were recorded on 29 dates during the growing seasons 2012-2014. This number of days ensured that all vegetative and reproductive growth stages of the vegetation were covered throughout several years.

To limit effects of changing observation angles and sensor heights, we used an automatic rail-based crane system along the five investigated plots (Figure 4-1). This setup allowed repeated sampling of spectral reflectance at exactly the same positions from nadir in 2 m height above ground (25° viewing angle), resulting in a field of view of 0.64 m². Within each plot, reflectance was measured in three different subplots (a, b, c) to account for naturally occurring spatial variability in grassland (Butterfield and Malmström, 2009; Psomas et al., 2011). These measurements were repeated in each of the five plots between 12 and 33 times on each measurement day between 10 am and 4 pm. To mitigate variations of incoming solar radiation, collection of RS data was conducted under clear, cloud-free weather-conditions. Radiance of a Spectralon ® zenith polymer white reference target (95% reflectance; Labsphere Inc., North Hutton, NH, USA) was recorded after every three measurements to adapt reflectance recordings to changes in irradiation conditions. The entire spectral dataset included 2689 measurements.

To smooth the transitions between the three sensors integrated in the spectroradiometer (VNIR: 350-1000 nm, SWIR-1:1000-1800 nm, SWIR-2:1800-2500 nm), splice correction (Stevens and Ramirez-Lopez, 2013) with a filter size of n=25 bands was performed. To reduce high-frequency noise in the spectral signal, second order polynomial filters (Savitzky and Golay, 1964) with a size of 31 bands between 350 and 1350 nm, 51 bands between 1350 and 1800 nm and 101 bands between 1800 and 2500 nm were applied.
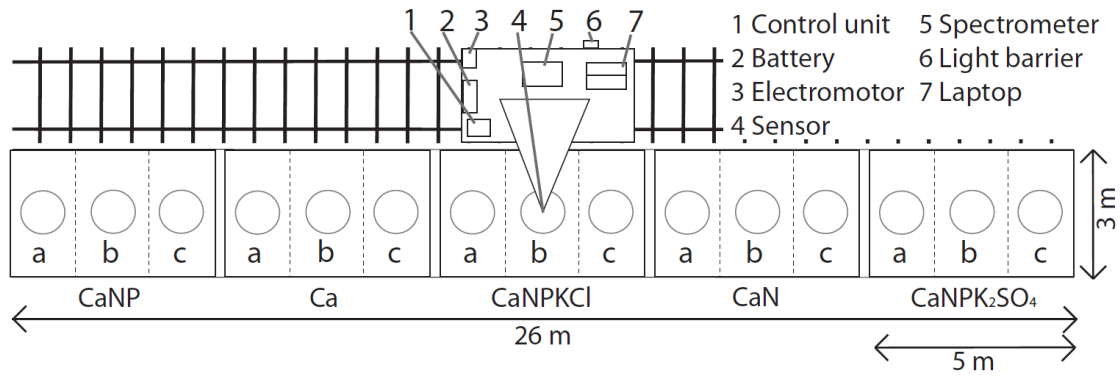
Figure 4-1. Setup of the rail system and the crane. The single fertilizer treatments Ca, CaN, CaNP, CaNPKCl and CaNPK₂SO₄ are separated into three subplots (a-c). The sensor field of views are indicated by circles.

4.2.3   Simulation of different remote sensing sensors

We decided to test the performance of six different sensors for detecting the FTs in a multitemporal analysis. The following six sensors were selected because they (1) are mainly designed for assessing plant biophysical properties, (2) have a high spatial resolution that is suitable for detecting FTs at the field scale, (3) feature large differences in band numbers and (4) measure reflectance in differently broad ranges of the spectrum (Figure 4-1).

Table 4-1. The five tested sensors, including their year launched, spectral range, full width half maximum (FWHM), spatial resolution, band number as well as the source of the spectral response functions (SRF) used for sensor simulation..

Platform	Sensor	Year launched	Spectral range (nm)	FWHM (nm)	Spatial res. (m)	No. of bands	Source of SRF
Ground	FS 3	-	350-2500	3/10	-	2150	-
Ground	HH 2	-	325-1075	3	-	725	-
Satellite	EnM	2019	420-2450	>8, <12	30	242	*
Satellite	S-2	2015	443-2190	>15, <180	>10, <60	13	ESA, 2015
Satellite	L 7	1999	450-2350	>60, <260	>15, <60	8	USGS (ed.), 2016
Satellite	RE	2008	440-850	>55, <90	6.5	5	BlackBridge (ed.), 2012

* Personal communication, Segl, K. 2016 October 27, 2016.

To simulate the half range spectroradiometer HH 2, spectral reflectance of the FS 3 was cut off at 1075 nm. Reflectance of EnM, S-2, L 7 and RE was simulated based on FS 3 measurements and the appropriate SRF (Table 4-1) applied in the given formula:

$$\gamma_x = \frac{\int_{n0}^{nmax} \gamma_n * \rho_n}{\Sigma \rho_n} \qquad (4.1)$$

where γ_x is the reflectance of the simulated band of the satellite sensor, n is the total band number of the spectral measurement, γ_n is the reflectance of band n, ρ_n is the response of band

n, given in the SRF, and $\sum \rho_n$ is the sum of relative reflectance given in the SRF of a given band.

Spectral information between 350-365 nm, 1330-1440 nm, 1790-1990 nm and 2360-2500 nm was severely affected by noise and thus excluded from further analyses. This reduced the number of bands to 1683 for the FS 3, 711 for the HH 2, 192 for EnM, 12 for S-2, 8 for L 7 and 5 for RE. For all sensor simulations, reflectance data averaged for the plot level for each measurement day was used (in total 189 averaged spectra).

4.2.4 Manual measurements and calculations of plant functional traits

For the purpose of relating spectral data to FTs, extensive in-situ measurements in the grass crops have been realized in the growing seasons 2012-2014. A total of 23 FTs were derived (Table 4-2).

FTs measured at the plant level: Seven of these FTs were measured on individual plants, from which ten additional FTs were calculated. Therefore, at the maximum in one day distance in time from the spectral measurements, ten plants per subplot (30 per plot) were randomly selected and removed. On the one hand, pre-trials have shown that this sample size is sufficient to scale up FTs to the community level (cf. mass-ratio hypotheses; Grime, 1998). On the other hand, the relatively low number of extracted plants ensured that vegetation in the plots was not considerably thinned out. To maintain vegetation density in the FOV of the spectroradiometer, vegetation sampling was conducted in the entire subplots. On each individual plant, PH, PFM and LFM as well as the SPAD value and the LA were measured. To estimate PDM and LDM, fresh material was dried for 48 hours at 60 °C and subsequently weighed. Based on the seven FTs measured for individual plants, ten more FTs were calculated according to Table 4-2. Results were finally averaged per plot.

FTs measured at the subplot level: Four FTs were measured at the subplot level. Therefore, dried plant material of the ten extracted individual plants (per subplot) was mixed and subsequently grinded for 120 seconds and 30 tilts per second using a ball mill (Retsch MM 400, Haan, Germany). To measure plant C- and N-content, samples of 0.2 g (± 0.005 g) from the grinded plant material were wrapped in Zn capsules (5 x 9 mm, IVA Analysetechnik GmbH & Co KG, Meerbusch, Germany). The material was then analyzed in a Euro EA 3000 elemental analyzer (Redavalle, Italy). C/N-ratio was calculated as the simple quotient of C- divided by N-content on a dry matter basis. NDF-content was determined for the grinded plant material according to van Soest et al., (1991). Finally, FTs were averaged at plot level.

FTs measured at the plot level: CSH and fPAR$_{abs}$ were recorded at the plot level. Therefore, ten measurements of CSH per plot were derived on 14 dates using a rising plate meter (30 cm diameter, 238 g, pressure of 3.4 kg * m^{-2}). CSH is highly correlated to the biomass of grassland canopies (Harmoney et al., 1997). Furthermore, ten measurements of fPAR$_{abs}$ per plot were recorded on 27 days. Both, CSH and fPAR$_{abs}$ were subsequently averaged at plot level.

Table 4-2. Definition, unit and used instrument for manual measurement of FTs; I= incoming solar radiation below ($_s$) and above canopy ($_i$). The levels indicate whether a FT was measured for individual plants, the subplot or the plot (adapted from chapter 3.2.3).

Level	FT	Definition	Unit	Instrument	Formula
Individual	PH	Plant height	cm	yardstick	-
	SPAD	SPAD value of two leaves	-	SPAD meter (Minolta 502, Marunouchi, Japan)	-
	LA	Area of plant leaves	cm²	Scanner (Epson Expression 1100, Suwa, Japan)	-
	PWC	Plant water content	%	-	((PFM-PDM)/PFM)*100
	TWC	Tiller water content	%	-	((TFM-TDM)/TFM)*100
	LWC	Leaf water content	%	-	((LFM-LDM)/LFM)*100
	SLA	Specific leaf area	cm² g^{-1}	-	LA/LDM
	PDMC	Plant dry matter content	%	-	PDM/PFM*100
	TDMC	Tiller dry matter content	%	-	TDM/TFM*100
	LDMC	Leaf dry matter content	%	-	LDM/LFM*100
	LS	Leaf-tiller ratio	-	-	LDM/SDM
	PFM	Plant fresh matter	%	Scale (Sartorius BP 110 S, Göttingen, Germany)	-
	TFM	Tiller fresh matter	g	-	PFM-LFM
	LFM	Leaf fresh matter	g	Scale (Sartorius BP 110 S, Göttingen, Germany)	-
	PDM	Plant dry matter	g	Scale (Sartorius BP 110 S, Göttingen, Germany)	-
	TDM	Tiller dry matter	g	-	PDM-LDM
	LDM	Leaf dry matter	g	Scale (Sartorius BP 110 S, Göttingen, Germany)	-
Subplot	N	N (g) per g dry matter	%	Elemental analyzer (Euro EA 3000, Redavalle, Italy)	-
	C	C (g) per g dry matter	%	Elemental analyzer (Euro EA 3000, Redavalle, Italy)	-
	C/N	C (g) per N (g)	%	Elemental analyzer (Euro EA 3000, Redavalle, Italy)	C/N
	NDF	Neutral detergent fiber content per unit dry matter	%	Scale (Sartorius BP 110 S, Göttingen, Germany)	-
Plot	CSH	Compressed sward height	cm	Rising plate meter	-
	fPAR$_{abs}$	Fraction of photosynthetically active radiation absorbed	µmol s^{-1} m^{-2}	Ceptometer (Delta-T Devices Sun Scan SS1, Cambridge, UK)	I$_s$/I$_i$

4.2.5   Data analysis

We selected brightness normalized PLSR (Feilhauer et al., 2010) using backward selection of predictor variables as implemented in *autopls* package for R (Schmidtlein et al., 2015) for relating the spectral reflectance of the six sensors to the 23 FTs. This choice had several reasons. First, recent studies have shown that PLSR is a valuable technique for deriving highly accurate models of grassland FTs based on hyperspectral RS data (chapter 3.2.3; Roelofsen et al., 2013). Second, PLSR performs well when relating spectral information to plant properties because it is less affected by collinearity and model overfitting than multiple regression techniques (Chong and Jun, 2005; Kawamura et al., 2008; Ramoelo et al., 2013; Schmidtlein et al., 2012). Third, PLSR efficiently summarizes high-dimensional (i.e. hyperspectral) information and has also proven to be a good choice when relating a low number of observations to a high number of predictor variables (which is the case when processing hyperspectral reflectance data) (Bolster et al., 1996; Psomas et al., 2011; Wold et al., 2001). Brightness normalization according to Feilhauer et al., (2010) was applied to limit effects of seasonal shifts in irradiation intensity as well as shadows within the canopy (Middleton, 1991; Shibayama and Wiegand, 1985). As PLSR requires normal distribution of dependent variables (i.e. FTs), PH, LA, PWC, TWC, TDMC, PFM, TFM, LFM, PDM, TDM, C/N-ratio, NDF-content and CSH were transformed using decadal logarithm.

In PLSR, a set of latent vectors (similar to principal components) is created representing the most important spectral information for predicting the dependent variable (a FT). For creating these latent vectors, we applied backward selection of bands with an automated search criterion, which removes 25% of the predictors in each iteration based on significance jackknifing. Thus, irrelevant information for predicting a variable was removed from LVs and only important information was included in the models (Feilhauer et al., 2010). Model validation was performed using LOO-CV. This method allows a balanced estimation of model accuracy (Darvishzadeh et al., 2008a; Schlerf et al., 2005). In LOO-CV, models are calibrated using all but one observations. The remaining observation is subsequently used for model validation. To produce the best possible PLSR models, calibration and validation were performed iteratively until the most suitable compromise between model fit and parsimony enabling a minimal root-mean-squared error was found (Feilhauer and Schmidtlein, 2011). PLSR models were created for every FT and sensor using pooled data from all plots, both growths and all three years. Creating one model for all treatments has shown to provide equal or higher accuracies than producing several models stratified by plant communities (cf. chapter 3). Thus, we derived twenty-three models for each of the six sensors (138 models in total). To compare the average

performance of the six sensors, a two-tailed t-test comparing the R^2_{val} for all FTs of one sensor to those of the five other sensors was used.

4.3 Results

4.3.1 Overall accuracies of the partial least squares regression models by sensor

The average performance of the models based on hyperspectral data (FS 3, HH 2 and EnM) significantly outperformed the models created based on multispectral data (Figure 4-2). Thereby, FS 3 data achieved the highest average R^2_{val} (0.42) for detecting the set of 23 FTs and performed best for detecting 14 FTs. Nevertheless, a two sample t-tests showed that data of simulated HH 2 and EnM reflectance were on average not significantly less accurate than the FS 3 data for estimating FTs (Figure 4-2).
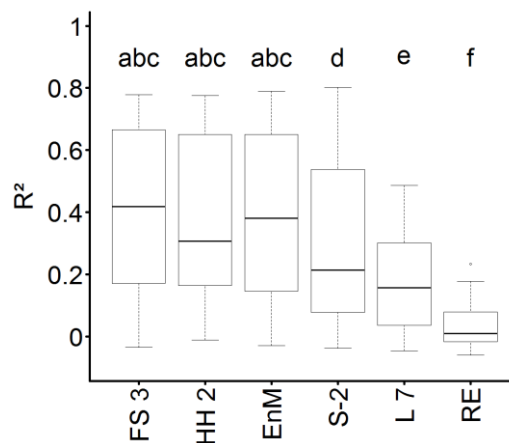
Figure 4-2. Boxplots representing the performance of models created for all FTs by sensor. Letters a-f represent significant differences (paired t-test, n=23, p=0.05).

4.3.2 Model accuracies achieved by the tested sensors for detecting single functional traits

Large differences in model performances were observed between the single FTs (Table 4-3). Our data show that PH, CSH and $fPAR_{abs}$ were detected with high accuracies of $R^2_{val} > 0.6$ using FS 3, HH 2, EnM and S-2 data. Pearson correlation between the number of bands of the six sensors and the averaged R^2_{val} of the 23 FTs was estimated as $\lambda_{Pearson}=0.64$. This shows that the decreasing band number of the sensor systems lead to significantly lower model fits. Although hyperspectral sensors reached higher R^2 values for most of these FTs, it is interesting that S-2 achieved the highest accuracy for detecting PH. Other FTs, such as SPAD, TFM, C/N-ratio and NDF-content were also detected with high accuracy using hyperspectral data. Acceptable accuracies ($0.4 < R^2_{val} < 0.6$) were reached for TDMC with FS 3 and HH 2, for TWC and PDMC with FS 3 and EnM and for PDMC and LDMC with FS 3 data only. Using

the L 7 sensor, four FTs, including PH, SPAD, NDF-content and CSH were detected with acceptable accuracy, but none with high accuracy. No FT was detected with high or acceptable accuracy using the RE sensor.

Table 4-3. PLSR model statistics for the 23 FTs by sensor, including number of observations (N), number of predictors (# pred.), number of latent vectors (# LV), normalized root mean squared errors in calibration (nRMSE_cal) and validation (nRMSE_val) as well as coefficients of determination in calibration (R²_cal) and validation (R²_val).

FT	N	# pred.	# LV	nRMSE_cal [%]	nRMSE_val [%]	R²_cal	R²_val	# pred.	# LV	nRMSE_cal [%]	nRMSE_val [%]	R²_cal	R²_val
					FS 3						HH 2		
PH	138	1135	6	10.78	11.83	0.82	0.78	269	6	9.83	10.34	0.81	0.78
fPAR_abs	130	259	7	10.63	10.45	0.79	0.73	261	7	12.85	13	0.73	0.66
C/N	134	348	6	11.36	10.87	0.77	0.74	108	7	11.85	12.71	0.73	0.67
TFM	138	709	9	12.26	13.47	0.75	0.68	242	6	11.91	12.52	0.73	0.68
N	134	40	7	10.66	11.23	0.75	0.71	168	7	11.27	11.59	0.72	0.67
CSH	69	195	5	13.27	16.27	0.81	0.75	399	4	14.73	16.18	0.75	0.69
SPAD	138	358	7	12.99	14.2	0.71	0.65	63	7	12.98	13.44	0.67	0.62
NDF	134	210	6	15.68	16.66	0.64	0.6	112	7	15.02	15.7	0.67	0.62
LA	139	203	3	23.92	28.02	0.33	0.31	175	5	19.93	21.83	0.4	0.31
PFM	138	43	7	16.17	17.97	0.65	0.59	113	5	12.98	13.47	0.68	0.64
LFM	138	1135	2	108.43	95.38	0.04	-0.01	711	12	21.7	18.95	0.43	0.2
LDM	137	1135	2	116.39	100.08	0.04	-0.04	711	12	19.5	19.22	0.44	0.2
LDMC	136	216	7	17.89	17.52	0.51	0.46	126	5	22.4	23.59	0.42	0.33
PDM	126	9	5	23.05	25.5	0.4	0.33	34	2	35.35	38.09	0.3	0.25
TDMC	126	33	5	18.3	19.25	0.5	0.45	711	17	13.21	17.13	0.66	0.4
PWC	126	1683	2	59.02	52.57	0.1	0.02	575	2	62.26	51.97	0.06	-0.01
TWC	126	29	4	20.8	21.73	0.46	0.42	9	8	20.54	20.06	0.41	0.28
PDMC	126	298	7	22.59	25	0.5	0.41	10	2	47.94	50.09	0.17	0.13
TDM	126	216	10	15.71	18.12	0.52	0.34	12	2	30.19	30.31	0.33	0.27
LWC	136	387	6	23.99	24.72	0.29	0.19	575	2	60.86	47.34	0.05	0
C	134	72	5	35.99	38.8	0.21	0.13	78	2	56.17	55.26	0.13	0.1
LS	126	557	4	33.19	34.14	0.21	0.14	175	3	32.25	32.89	0.2	0.12
SLA	137	37	2	45.4	47.47	0.18	0.15	242	3	38.93	43.66	0.2	0.13
					EnM						S-2		
PH	138	41	7	9.67	10.24	0.83	0.79	12	5	10.3	10.81	0.82	0.8
fPAR_abs	130	43	8	10.49	11.21	0.78	0.73	12	6	15.47	16.11	0.66	0.61
C/N	134	18	6	10.77	11.16	0.77	0.75	9	9	16.37	18.1	0.63	0.54
TFM	138	48	5	14.12	15.37	0.71	0.67	12	4	17.11	17.48	0.61	0.57
N	134	18	6	12.55	12.37	0.71	0.69	12	10	15.81	16.81	0.59	0.51
CSH	69	13	6	13.89	16.16	0.81	0.74	12	8	13.43	15.82	0.78	0.69
SPAD	138	17	7	15.66	16.82	0.67	0.63	9	5	19.5	20.68	0.58	0.53
NDF	134	129	9	15.59	16.51	0.7	0.6	12	4	16.93	17.56	0.61	0.57
LA	139	36	3	29.78	31.95	0.31	0.3	9	4	27.67	30.3	0.31	0.21
PFM	138	64	5	15.87	16.93	0.65	0.6	12	4	17.87	19.53	0.58	0.53
LFM	138	192	4	50.31	49.06	0.13	0.05	9	6	39.07	38.58	0.19	0.07
LDM	137	129	2	111.2	82.13	0.03	-0.03	12	3	82.14	78.29	0.06	-0.04
LDMC	136	64	7	21.52	21.39	0.44	0.34	9	2	33.83	27.25	0.17	0.09
PDM	126	9	2	35.78	36.88	0.3	0.26	9	4	31.92	31.35	0.3	0.22
TDMC	126	27	5	24.84	26.25	0.44	0.38	9	3	33.49	31.89	0.25	0.19
PWC	126	144	2	53.81	50.53	0.1	0.03	12	2	56.06	46.37	0.06	-0.02
TWC	126	12	6	19.08	20.65	0.5	0.43	10	2	46.46	49.49	0.2	0.15
PDMC	126	22	7	19.46	21.29	0.5	0.41	7	3	52.13	41.58	0.16	0.09
TDM	126	26	5	25.67	30	0.4	0.31	7	4	31.41	31.85	0.31	0.23
LWC	136	108	3	61.94	66.03	0.08	0.02	12	2	68	50.99	0.04	-0.02
C	134	9	3	43.27	41.36	0.14	0.09	7	5	54.34	55	0.14	0.05
LS	126	72	4	34.11	36.06	0.21	0.13	9	2	60.87	63.14	0.08	0.02
SLA	137	129	3	41.48	45.51	0.23	0.16	9	5	37.64	42.5	0.22	0.13

Table 4-3 (continued). PLSR model statistics for the 23 FTs by sensor, including number of observations (N), number of predictors (# pred.), number of latent vectors (# LV), normalized root mean squared errors in calibration (nRMSE$_{cal}$) and validation (nRMSE$_{val}$) as well as coefficients of determination in calibration (R²$_{cal}$) and validation (R²$_{val}$).

FT	N	# pred.	# LV	nRMSE$_{cal}$ [%]	nRMSE$_{val}$ [%]	R²$_{cal}$	R²$_{val}$	# pred.	# LV	nRMSE$_{cal}$ [%]	nRMSE$_{val}$ [%]	R²$_{cal}$	R²$_{val}$
					L 7						RE		
PH	138	5	3	22.07	20.79	0.49	0.44	5	2	38	39.72	0.06	0.02
fPAR$_{abs}$	130	6	3	26.88	28.54	0.43	0.37	5	3	46.44	41.2	0.07	-0.01
C/N	134	4	3	23.57	19.03	0.38	0.29	4	1	30.58	28.73	0.13	0.08
TFM	138	6	3	26.87	22.63	0.36	0.29	4	2	81.61	65.56	0.01	-0.03
N	134	6	3	29.79	22.64	0.23	0.14	5	3	41.02	44.17	0.12	0.07
CSH	69	5	3	19.71	20.51	0.56	0.49	3	1	104.45	88.38	0.01	-0.06
SPAD	138	5	4	20.9	21.45	0.5	0.46	5	3	27.58	25.08	0.26	0.23
NDF	134	5	4	21.57	21.68	0.44	0.43	5	2	46.29	37.86	0.02	-0.02
LA	139	5	2	60.69	58.61	0.13	0.08	5	2	82.97	56.5	0.05	0.06
PFM	138	4	3	29	27.15	0.37	0.31	5	3	51.04	39.51	0.05	-0.01
LFM	138	6	3	68.14	72.89	0.07	0	5	3	44.27	46.52	0.15	0.1
LDM	137	6	3	89.8	69.16	0.05	-0.05	5	3	66.1	52.03	0.08	-0.01
LDMC	136	4	1	127.64	124.41	0.04	0.01	3	1	48.36	44.86	0.13	0.1
PDM	126	5	3	29.25	26.88	0.28	0.19	5	3	50.96	43.45	0.06	-0.01
TDMC	126	4	1	49.9	51.27	0.19	0.17	3	1	43.57	40.93	0.21	0.18
PWC	126	4	1	205.09	178.86	0.01	-0.02	3	1	91.12	85.09	0.05	0.01
TWC	126	4	2	46.61	48.39	0.2	0.16	3	1	54.92	52.15	0.15	0.12
PDMC	126	4	2	51.25	51.69	0.17	0.11	3	1	64.17	58.78	0.11	0.07
TDM	126	5	3	27.16	26.03	0.31	0.22	4	1	92.03	88.14	0.02	-0.03
LWC	136	4	1	235.83	213.29	0.01	-0.01	3	1	70.39	55.47	0.04	-0.01
C	134	4	3	62.94	64.17	0.12	0.06	4	3	62.89	62.14	0.1	0.03
LS	126	6	2	60.46	68.61	0.07	0	5	2	208.3	83.86	0.01	-0.06
SLA	137	5	3	59.8	53.86	0.12	0.07	3	1	162.74	140.67	0.02	-0.02

4.3.3 Number of bands and spectral regions used for modelling of plant functional traits

For model calibration of only four FTs more than 50% of the bands of the FS 3 were used (Figure 4-3). This number increased to five for HH 2 and six for EnM. For S-2, L 7 and RE, all models included more than 50% of the respective sensor's spectral bands, which indicates that these sensors produced few redundant spectral information. However, low prediction accuracies of multispectral systems also show that important information for estimating FTs was missing.

The number of bands selected by *autopls* differed considerably between FTs (Table 4-3). Especially the models created using FS 3 and EnM data frequently integrated similar spectral regions and featured strong relations between the numbers of bands used for prediction (Figure 4-3). Different spectral bands were included in the models created based on HH 2 data because this system did not use the entire spectral range of the previously mentioned sensors. We did not display model results of the multispectral systems in Figure 4-3 because the majority of

bands was used for modelling all FTs. For predicting eight (PH, SPAD, LDMC, TFM, C/N-ratio, NDF-content, CSH and $fPAR_{abs}$) of the 13 FTs detected with acceptable or high accuracy ($R^2_{val} > 0.4$) using the FS 3 data, bands from all regions of the spectrum, i.e. UV and VIS (350-700 nm), NIR (700-1400 nm), nSWIR (1400-1800 nm) and fSWIR (1800-2360 nm), were used. For detecting TWC and PFM, backward selection identified only bands from the NIR and the nSWIR regions to provide significant additional information. NIR and fSWIR data did not carry no relevant information for improving model performance for predicting PDM and N-content. Solely nSWIR and fSWIR data were used for detecting PFM. No highly correlated spectral information was found for LA, PWC, LWC, SLA, LS-ratio, LFM, PDM, TDM, LDM and C-content, as $R^2_{val} < 0.4$ indicate.
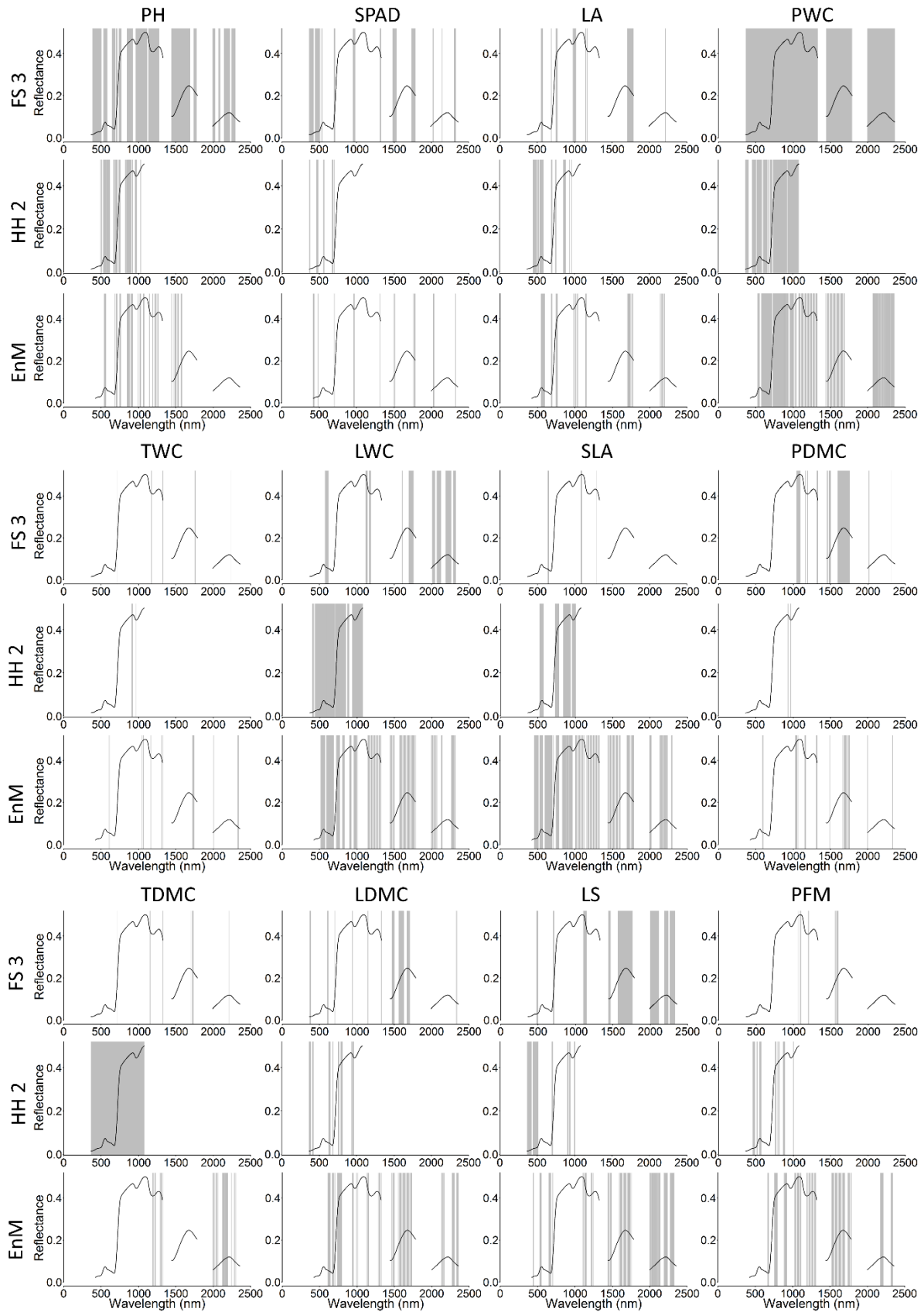
Figure 4-3. Bands selected in the PLSR models to detect the single FTs for FS 3, HH 2 and EnM sensors, indicated by vertical grey bars. The shown spectrum (black) is based on the average of all spectra simulated for the concerning sensor.
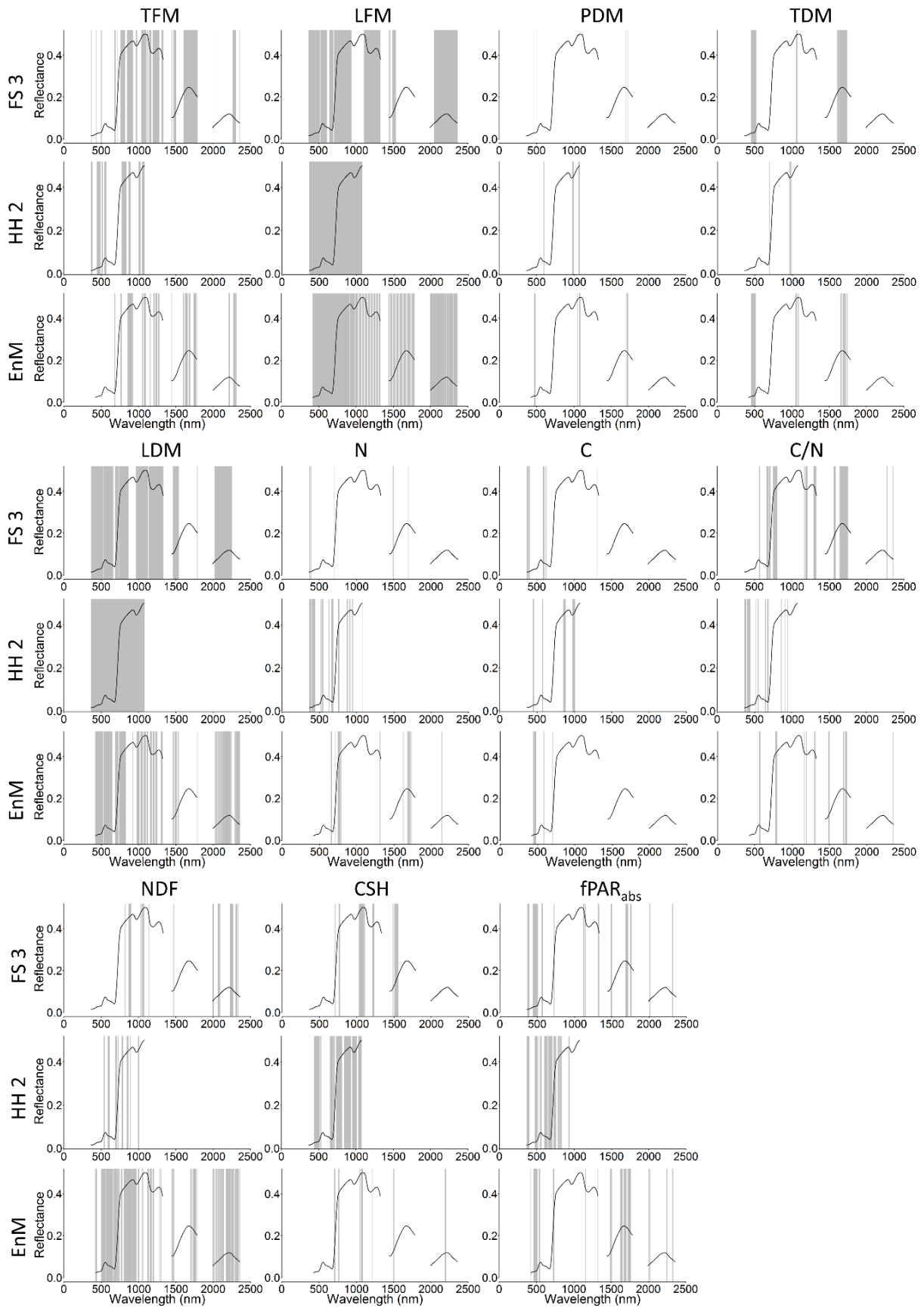
Figure 4.3 (continued). Bands selected in the PLSR models to detect the single FTs for FS 3, HH 2 and EnM sensors, indicated by vertical grey bars. The shown spectrum (black) is based on the average of all spectra simulated for the concerning sensor.

4.4   Discussion

In the presented study, the potentials of six RS sensors featuring various bandwidths, band numbers and spectral ranges were investigated for estimating 23 FTs of five different grassland communities. To exclude effects of sensor noise and differences in the spatial and radiometric resolution from our analysis, the entire spectral dataset was acquired using a FS 3 field spectroradiometer. Subsequently, the reflectance of a HH 2 field spectroradiometer as well as the reflectances of the satellite sensors EnM, S-2, L 7 and RE were simulated using their SRFs.

Acquisition of spectral measurements using a field spectroradiometer allowed us to (1) minimize BRDF effects by collecting spectral data several times on each day, (2) ensure that the spectral measurements and vegetation samples were solely acquired in the defined plots, (3) collect data with sufficient temporal resolution to cover all growing stages of vegetation and (4) use data collected at exactly the same time and vegetation stage for sensor comparison. The utilization of an automated crane system further ensured that samples were recorded from a constant viewing geometry, i.e. sensor angle and height (Stagakis et al., 2010). Collection of spectral signatures in three different positions within each plot has shown in previous tests to cover the naturally occurring variance in reflectance within plots and was thus representative of the plots' average spectral properties. Furthermore, 30 plant samples acquired within each plot were observed in preliminary trials to provide stable means of FTs. Thus, representative models on the plot level were created, although spectral measurements did not exactly resemble the positions of the plant samples. As the spatial resolutions of the real satellite sensors differ from those of our field spectroradiometer measurements, our results may only provide a gross estimation of real sensor accuracy. However, it was shown that up-scaling of models using field spectroradiometer data to satellite data is possible, when the spatial resolutions of both instruments are well above the size of individual plants (Psomas et al., 2011; Verrelst et al., 2009). As this requirement was fulfilled here, we are confident that the produced results provide an insight into the potential of the different satellite sensors for detecting grassland FTs.

PLSR was used to relate the response of remotely sensed information to changes in FTs. For validating our model results, LOO-CV was applied. This method may be affected by problems of overfitting for datasets with a large number of predictors (Allen, 1974), and thus tends to provide optimistic prediction accuracies, especially for hyperspectral data. However, it has the advantage to create almost unbiased estimations of target variables based on the input data (Luntz and Brailovsky, 1969). We further argue that overfitting in this study may be limited due to the creation of a relatively low number of latent vectors used in the PLSR models.

4.4.1   Overall Performances of the six tested sensors for detecting plant functional traits

Best suited for detecting FTs were hyperspectral sensors, i.e. FS 3, EnM and HH 2, which provided data to successfully estimate 13, 11 and ten FTs, respectively ($R^2_{val} > 0.4$). This confirms the results of previous studies that hyperspectral systems with narrow bands allow improved insights into variations in specific chemical compounds, compared to multispectral data (Blackburn, 1998; Stagakis et al., 2010; Thenkabail et al., 2004a). However, also simulated S-2 data featured R^2_{val} greater than 0.4 for estimating nine of the 23 tested FTs. Only three FTs were detected with acceptable accuracies using L 7 and none using simulated RE bands. This shows that these two sensors are not suitable for deriving FTs of mixed grasslands on a multitemporal scale.

The performance for detecting FTs was thereby related to a sensor's band number ($\lambda_{Pearson}=0.64$). Similar findings were made by Cho et al., (2007) and Thenkabail et al., (2004a), who observed that accuracies for detecting biophysical or chemical plant properties increase with the band number of a sensor. Furthermore, the presented study shows that the spectral range of a RS system strongly influences its performance for detecting FTs: although the HH 2 sensor exhibits a significantly higher number of bands (711) than EnM (192), slightly better (albeit non-significant) model fits were achieved by data based of the latter RS system. In addition, the 1683 bands of the FS 3 did not enable a significantly higher average accuracy than HH 2- and EnM-bands. We assume that the closely spaced bands of FS 3 and HH 2 did not carry additional information and hence did not lead to increased model accuracies (Broge and Leblanc, 2000; Thenkabail et al., 2000, 2002). Interestingly, although S-2 had a significantly lower number of bands (11), this sensor yielded comparable accuracies to hyperspectral sensors for some FTs (i.e. PH, NDF-content and CSH), but performed significantly weaker on average. This observation is supported by Kawamura et al., (2008), who showed that for detecting biomass and fiber content a high spectral detail in the red-edge region (as provided by S-2) may contain most of the important information. The low accuracies of models based on L 7 and RE data are caused by the missing spectral detail as well as by limitations in their spectral range.

These results show that hyperspectral data is needed for creating stable relations between spectral reflectance and the majority of investigated FTs. Thereby for estimating FTs, a very high band number (thousands of spectral bands) does not always perform significantly better than 100-200 bands located in relevant regions of the spectrum. Although, on average half-range (365-1075 nm) data were not significantly less suited for predicting FTs, improvements

in the strength of the relations for predicting a number of FTs were achieved by adding bands at longer wavelengths than 1075 nm.

4.4.2   Accuracies reached for detecting individual plant functional traits

FTs were predicted with R^2_{val} ranging between -0.06 and 0.8. As we collected datasets in species-rich grasslands, the accuracies for estimating many of the FTs were relatively low compared to other studies, which collected data in grass monocultures (cf. Table 1-3; Kawamura et al., 2008). Although, applying first derivations of spectra may enable improved model accuracies (cf. chapter 3), it was decided not to use this technique. Instead, we intended to compare raw reflectance of different sensors rather than to maximize model accuracies. Thereby, we created one single model using pooled data from 5 plant communities and six growths within three years. This was preferred because we aimed at creating models which were applicable to a large variety of plant communities, vegetation phenological stages, growths, years and weather conditions.

FTs related to biomass (i.e. PH, CSH, PFM and TFM), LAI (i.e. $fPAR_{abs}$), chlorophyll content (i.e. SPAD, N-content and C/N-ratio) and fiber content (i.e. NDF-content) were detected with relatively high accuracies. This was expected because several studies have shown that grassland biomass can be detected fairly well using remotely sensed data (Boschetti et al., 2007; Kawamura et al., 2008; Psomas et al., 2011). Furthermore, strong correlations between spectral data and LAI, chlorophyll content, N-content and NDF-content were also observed by other scientists (Darvishzadeh et al., 2008b; García-Ciudad et al., 1993; Hansen and Schjoerring, 2003; Ling et al., 2014; Redshaw et al., 1986; Rossini et al., 2012; Stagakis et al., 2010).

FTs related to dry matter content (i.e. PDMC, TDMC and LDMC) as well as to water content (i.e. PWC, TWC and LWC) were more difficult to detect. We assume that rain events before plant sample collection may have severely influenced the water content of samples because these events attached large amounts of adhesive water to the plant leaves. This adhesive water was not detected isolated from water contained in the plants using RS information. Similarly, adhesive water may have also been responsible for the low model accuracies for detecting LFM. Furthermore, PDM, TDM and LDM were difficult to detect. We argue that the estimation of these FTs was exacerbated because dry matter of senesced vegetation resembles dry matter of green vegetation. However, the spectral signatures between senescent and green vegetation distinctly differ. As LS-ratio was calculated based on LDM and TDM, low accuracy for detecting this FT is reasonable. C-content varied only marginally between treatments and over

time and these changes appeared to be too small to be evident in the spectral signatures, as bad performance of models for detecting this FT indicate. Low model accuracies for detecting LA and SLA were also expected because LA was measured on individual plants, regardless of stand density (which also plays an important role for the relations between LA and spectra). Poor performances to estimate SLA using remotely sensed data are also reported in Homolová et al., (2013).

4.5   Conclusions

Spectral resolution and spectral range – these two parameters have a strong impact on the performance of RS systems for detecting FTs. We showed that hyperspectral remotely sensed information allows significantly higher accuracies for deriving FTs than multispectral information. Thus, up to 13 of 23 tested FTs could be estimated with acceptable or high accuracies ($R^2_{val} > 0.4$) using hyperspectral RS data. By simulating different hyperspectral and multispectral RS sensors, it was shown that with decreasing band number, the amount of successfully detected FTs significantly dropped. However, more important than band number was that the spectral bands were located in relevant sections of the spectral range between 350 and 2500 nm. Among the most accurately detected FTs were those related to biomass, LAI, chlorophyll content or fiber content, whereas FTs related to plant water content, dry matter content, leaf area, leaf-stem ratio or C-content were more difficult to detect.

We conclude that modern hyperspectral satellite sensors featuring a high spectral, spatial and temporal resolution as well as a broad spectral range (such as EnM) have the potential to monitor changes in many important FTs in the spatial domain. These products can contain per-pixel estimates on the status of single FTs, which may be further analyzed in the ecological context, e.g. for indicating shifts in the growth conditions due to management or climate, for deducing other site attributes, such as Ellenberg indicator values, or for creating maps of plant C-S-R strategy types. Furthermore, successful monitoring of FTs and the supply of spatially contiguous information on grassland status are of large value for precision agriculture and may thus add to a more sustainable agricultural use of these ecosystems.

The next steps in research should aim at transferring models based on field spectrometry to real satellite imagery. An important question to be answered is if large components of noise occurring when collecting earth observation data with a very high spectral and spatial resolution from space can be diminished to recognize subtle changes in the reflectance of plant canopies caused by variations in the FTs.

5   General conclusions and outlook

In Central Europe, centuries of agricultural use of grasslands have led to the development of unique ecosystems. These represent the habitat for many endemic species and provide important ecosystem services, e.g. as a source of fodder for livestock. The current condition of grassland ecosystems can only be maintained if their management is adapted to increasing pressures caused by changes in climate and in the intensities of use. However, plant communities found in these ecosystems are complex in their floristic composition and their responses to management actions. As the conventional taxonomic approach based on species classification has shown to be little effective for assessing changes in the state, quality and health grassland vegetation, ecologists and agronomists use FTs. Current techniques for estimating many grassland FTs require a manual and destructive data collection and cause high monetary and temporal costs. Thus, agronomists and ecologists are seeking for novel methods for solving these problems. RS may provide a universal solution to derive estimates of FTs on local and regional scale with high temporal resolution.

In this thesis, the potential of RS for monitoring changes in the FTs of grassland was explored. Under progressive climate change and transformations in grassland use, such estimates are necessary to support grassland managers to conserve the diversity and productivity of these ecosystems and to prevent negative effects on the underlying soils and adjacent water bodies.

5.1   How can we distinguish grassland intensity levels using remote sensing?

Depending on the given biotic and abiotic site-conditions, grassland communities are composed of characteristic stakes of plant species pursuing certain CSR-strategies (Grime, 1977). Under temperate-maritime climate conditions, species rapidly developing in LA and biomass (i.e. species belonging to the competitive strategy (C) type) are dominant in nutrient-rich habitats. In contrast, species developing slower in these parameters, but featuring a long reproductive phase and low SLA (i.e. species of the conservative strategy (S) type) are characteristic for nutrient-limited habitats. Accordingly, plants belonging to different PFTs and featuring differences in their FTs predominate, depending on the soil nutrient status at a site. The optical characteristics of CSR-strategy types and PFTs differ from each other according to their FTs. In other words, intensity levels of grasslands, are dominated by different PFTs, which consequently feature different expressions of FTs.

As VIs respond to these differences in the FTs, they can be used to distinguish grassland intensity levels. However, expressions of numerical FTs may vary throughout a growing

season. The performance of each VI for separating grassland intensity levels thus depends on its sensitivity to certain FTs that differ between grassland communities at a given phenological state. For example, VIs sensitive to green LA and green biomass can reliably be used to distinguish grasslands as long as the communities feature significant differences in these FTs. However, during some phases of phenological development, plant communities may exhibit similar values in these variables. At these phases, VIs sensitive to other FTs (e.g. to plant water content or fiber content), may allow a more successful classification. Consequently, mapping studies of grassland vegetation using single VIs require a prior assessment of their individual phenological state to identify the best VIs for grassland separation.

To overcome this drawback of single VIs, a multiple VI approach was developed using random forests. This algorithm selects the ideal set of VIs for distinguishing different grassland intensity levels from each other according to their phenological state and allows a relatively stable grassland classification. Thus, this approach helps to improve classification accuracies and, at the same time, simplifies the selection of efficient VIs for distinguishing grassland intensity levels.

5.2   Monitoring of plant functional traits using remote sensing – lessons learned

Hyperspectral RS has shown to be an effective tool for assessing changes in the FTs of different grassland intensity levels throughout the entire growing season (cf. chapter 3). As non-destructive, cost-efficient and time-saving technique, field spectroscopy enables grassland managers to record spectral data on demand. Field spectroradiometers can be transported and used even at remote locations and are of great value for improving grassland management techniques on a local scale. Additionally, our results suggest that RS of FTs for small-scale agriculturally used areas may also be possible using UAVs, which can collect imagery featuring a high spatial and spectral resolution from low flight altitudes. FTs of larger areas may best be monitored using space-borne platforms, which provide hyperspectral data with lower spatial resolutions.

To enhance information content of RS data to detect FTs, different transformations of spectra as well as analysis techniques can be applied. Spectral derivations have shown to allow improved estimates of FTs compared to raw spectra and continuum removed spectra and may be used to limit bidirectional reflectance effects occurring in multitemporal datasets. Although difficulties remain in understanding the absorbance, transmittance and reflectance processes existing in the studied species-rich (i.e. complex) grassland canopies, our empirical approach

using PLSR has shown to provide moderately to highly accurate models for many important FTs. Furthermore, our results show that the flexible algorithm of PLSR allows creating one statistical model for assessing one FT of different grassland communities throughout entire growing seasons. These findings also suggests that the models are transferable between different grassland canopies and consequently also to other regions. In addition, it is shown that RS is an efficient technique to monitor FT development.

However, accuracies of the created models were highly variable. Using spectral reflectance measurements, FTs related to plant morphology (i.e. PH and fPAR$_{abs}$), biomass (i.e. CSH and TFM) and chlorophyll content (i.e. N-content, C/N-ratio and SPAD value) as well as FTs related to NDF-content and LA can be estimated with high accuracy ($R^2_{val} > 0.6$). Moderate accuracies (≥ 0.4 in R^2_{val}) were reached for estimating PFM, LFM, LDM and LDMC. Finally, PWC, TWC, LWC, PDMC, TDMC, PDM, TDM, C-content, L-S-ratio and SLA were detected with low accuracies ($R^2_{val} < 0.4$).

These findings are of great importance for grassland scientists because they underline the potential of RS to provide spatiotemporal data on grassland development. Such datasets are currently rarely available but urgently needed. Combining RS with ecological theory may thus contribute to a sustainable use of grassland ecosystems.

5.3 How to estimate numerical plant functional traits using hyperspectral remote sensing

As stated in chapter 3, an estimation of many (13 of 23 tested) important numerical FTs of grassland communities is possible by relating their manually measured expressions to hyperspectral RS data. To allow such estimates over entire growing seasons, the following procedures should be conducted:

1. The first step is the collection of RS data and the manual measurement of FTs. To allow a monitoring of FTs over time, it is necessary to collect spectral signatures and FT expressions over the entire growing seasons of several years and to integrate these observations in flexible statistical models, e.g. using PLSR. It is thereby important that the manual samples and RS data match in time to ensure that both datasets were collected at the same phenological state. To consider the spatial heterogeneity naturally occurring within grassland communities, a number of both, RS estimates and manual samples of FTs, should be collected within each vegetation stand at each sampling date. Furthermore, RS systems measure reflectance typically above the spatial extent of single grasses or forbs. Therefore,

FTs of a number of plants should be recorded in order to produce stable estimates of community mean FTs.

2. The strength of the relations between RS data and FTs could be increased by using first derivation spectra. We assume that BRDF effects and variations in incoming solar radiation were diminished by this technique, which lead to a more efficient use of spectral information. To delete random noise, smoothing of the spectral signatures (e.g. according to Savitzky and Golay, 1964) and a correction of sensor offset (i.e. by splice correction, cf. Stevens and Ramirez-Lopez, 2013) are also recommended.

3. PLSR was identified as an efficient algorithm to relate the spectral reflectance of grassland canopies to manual measurements of FTs. This algorithm can solve problems related to the high dimension of hyperspectral RS data, such as effects of overfitting. Furthermore, backward selection of predictors removes redundant information or bands uncorrelated to the target variables (i.e. FTs) from the models and thus limits effects of multicollinearity. In addition, PLSR was flexible enough to produce one model for relating RS data to a FT and to cover different plant communities throughout the growing seasons of several years.

4. For model calibration and validation, LOO-CV was identified as appropriate approach. As models developed using this method may be subject to overfitting (i.e. a too positively calculated model accuracy caused by a high number of integrated independent variables), the dimensionality of spectral data was minimized using LVs. Using LOO-CV, we were thus able to create a balanced assessment of the sets of relevant bands for detecting each FT and to compare model accuracies produced by different RS sensors efficiently.

5.4 Which spectral range and resolution are suitable for remote sensing of plant functional traits?

Although large efforts have been made in recent years to detect grassland FTs using field spectroradiometers, it remained unclear, which available satellite sensors provide the potential to produce contiguous spatial information in this domain. In chapter 4 of this thesis, this topic is addressed. It was shown that traditional broadband satellite sensors, such as RE and L7, are not suited for monitoring FTs due to their low spectral resolutions (i.e. low band numbers and broad bandwidths) and their limited spectral ranges. Nevertheless, modern multispectral systems providing higher spectral resolutions and covering a wider range of wavelengths (such as S-2) may allow improved results and enable moderate to high accuracies for mapping selected FTs.

However, new-generation hyperspectral satellite sensors, such as EM (planned launch in 2019), have the greatest potential for providing spatiotemporal information on important FTs. These systems may even produce comparable accuracies for estimating many important FTs to full-range field spectroradiometers (providing the 10-fold number of spectral bands) and mostly higher accuracies than half-range field spectroradiometers (providing the 5-fold number of spectral bands). For the design of future hyperspectral sensors, these findings suggest that pure band number is not the main determinant for producing highly accurate estimates of FTs. In fact, it is more important to cover relevant spectral regions within a broad spectral range. Thereby, a number of approximately 200 bands distributed across the spectral range between 350-2500 nm is suitable for mapping many FTs with moderate to high accuracy.

New imaging spectrometers, such as EnM or HyspIRI, may thus allow observing changes in FTs due to transitions in management on the short-term as well as to variations in climate on the long-term. Furthermore, hyperspectral RS may provide information on the nutrient status of grasslands at different spatial scales. Such datasets are of large value for precision agriculture because they can support grassland managers in applying fertilizers according to the identified nutrient-demand of the plants and can consequently help to maximize yields. Finally, such precise dosage of nutrients will contribute to maintaining the soil quality and species diversity of grassland ecosystems and, at the same time, prevent negative side effects on adjacent water bodies.

5.5   Recommendations for future studies and outlook

Although it was shown that RS may allow to gather insights into the status and functional properties of grassland, more research is needed to map the current distribution of different grassland communities and to monitor changes in their functioning on a global scale.

As stated in chapter 2, distinguishing different intensity levels of grassland is possible using the proposed multiple VI approach. For developing and testing this approach, clearly separable vegetation communities were used. However, when applying airborne or satellite-borne RS systems in classification studies, problems related to mixed pixels (i.e. a mixture of land-cover classes, e.g. grassland communities, occurring within one pixel) exist. These problems may even increase when RS systems featuring coarse spatial resolutions are used for mapping the global distribution of grassland types. A solution for the mixed pixel problem may provide multiple endmember spectral mixture analysis (MESMA). This technique can be applied to identify the proportions of different grassland communities within one pixel. Using MESMA it

is thus possible to create estimates of land-cover-types on the sub-pixel level and consequently to produce maps of the occurrence of grassland communities, which are also comparable across different spatial scales.

To detect the FTs of the different studied grassland intensity levels using RS, an empirical modelling approach based on PLSR was used. The results, as given in chapter 3, demonstrate that the detection of many (13 of 23 tested) grassland FTs is possible using field spectrometry. Thereby, the developed PLSR-models have shown to be valid over a wide range of European grasslands and phenological stages at one experimental site. However, it still needs to be addressed if and how these models can be transferred between different regions and climatic conditions in order to enable scientists to detect changes in the FTs of grassland communities globally and on different scales.

Physically based RTMs may allow such an application of RS data for detecting FTs over a wide range of grassland types and environmental (i.e. climate and soil) conditions. For example, recent studies have attained promising results in the derivation of different FTs, such as LAI and biomass, of species-rich grassland canopies using RTMs (e.g. Atzberger et al., 2013; Darvishzadeh et al., 2011; Kattenborn et al., 2017). Thus, RTMs may provide the potential to estimate some of those ten FTs, which were not successfully detected using PLSR. However, much research still needs to be undertaken to explore the full potential of these modelling approaches for estimating FTs.

Besides the transferability of models between regions, it further remains unanswered, which impact the spatial resolution of a RS sensor has on its possible accuracy for estimating FTs. For this purpose, UAVs may provide valuable datasets because they can produce imagery from different altitudes, i.e. featuring different spatial resolutions, using the same sensor. Such scaling studies may represent the next step for transferring models developed using ground-based or airborne RS data to satellite systems.

In addition, future research may also focus on investigating the potential of active RS sensors, such as radar and lidar, for detecting FTs. High accuracies using these systems were especially reached for retrieving the water content and the morphological properties of vegetation (cf. Bork and Su, 2007; Jones and Vaughan, 2012). Thus, following studies may investigate the fusion of optical and radar or lidar RS data in order to increase the accuracies for detecting many FTs.

Although first attempts have been made to connect ecological theory with RS data, it is yet not clearly identified how direct relationships between these two fields in research can be

established. The concept of "optical types" stated in Ustin and Gamon, (2010) was a first approach on connecting PFTs (i.e. plants exhibiting similar sets of FTs) with remotely sensed information. In this respect, it is still subject to research how strongly certain FTs influence the spectral signal and so determine the classification of a plant as a specific optical type. Thus, enabling clearly defined sets of FTs affecting the optical type of a plant may further add to a more direct applicability of RS for ecological studies. Thereby, it needs to be considered which FTs are detectable by RS and how important these FTs are for assessing ecosystem functioning.

Finally, the use of RS in grassland ecology needs to be supported and promoted. Therefore, RS data or RS-based estimates of FTs need to be made available to the concerning stakeholders, including scientists (i.e. agronomists and ecologists), government authorities and farmers. Furthermore, programs need to be established, which aim at assessing changes in grassland FTs in the spatial domain and on an operational scale. Such estimates may add to a warning system, which identifies unintended trends in grassland development and enables grassland managers and legislative institutions to undertake measures preventing negative effects on grassland health, production and species-richness. Thus, RS can support an efficient agricultural valorization of grassland ecosystems and at the same time enable their sustainable use.

6 References

Adams, J.B., Sabol, D.E., Kapos, V., Almeida Filho, R., Roberts, D.A., Smith, M.O., Gillespie, A.R., 1995. Classification of multispectral images based on fractions of endmembers: application to land-cover change in the Brazilian Amazon. Remote Sens. Environ. 52, 137–154. doi:10.1016/0034-4257(94)00098-8

Adler, P., Raff, D., Lauenroth, W., 2001. The effect of grazing on the spatial heterogeneity of vegetation. Oecologia 128, 465–479.

Aerts, R., Chapin III, F.S., 2000. The mineral nutrition of wild plants revisited: re-evaluation of processes and patterns. Adv. Ecol. Res. 30, 1–67. doi:http://dx.doi.org/10.1016/S0065-2504(08)60016-1

Al Haj Khaled, R., Duru, M., Theau, J.P., Plantreux, S., Cruz, P., 2005. Variation in leaf traits through seasons and N-availability levels and its consequences for ranking grassland species. J. Veg. Sci. 16, 391–398.

Allen, D.M., 1974. The relationship between variable selection and data agumentation and a method for prediction. Technometrics 16, 125–127. doi:10.2307/1267500

Anderson, M.C., Neale, C.M.U., Li, F., Norman, J.M., Kustas, W.P., Jayanthi, H., Chavez, J., 2004. Upscaling ground observations of vegetation water content, canopy height, and leaf area index during SMEX02 using aircraft and Landsat imagery. Remote Sens. Environ. 92, 447–464. doi:10.1016/j.rse.2004.03.019

Aragón, R., Oesterheld, M., 2008. Linking vegetation heterogeneity and functional attributes of temperate grasslands through remote sensing. Appl. Veg. Sci. 11, 117–130. doi:10.1111/j.1654-109X.2008.tb00210.x

ASD Inc. [Analytical Spectral Devices Inc.] (ed.), 2010. Fieldspec® user manual. ASD Inc., Boulder, CO, USA.

Asner, G.P., 1998. Biophysical and biochemical sources of variability in canopy reflectance. Remote Sens. Environ. 64, 234–253. doi:10.1016/S0034-4257(98)00014-5

Asner, G.P., Heidebrecht, K.B., 2003. Imaging spectroscopy for desertification studies: Comparing AVIRIS and EO-1 Hyperion in Argentina drylands. IEEE Trans. Geosci. Remote Sens. 41, 1283–1296.

Asner, G.P., Martin, R.E., 2009. Airborne spectranomics: mapping canopy chemical and taxonomic diversity in tropical forests. Front. Ecol. Environ. 7, 269–276.

Atzberger, C., Darvishzadeh, R., Schlerf, M., le Maire, G., 2013. Suitability and adaptation of PROSAIL radiative transfer model for hyperspectral grassland studies. Remote Sens. Lett. 4, 55–64. doi:https://doi.org/10.1016/j.rse.2007.12.003

Atzberger, C., Richter, K., Vuolo, F., Darvishzadeh, R., Schlerf, M., 2011. Why confining to vegetation indices? Exploiting the potential of improved spectral observations using radiative transfer models. Presented at the SPIE: Remote Sensing for Agriculture, Ecosystems, and Hydrology XIII, Prague, Czech Republic, pp. Q1–Q16. doi:doi:10.1117/12.898479

Bacour, C., Baret, F., Béal, D., Weiss, M., Pavageau, K., 2006. Neural network estimation of LAI, fAPAR, fCover and LAI×Cab, from top of canopy MERIS reflectance data: Principles and validation. Remote Sens. Environ. 105, 313–325. doi:10.1016/j.rse.2006.07.014

Bai, Y., Abouguendia, Z., Redmann, R.E., 2001. Relationship between plant species diversity and grassland condition. J. Range Manag. 54, 177–183. doi:10.2307/4003180

Bailey, D.W., Gross, J.E., Laca, E.A., Rittenhouse, L.R., Coughenour, M.B., Swift, D.M., Sims, P.L., 1996. Mechanisms that result in large herbivore grazing distribution patterns. J. Range Manag. 49, 386–400.

Barnes, J.D., Balaguer, L., Manrique, E., Elvira, S., Davison, A.W., 1992. A reappraisal of the use of DMSO for the extraction and determination of chlorophylls a and b lichens and higher plants. Environ. Exp. Bot. 32, 85–100. doi:10.1016/0098-8472(92)90034-Y

Barnsley, M., Allison, D., Lewis, P., 1997. On the information content of multiple view angle (MVA) images. Int. J. Remote Sens. 18, 1937–1960.

Bauer, M.E., Daughtry, C.S.T., Vanderbilt, V., 1981. Spectral-agronomic relationships of corn, soybean and wheat canopies. Report SR-P1-04187. Laboratory for Applications of Remote Sensing, Purdue University, West Lafayette, IN, USA.

BlackBridge (ed.), 2012. Spectral response curves of the RapidEye Sensor [WWW Document]. URL http://blackbridge.com/rapideye/upload/Spectral_Response_Curves.pdf (accessed 1.20.16).

Blackburn, G.A., 1998. Spectral indices for estimating photosynthetic pigment concentrations: a test using senescent tree leaves. Int. J. Remote Sens. 19, 657–675. doi:10.1080/014311698215919

Blackburn, G.A., Steele, C.M., 1999. Towards the remote sensing of matorral vegetation physiology: relationships between spectral reflectance, pigment, and biophysical characteristics of semiarid bushland canopies. Remote Sens. Environ. 70, 278–292.

Blair, J., Nippert, J., Briggs, J., 2014. Grassland ecology, in: Ecology and the Environment. The Plant Sciences 8. Springer, New York, USA, pp. 389–422.

Bolster, K.L., Martin, M.E., Aber, J.D., 1996. Determination of carbon fraction and nitrogen concentration in tree foliage by near infrared reflectances: a comparison of statistical methods. Can. J. For. Res. 26, 590–600. doi:10.1139/x26-068

Bork, E.W., Su, J.G., 2007. Integrating LIDAR data and multispectral imagery for enhanced classification of rangeland vegetation: A meta analysis. Remote Sens. Environ. 111, 11–24. doi:http://doi.org/10.1016/j.rse.2007.03.011

Boschetti, M., Bocchi, S., Brivio, P.A., 2007. Assessment of pasture production in the Italian Alps using spectrometric and remote sensing information. Agric. Ecosyst. Environ. 118, 267–272. doi:10.1016/j.agee.2006.05.024

Brantley, S.T., Zinnert, J.C., Young, D.R., 2011. Application of hyperspectral vegetation indices to detect variations in high leaf area index temperate shrub thicket canopies. Remote Sens. Environ. 115, 514–523. doi:10.1016/j.rse.2010.09.020

Breiman, L., 2001. Random forests. Mach. Learn. 45, 5–32. doi:10.1023/A:1010933404324

Broge, N.H., Leblanc, E., 2000. Comparing prediction power and stability of broadband and hyperspectral vegetation indices for estimation of green leaf area index and canopy chlorophyll density. Remote Sens. Environ. 76, 156–172. doi:10.1016/S0034-4257(00)00197-8

Bryant, J.P., Chapin, F.S., Klein, D.R., 1983. Carbon/nutrient balance of boreal plants in relation to vertebrate herbivory. Oikos 40, 357–368. doi:10.2307/3544308

Butterfield, H.S., Malmström, C.M., 2009. The effects of phenology on indirect measures of aboveground biomass in annual grasses. Int. J. Remote Sens. 30, 3133–3146. doi:10.1080/01431160802558774

Campbell, J.B., Wynne, R.H. (Eds.), 2011. Introduction to remote sensing. Fifth edition. Guilford Publications.

Carter, G.A., 1998. Reflectance wavebands and indices for remote estimation of photosynthesis and stomatal conductance in pine canopies. Remote Sens. Environ. 63, 71–72.

Carter, G.A., 1994. Ratios of leaf reflectances in narrow wavebands as indicators of plant stress. Remote Sens. 15, 697–703.

Carter, G.A., Knapp, A.K., 2001. Leaf optical properties in higher plants: linking spectral characteristics to stresses and chlorophyll concentration. Am. J. Bot. 88, 677–684.

Cebrian, J., Williams, M., McLelland, J., Valiela, I., 1998. The dependence of heterotrophic consumption and C accumulation on autotrophic nutrient content in. Ecol. Lett. 1, 165–170.

Chambers, J.M., Hastie, T.J., 1992. Statistical models in S. Chapman & Hall, Boca Raton, FL, USA.

Chen, J., Gu, S., Shen, M., Tang, Y., Matsushita, B., 2009. Estimating aboveground biomass of grassland having a high canopy cover: an exploratory analysis of in situ hyperspectral data. Int. J. Remote Sens. 30, 6497–6517. doi:10.1080/01431160902882496

Cho, M.A., Skidmore, A., Corsi, F., Van Wieren, S.E., Sobhan, I., 2007. Estimation of green grass/herb biomass from airborne hyperspectral imagery using spectral indices and partial least squares regression. Int. J. Appl. Earth Obs. Geoinf. 9, 414–424. doi:10.1016/j.jag.2007.02.001

Cho, M.A., van Aardt, J., Main, R., Majeke, B., 2010. Evaluating variations of physiology-based hyperspectral features along a soil water gradient in a Eucalyptus grandis plantation. Int. J. Remote Sens. 31, 3143–3159. doi:10.1080/01431160903154390

Chong, I.-G., Jun, C.-H., 2005. Performance of some variable selection methods when multicollinearity is present. Chemom. Intell. Lab. Syst. 78, 103–112. doi:10.1016/j.chemolab.2004.12.011

Chytrý, M., Hejcman, M., Hennekens, S.M., Schellberg, J., 2009. Changes in vegetation types and Ellenberg indicator values after 65 years of fertilizer application in the Rengen Grassland Experiment, Germany. Appl. Veg. Sci. 12, 167–176.

Cingolani, A.M., Posse, G., Collantes, M.B., 2005. Plant functional traits, herbivore selectivity and response to sheep grazing in Patagonian steppe grasslands. J. Appl. Ecol. 42, 50–59. doi:10.1111/j.1365-2664.2004.00978.x

Cingolani, A.M., Renison, D., Zak, M.R., Cabido, M.R., 2004. Mapping vegetation in a heterogeneous mountain rangeland using Landsat data: an alternative method to define and classify land-cover units. Remote Sens. Environ. 92, 84–97. doi:10.1016/j.rse.2004.05.008

Cleveland, W.S., Grosse, E., Shyu, W.M., 1992. Local regression models, in: Chambers, J.M., Hastie, T.J. (Eds.), Statistical Models in S. Chapman & Hall, Boca Raton, FL, USA, pp. 309–377.

Clevers, J.G.P.W., Kooistra, L., Schaepman, M.E., 2008. Using spectral information from the NIR water absorption features for the retrieval of canopy water content. Int. J. Appl. Earth Obs. Geoinformation 10, 388–397. doi:10.1016/j.jag.2008.03.003

Cochrane, M.A., 2000. Using vegetation reflectance variability for species level classification of hyperspectral data. Int. J. Remote Sens. 21, 2075–2087.

Coley, P.D., Bryant, J.P., Chapin III, F.S., 1985. Resource availability and plant antiherbivore defense. Science 230, 895–900.

Cornelissen, J.H.C., Lavorel, S., Garnier, E., Diaz, S., Buchmann, N., Gurvich, D.E., Reich, P.B., ter Steege, H., Morgan, H.D., van der Heijden, M.G.A., Pausas, J.G., Poorter, H., 2003. A handbook of protocols for standardised and easy measurement of plant functional traits worldwide. Aust. J. Bot. 51, 335–380.

Cousins, S.A.O., Lavorel, S., Davies, I., 2003. Modelling the effects of landscape pattern and grazing regimes on the persistence of plant species with high conservation value in grasslands in south-eastern Sweden. Landsc. Ecol. 18, 315–332. doi:10.1023/A:1024400913488

Craine, J.M., Froehle, J., Tilman, D.G., Wedin, D.A., Chapin, I., F.S., 2001. The relationships among root and leaf traits of 76 grassland species and relative abundance along fertility and disturbance gradients. Oikos 93, 274–285. doi:10.1034/j.1600-0706.2001.930210.x

Craine, J.M., Lee, W.G., Bond, W.J., Williams, R.J., Johnson, L.C., 2005. Environmental constraints on a global relationship among leaf and root traits of grasses. Ecology 86, 12–19.

Craine, J.M., Tilman, D., Wedin, D., Reich, P., Tjoelker, M., Knops, J., 2002. Functional traits, productivity and effects on nitrogen cycling of 33 grassland species. Funct. Ecol. 16, 563–574. doi:10.1046/j.1365-2435.2002.00660.x

Cruz, P., Duru, M., Therond, O., Theau, J.P., Ducourtieux, C., Jouany, C., Al Haj Khaled, R., Ansquer, P., 2002. Une nouvelle approche pour caractériser les prairies naturelles et leur valeur d'usage. Fourrages 172, 335–354.

Curran, P.J., 1994. Imaging spectroscopy. Prog. Phys. Geogr. 18, 247–266.

Curran, P.J., 1989. Remote sensing of foliar chemistry. Remote Sens. Environ. 30, 271–278. doi:10.1016/0034-4257(89)90069-2

Danson, F.M., Steven, M.D., Malthus, T.J., Clark, J.A., 1992. High-spectral resolution data for determining leaf water content. Int. J. Remote Sens. 13, 461–470. doi:10.1080/01431169208904049

Darvishzadeh, R., Atzberger, C., Skidmore, A., Schlerf, M., 2011. Mapping grassland leaf area index with airborne hyperspectral imagery: a comparison study of statistical approaches and inversion of radiative transfer models. ISPRS J. Photogramm. Remote Sens. 66, 894–906. doi:10.1016/j.isprsjprs.2011.09.013

Darvishzadeh, R., Skidmore, A., Atzberger, C., van Wieren, S., 2008a. Estimation of vegetation LAI from hyperspectral reflectance data: effects of soil type and plant architecture. Int. J. Appl. Earth Obs. Geoinformation 10, 358–373. doi:10.1016/j.jag.2008.02.005

Darvishzadeh, R., Skidmore, A., Schlerf, M., Atzberger, C., Corsi, F., Cho, M., 2008b. LAI and chlorophyll estimation for a heterogeneous grassland using hyperspectral measurements. ISPRS J. Photogramm. Remote Sens. 63, 409–426. doi:10.1016/j.isprsjprs.2008.01.001

Datt, B., 1999. A new reflectance index for remote sensing of chlorophyll content in higher plants: Tests using eucalyptus leaves. J. Plant Physiol. 154, 30–36.

Daughtry, C.S.T., Walthall, C.L., Kim, M.S., Brown de Colstoun, E., McMurtey, J.E., 2000. Estimating corn leaf chlorophyll concentration from leaf and canopy reflectance. Remote Sens. Environ. 74, 229–239. doi:10.1016/S0034-4257(00)00113-9

De Bello, F., Thuiller, W., Lepš, J., Choler, P., Clément, J.-C., Macek, P., Sebastià, M.-T., Lavorel, S., 2009. Partitioning of functional diversity reveals the scale and extent of trait convergence and divergence. J. Veg. Sci. 20, 475–486. doi:10.1111/j.1654-1103.2009.01042.x

DeFries, R.S., Field, C.B., Fung, I., Justice, C.O., Los, S., Matson, P.A., Matthews, E., Mooney, H.A., Potter, C.S., Prentice, K., 1995. Mapping the land surface for global atmosphere-biosphere models: Toward continuous distributions of vegetation's functional properties. J. Geophys. Res. Atmospheres 100, 20867–20882.

Díaz, S., Hodgson, J.G., Thompson, K., Cabido, M., Cornelissen, J.H.C., Jalili, A., Montserrat-Martí, G., Grime, J.P., Zarrinkamar, F., Asri, Y., Band, S.R., Basconcelo, S., Castro-Díez, P., Funes, G., Hamzehee, B., Khoshnevi, M., Pérez-Harguindeguy, N., Pérez-Rontomé, M.C., Shirvany, A., Vendramini, F., Yazdani, S., Abbas-Azimi, R., Bogaard, A., Boustani, S., Charles, M., Dehghan, M., de Torres-Espuny, L., Falczuk, V., Guerrero-Campo, J., Hynd, A., Jones, G., Kowsary, E., Kazemi-Saeed, F., Maestro-Martínez, M., Romo-Díez, A., Shaw, S., Siavash, B., Villar-Salvador, P., Zak, M.R., Rapson, G., 2004. The plant traits that drive ecosystems: evidence from three continents. J. Veg. Sci. 15, 295–304. doi:10.1658/1100-9233(2004)015[0295:TPTTDE]2.0.CO;2

Díaz, S., Lavorel, S., De Bello, F., Quétier, F., Grigulis, K., Robson, T.M., 2007a. Incorporating plant functional diversity effects in ecosystem service assessments. Proc. Natl. Acad. Sci. USA 104, 20684–20689.

Díaz, S., Lavorel, S., McIntyre, S., Falczuk, V., Casanoves, F., Milchunas, D.G., Skarpe, C., Rusch, G., Sternberg, M., Noy-Meir, I., 2007b. Plant trait responses to grazing–a global synthesis. Glob. Change Biol. 13, 313–341.

Diner, D.J., Asner, G.P., Davies, R., Knyazikhin, Y., Muller, J.-P., Nolin, A.W., Pinty, B., Schaaf, C.B., Stroeve, J., 1999. New directions in earth observing: scientific applications of multiangle remote sensing. Bull. Am. Meteorol. Soc. 80, 2209–2228.

Disney, M., Lewis, P., Saich, P., 2006. 3D modelling of forest canopy structure for remote sensing simulations in the optical and microwave domains. Remote Sens. Environ. 100, 114–132. doi:10.1016/j.rse.2005.10.003

Duru, M., Ansquer, P., Jouany, C., Theau, J.P., Cruz, P., 2010. Comparison of methods for assessing the impact of different disturbances and nutrient conditions upon functional characteristics of grassland communities. Ann. Bot. 106, 823–831. doi:https://doi.org/10.1093/aob/mcq178

Duru, M., Cruz, P., Magda, D., Pfadenhauer, J., 2004. Using plant traits to compare sward structure and composition of grass species across environmental gradients. Appl. Veg. Sci. 7, 11–18. doi:10.1658/1402-2001(2004)007[0011:UPTTCS]2.0.CO;2

DWD [Deutscher Wetterdienst], 2015. 1x1 km Wetterdaten [WWW Document]. URL http://www.dwd.de/DE/leistungen/webwerdis/webwerdis.html (accessed 5.15.16).

EEA [European Environment Agency], 2001. Pressures on grasslands. Indicator fact sheet [WWW Document]. URL http://www.eea.europa.eu/data-and-maps/indicators/pressures-on-grasslands#tab-figures-supporting-this (accessed 1.31.17).

Efron, B., Gong, G., 1983. A leisurely look at the bootstrap, the jackknife, and cross-validation. Am. Stat. 37, 36–48. doi:10.1080/00031305.1983.10483087

Egbert, D.D., Ulaby, F.T., 1972. Effect of angles on reflectivity. Photogramm. Eng. Remote Sens. 38, 556–564.

Elvidge, C.D., 1990. Visible and near infrared reflectance characteristics of dry plant materials. Int. J. Remote Sens. 11, 1775–1795. doi:10.1080/01431169008955129

Elvidge, C.D., Chen, Z., 1995. Comparison of broad-band and narrow-band red and near-infrared vegetation indices. Remote Sens. Environ. 54, 38–48. doi:10.1016/0034-4257(95)00132-K

Ernst, P., Loeper, E.G., 1976. Temperaturentwicklung und Vegetationsbeginn auf dem Grünland. Wirtschaftseigene Futter 22, 5–11.

ESA [European Space Agency] (ed.), 2015. Sentinel-2A spectral response functions (S2A-SRF) [WWW Document]. URL https://sentinel.esa.int/web/sentinel/user-guides/sentinel-2-msi/document-library/-/asset_publisher/Wk0TKajiISaR/content/sentinel-2a-spectral-responses (accessed 11.4.16).

Eurostat (ed.), 2017. Agri-environmental indicator - cropping patterns [WWW Document]. URL http://ec.europa.eu/eurostat/statistics-explained/index.php/Agri-environmental_indicator_-_cropping_patterns (accessed 1.8.17).

FAO [Food and Agricultural Organization of the United Nations], 2008. Are grasslands under threat? Brief analysis of FAO statistical data on pasture and fodder crops [WWW Document]. URL http://www.fao.org/ag/agp/agpc/doc/grass_stats/grass-stats.htm (accessed 1.31.17).

Fava, F., Colombo, R., Bocchi, S., Meroni, M., Sitzia, M., Fois, N., Zucca, C., 2009. Identification of hyperspectral vegetation indices for Mediterranean pasture characterization. Int. J. Appl. Earth Obs. Geoinf. 11, 233–243. doi:10.1016/j.jag.2009.02.003

Fava, F., Parolo, G., Colombo, R., Gusmeroli, F., Della Marianna, G., Monteiro, A.T., Bocchi, S., 2010. Fine-scale assessment of hay meadow productivity and plant diversity in the European Alps using field spectrometric data. Agric. Ecosyst. Environ. 137, 151–157.

Feilhauer, H., Asner, G.P., Martin, R.E., Schmidtlein, S., 2010. Brightness-normalized partial least squares regression for hyperspectral data. J. Quant. Spectrosc. Radiat. Transf. 111, 1947–1957. doi:10.1016/j.jqsrt.2010.03.007

Feilhauer, H., Schmidtlein, S., 2011. On variable relations between vegetation patterns and canopy reflectance. Ecol. Inform. 6, 83–92. doi:10.1016/j.ecoinf.2010.12.004

Feilhauer, H., Thonfeld, F., Faude, U., He, K.S., Rocchini, D., Schmidtlein, S., 2013. Assessing floristic composition with multispectral sensors - a comparison based on monotemporal and multiseasonal field spectra. Int. J. Appl. Earth Obs. Geoinformation 21, 218–229. doi:http://dx.doi.org/10.1016/j.jag.2012.09.002

Feret, J.-B., François, C., Asner, G.P., Gitelson, A.A., Martin, R.E., Bidel, L.P.R., Ustin, S.L., le Maire, G., Jacquemoud, S., 2008. PROSPECT-4 and 5: Advances in the leaf optical properties model separating photosynthetic pigments. Remote Sens. Environ. 112, 3030–3043. doi:10.1016/j.rse.2008.02.012

Ferner, J., Linstädter, A., Südekum, K.-H., Schmidtlein, S., 2015. Spectral indicators of forage quality in West Africa's tropical savannas. Int. J. Appl. Earth Obs. Geoinformation 41, 99–106. doi:10.1016/j.jag.2015.04.019

Field, C.B., 1991. Ecological scaling of carbon gain to stress and resource, in: Response of Plants to Multiple Stresses. Academic Press, San Diego, CA, USA, pp. 35–65.

Field, C.B., Chapin III, F.S., Brivio, P.A., Mooney, H.A., 1992. Responses of terrestrial ecosystems to the changing atmosphere: a resource-based approach. Annu. Rev. Ecol. Syst. 23, 201–235.

Fuentes, D.A., Gamon, J.A., Qiu, H., Sims, D.A., Roberts, D.A., 2001. Mapping Canadian boreal forest using pigment and water absorption features derived from the AVIRIS sensor. J. Geophys. Res. Atmospheres 106. doi:10.1029/2001JD900110

Gamon, J.A., Cheng, Y., Claudio, H., MacKinney, L., Sims, D.A., 2006. A mobile tram system for systematic sampling of ecosystem optical properties. Remote Sens. Environ. 103, 246–254. doi:10.1016/j.rse.2006.04.006

García-Ciudad, A., García-Criado, B., Pérez-Corona, M.E., Aldana, D., Vázquez, B.R., Ruano-Ramos, A.M., 1993. Application of near-infrared reflectance spectroscopy to chemical analysis of heterogeneous and botanically complex grassland samples. J. Sci. Food Agric. 63, 419–426.

Garnier, E., Laurent, G., Bellmann, A., Debain, S., Berthelier, P., Ducout, B., Roumet, C., Navas, M.-L., 2001. Consistency of species ranking based on functional leaf traits. New Phytol. 152, 69–83. doi:10.1046/j.0028-646x.2001.00239.x

Gebhardt, S., Schellberg, J., Lock, R., Kühbauch, W., 2006. Identification of broad-leaved dock (Rumex obtusifolius L.) on grassland by means of digital image processing. Precis. Agric. 7, 165–178. doi:10.1007/s11119-006-9006-9

Geerken, R., Batikha, N., Celis, D., DePauw, E., 2005. Differentiation of rangeland vegetation and assessment of its status: field investigations and MODIS and SPOT VEGETATION data analyses. Int. J. Remote Sens. 26, 4499–4526. doi:10.1080/01431160500213425

Gianelle, D., Vescovo, L., 2007. Determination of green herbage ratio in grasslands using spectral reflectance. Methods and ground measurements. Int. J. Remote Sens. 28, 931–942. doi:10.1080/01431160500196398

Gitelson, A.A., Kaufman, Y.J., Merzlyak, M.N., 1996. Use of a green channel in remote sensing of global vegetation from EOS-MODIS. Remote Sens. Environ. 58, 289–298. doi:10.1016/S0034-4257(96)00072-7

Gitelson, A.A., Merzlyak, M.N., 1996. Signature analysis of leaf reflectance spectra: algorithm development for remote sensing of chlorophyll. J. Plant Physiol. 148, 494–500.

Gitelson, A.A., Viña, A., Ciganda, V., Rundquist, D.C., Arkebauer, T.J., 2005. Remote estimation of canopy chlorophyll content in crops. Geophys. Res. Lett. 32, n/a-n/a. doi:10.1029/2005GL022688

Glenn, E.P., Huete, A.R., Nagler, P.L., Nelson, S.G., 2008. Relationship between remotely-sensed vegetation indices, canopy attributes and plant physiological processes: what vegetation indices can and cannot tell us about the landscape. Sensors 8, 2136–2160.

Goel, N.S., 1988. Models of vegetation canopy reflectance and their use in estimation of biophysical parameters from reflectance data. Remote Sens. Rev. 4, 1–212. doi:http://dx.doi.org/10.1080/02757258809532105

Gong, P., Pu, R., Biging, G.S., Larieu, M.R., 2003. Estimation of forest leaf area index using vegetation indices derived from Hyperion hyperspectral data. IEEE Trans. Geosci. Remote Sens. 41, 1355–1362. doi:10.1109/TGRS.2003.812910

Göttlicher, D., Albert, J., Nauss, T., Bendix, J., 2011. Optical properties of selected plants from a tropical mountain ecosystem – traits for plant functional types to parametrize a land surface model. Ecol. Model. 222, 493–502. doi:10.1016/j.ecolmodel.2010.09.021

Govaerts, Y.M., Verstraete, M.M., Pinty, B., Gobron, N., 1999. Designing optimal spectral indices: a feasibility and proof of concept study. Int. J. Remote Sens. 20, 1853–1873. doi:10.1080/014311699212524

Grime, J.P., 1998. Benefits of plant diversity to ecosystems: immediate, filter and founder effects. J. Ecol. 86, 902–910. doi:10.1046/j.1365-2745.1998.00306.x

Grime, J.P., 1977. Evidence for the existence of three primary strategies in plants and its relevance to ecological and evolutionary theory. Am. Nat. 111, 1169–1194. doi:10.1086/283244

Guyot, G., Baret, F., Major, D.J., 1988. High spectral resolution: determination of spectral shifts between the red and the near infrared. Int. Arch. Photogramm. Remote Sens. 11, 750–760.

Haboudane, D., Miller, J.R., Pattey, E., Zarco-Tejada, P.J., Strachan, I.B., 2004. Hyperspectral vegetation indices and novel algorithms for predicting green LAI of crop canopies: modeling and validation in the context of precision agriculture. Remote Sens. Environ. 90, 337–352. doi:10.1016/j.rse.2003.12.013

Hansen, P.M., Schjoerring, J.K., 2003. Reflectance measurement of canopy biomass and nitrogen status in wheat crops using normalized difference vegetation indices and partial least squares regression. Remote Sens. Environ. 86, 542–553. doi:10.1016/S0034-4257(03)00131-7

Harmoney, K.R., Moore, K.J., George, J.R., Brummer, E.C., Russell, J.R., 1997. Determination of pasture biomass using four indirect methods. Agron. J. 89, 665–672.

Harris, A.T., Asner, G.P., Miller, M.E., 2003. Changes in vegetation structure after long-term grazing in pinyon-juniper ecosystems: integrating imaging spectroscopy and field studies. Ecosystems 6, 368–383. doi:10.1007/s10021-003-0168-2

He, Y., Guo, X., Wilmshurst, J., 2006. Studying mixed grassland ecosystems I: suitable hyperspectral vegetation indices. Can. J. Remote Sens. 32, 98–107. doi:10.5589/m06-009

Hejcman, M., Češková, M., Schellberg, J., Pätzold, S., 2010a. The Rengen Grassland experiment: effect of soil chemical properties on biomass production, plant species composition and species richness. Folia Geobot. 45, 125–142. doi:10.1007/s12224-010-9062-9

Hejcman, M., Klaudisová, M., Schellberg, J., Honsová, D., 2007. The Rengen Grassland experiment: plant species composition after 64 years of fertilizer application. Agric. Ecosyst. Environ. 122, 259–266. doi:10.1016/j.agee.2006.12.036

Hejcman, M., Schellberg, J., Pavlů, V., 2010b. Long-term effects of cutting frequency and liming on soil chemical properties, biomass production and plant species composition

of Lolio-Cynosuretum grassland after the cessation of fertilizer application. Appl. Veg. Sci. 13, 257–269.

Hill, M.J., 2013. Vegetation index suites as indicators of vegetation state in grassland and savanna: an analysis with simulated SENTINEL 2 data for a North American transect. Remote Sens. Environ. 137, 94–111. doi:10.1016/j.rse.2013.06.004

Hill, M.J., Donald, G.E., Hyder, M.W., Smith, R.C.G., 2004. Estimation of pasture growth rate in the south west of Western Australia from AVHRR NDVI and climate data. Remote Sens. Environ. 93, 528–545.

Hirata, M., 1998. Dynamics of the horizontal distribution of herbage mass in a bahiagrass (Paspalum notatum Flugge) pasture grazed by cattle: stability of spatial pattern of herbage mass. Grassl. Sci. 44, 169–172.

Hollberg, J.L., Ferner, J., Schmidtlein, S., Schellberg, J., 2017a. Can we detect grassland plant functional traits based on canopy reflectance? Unpubl. Results.

Hollberg, J.L., Ferner, J., Schmidtlein, S., Schellberg, J., 2017b. The potential of remote sensing sensors featuring different spectral resolution and range for detecting functional traits of grassland. Unpubl. Results.

Hollberg, J.L., Schellberg, J., 2017. Distinguishing intensity levels of grassland fertilization using vegetation indices. Remote Sens. 9, 1–20. doi:10.3390/rs9010081

Homolová, L., Malenovský, Z., Clevers, J.G.P.W., García-Santos, G., Schaepman, M.E., 2013. Review of optical-based remote sensing for plant trait mapping. Ecol. Complex. 15, 1–16. doi:10.1016/j.ecocom.2013.06.003

Hopkins, A., Holz, B., 2006. Grassland for agriculture and nature conservation: production, quality and multi-functionality. Agron. Res. 4, 3–20.

Houborg, R., Fisher, J.B., Skidmore, A.K., 2015. Advances in remote sensing of vegetation function and traits. Spec. Issue Adv. Remote Sens. Veg. Funct. Traits 43, 1–6. doi:10.1016/j.jag.2015.06.001

Huang, Z., Turner, B.J., Dury, S.J., Wallis, I.R., Foley, W.J., 2004. Estimating foliage nitrogen concentration from HYMAP data using continuum removal analysis. Remote Sens. Environ. 93, 18–29. doi:10.1016/j.rse.2004.06.008

Huber, S., Kneubühler, M., Psomas, A., Itten, K., Zimmermann, N.E., 2008. Estimating foliar biochemistry from hyperspectral data in mixed forest canopy. For. Ecol. Manag. 256, 491–501. doi:10.1016/j.foreco.2008.05.011

Hunt Jr., E.R., 1991. Airborne remote sensing of canopy water thickness scaled from leaf spectrometer data. Int. J. Remote Sens. 12, 643–649. doi:10.1080/01431169108929679

Hunt Jr., E.R., Doraiswamy, P.C., McMurtrey, J.E., Daughtry, C.S.T., Perry, E.M., Akhmedov, B., 2013. A visible band index for remote sensing leaf chlorophyll content at the canopy scale. Int. J. Appl. Earth Obs. Geoinformation 21, 103–112. doi:10.1016/j.jag.2012.07.020

Idso, S.B., Pinter Jr., P.J., Jackson, R.D., Reginato, R.J., 1980. Estimation of grain yields by remote sensing of crop senescence rates. Remote Sens. Environ. 9, 87–91. doi:10.1016/0034-4257(80)90049-8

Inoue, Y., Penuelas, J., 2001. An AOTF-based hyperspectral imaging system for field use in ecophysiological and agricultural applications. Int. J. Remote Sens. 22, 3883–3888.

Inoue, Y., Sakaiya, E., Zhu, Y., Takahashi, W., 2012. Diagnostic mapping of canopy nitrogen content in rice based on hyperspectral measurements. Remote Sens. Environ. 126, 210–221.

Jackson, R.D., Pinter, P.J., 1986. Spectral response of architecturally different wheat canopies. Remote Sens. Environ. 20, 43–56.

Jacquemoud, S., Verhoef, W., Baret, F., Bacour, C., Zarco-Tejada, P.J., Asner, G.P., François, C., Ustin, S.L., 2009. PROSPECT + SAIL models: a review of use for vegetation

characterization. Imaging Spectrosc. Spec. Issue 113, Supplement 1, S56–S66. doi:10.1016/j.rse.2008.01.026

Janzen, D.H., 1984. Dispersal of small seeds by big herbivores: foliage is the fruit. Am. Nat. 123, 338–353.

Jensen, J.R. (Ed.), 2007. Remote sensing of the environment. An Earth resource perspective. Second edition. Pearson Prentice Hall, Upper Saddle River, NJ, USA.

Jones, H.G., Vaughan, R.A., 2012. Remote sensing of vegetation. Principles, techniques, and applications. Oxford University Press, Oxford, UK.

Kahmen, S., Poschlod, P., Schreiber, K.-F., 2002. Conservation management of calcareous grasslands. Changes in plant species composition and response of functional traits during 25 years. Biol. Conserv. 104, 319–328. doi:10.1016/S0006-3207(01)00197-5

Karnieli, A., Gabai, A., Ichoku, C., Zaddy, E., 2002. Temporal dynamics of soil and vegetation spectral responses in a semi-arid environment. Int. J. Remote Sens. 23, 4073–4087. doi:http://dx.doi.org/10.1080/01431160110116338

Kattenborn, T., Fassnacht, F.E., Pierce, S., Lopatin, J., Grime, J.P., Schmidtlein, S., 2017. Linking plant strategies and plant traits derived by radiative transfer modelling. J. Veg. Sci. 28, 717–727. doi:10.1111/jvs.12525

Kawamura, K., Watanabe, N., Sakanoue, S., Inoue, Y., 2008. Estimating forage biomass and quality in a mixed sown pasture based on partial least squares regression with waveband selection. Grassl. Sci. 54, 131–145. doi:10.1111/j.1744-697X.2008.00116.x

Kemp, D.R., Guodong, H., Xiangyang, H., Michalk, D.L., Fujiang, H., Jianping, W., Yingjun, Z., 2013. Innovative grassland management systems for environmental and livelihood benefits. Proc. Natl. Acad. Sci. 110, 8369–8374.

Kleyer, M., Bekker, R.M., Knevel, I.C., Bakker, J.P., Thompson, K., Sonnenschein, M., Poschlod, P., Van Groenendael, J.M., Klimeš, L., Klimešová, J., Klotz, S., Rusch, G.M., Hermy, M., Adriaens, D., Boedeltje, G., Bossuyt, B., Dannemann, A., Endels, P., Götzenberger, L., Hodgson, J.G., Jackel, A.-K., Kühn, I., Kunzmann, D., Ozinga, W.A., Römermann, C., Stadler, M., Schlegelmilch, J., Steendam, H.J., Tackenberg, O., Wilmann, B., Cornelissen, J.H.C., Eriksson, O., Garnier, E., Peco, B., 2008. The LEDA traitbase: a database of life-history traits of the Northwest European flora. J. Ecol. 96, 1266–1274. doi:10.1111/j.1365-2745.2008.01430.x

Knox, N.M., Skidmore, A.K., Prins, H.H.T., Asner, G.P., van der Werff, H.M.A., de Boer, W.F., van der Waal, C., de Knegt, H.J., Kohi, E.M., Slotow, R., Grant, R.C., 2011. Dry season mapping of savanna forage quality, using the hyperspectral Carnegie Airborne Observatory sensor. Remote Sens. Environ. 115, 1478–1488. doi:10.1016/j.rse.2011.02.007

Knyazikhin, Y., Schull, M.A., Stenberg, P., Mõttus, M., Rautiainen, M., Yang, Y., Marshak, A., Carmona, P.L., Kaufmann, R.K., Lewis, P., Disney, M.I., Vanderbilt, V., Davis, A.B., Baret, F., Jacquemoud, S., Lyapustin, A., Myneni, R.B., 2012. Hyperspectral remote sensing of foliar nitrogen content. Proc. Natl. Acad. Sci. 110, E185–E192.

Kumar, L., Schmidt, K., Dury, S., Skidmore, A., 2001. Imaging spectrometry and vegetation science, in: van der Meer, F.D., Jong, S.M.D. (Eds.), Imaging Spectrometry: Basic Principles and Prospective Applications. Springer, Dordrecht, Netherlands, pp. 111–155.

Laba, M., Tsai, F., Ogurcak, D., Smith, S., Richmond, M.E., 2005. Field determination of optimal dates for the discrimination of invasive wetland plant species using derivative spectral analysis. Photogramm. Eng. Remote Sens. 71, 603–611. doi:https://doi.org/10.14358/PERS.71.5.603

Lavorel, S., Díaz, S., Cornelissen, J.H.C., Garnier, E., Harrison, S.P., McIntyre, S., Pausas, J.G., Pérez-Harguindeguy, N., Roumet, C., Urcelay, C., 2007. Plant functional types: are we getting any closer to the holy grail?, in: Canadell, J.G., Pataki, D.E., Pitelka, L.F. (Eds.),

Terrestrial Ecosystems in a Changing World. Springer, Berlin, Heidelberg, pp. 149–164.

Lavorel, S., Garnier, E., 2002. Predicting changes in community composition and ecosystem functioning from plant traits: revisiting the holy grail. Funct. Ecol. 16, 545–556. doi:10.1046/j.1365-2435.2002.00664.x

Lavorel, S., Grigulis, K., Lamarque, P., Colace, M.-P., Garden, D., Girel, J., Pellet, G., Douzet, R., 2011. Using plant functional traits to understand the landscape distribution of multiple ecosystem services. J. Ecol. 99, 135–147. doi:10.1111/j.1365-2745.2010.01753.x

Lavorel, S., McIntyre, S., Landsberg, J., Forbes, T.D.A., 1997. Plant functional classifications: from general groups to specific groups based on response to disturbance. Trends Ecol. Evol. 12, 474–478. doi:10.1016/S0169-5347(97)01219-6

Liancourt, P., Callaway, R.M., Michalet, R., 2005. Stress tolerance and competitive-response ability determine the outcome of biotic interactions. Ecology 86, 1611–1618. doi:10.1890/04-1398

Lindberg, W., Persson, J.-Å., Wold, S., 1983. Partial least-squares method for spectrofluorimetric analysis of mixtures of humic acid and lignin sulfonate. Anal. Chem. 55, 643–648.

Ling, B., Goodin, D.G., Mohler, R.L., Laws, A.N., Joern, A., 2014. Estimating canopy nitrogen content in a heterogeneous grassland with varying fire and grazing treatments: Konza Prairie, Kansas, USA. Remote Sens. 6, 4430–4453.

Loarie, S.R., Joppa, L.N., Pimm, S.L., 2007. Satellites miss environmental priorities. Trends Ecol. Evol. 22, 630–632. doi:http://dx.doi.org/10.1016/j.tree.2007.08.018

Lobell, D.B., Asner, G.P., Law, B.E., Treuhaft, R.N., 2002. View angle effects on canopy reflectance and spectral mixture analysis of coniferous forests using AVIRIS. Int. J. Remote Sens. 23, 2247–2262. doi:10.1080/01431160110075613

Lorber, A., Wangen, L.E., Kowalski, B.R., 1987. A theoretical foundation for the PLS algorithm. J. Chemom. 1, 19–31. doi:10.1002/cem.1180010105

Lorenzen, B., Jensen, A., 1988. Reflectance of blue, green, red and near infrared radiation from wetland vegetation used in a model discriminating live and dead above ground biomass. New Phytol. 108, 345–355. doi:10.1111/j.1469-8137.1988.tb04173.x

Los, S.O., North, P.R.J., Grey, W.M.F., Barnsley, M.J., 2005. A method to convert AVHRR normalized difference vegetation index time series to a standard viewing and illumination geometry. Remote Sens. Environ. 99, 400–411. doi:10.1016/j.rse.2005.08.017

Lu, D., 2006. The potential and challenge of remote sensing-based biomass estimation. Int. J. Remote Sens. 27, 1297–1328. doi:10.1080/01431160500486732

Lucas, R.M., Honzak, M., Foody, G.M., Curran, P.J., Corves, C., 1993. Characterizing tropical secondary forests using multi-temporal Landsat sensor imagery. Int. J. Remote Sens. 14, 3061–3067. doi:10.1080/01431169308904419

Luntz, A., Brailovsky, V., 1969. On estimation of characters obtained in statistical procedure of recognition. Tech. Kibern. 3, 6–12.

Magiera, A., Feilhauer, H., Otte, A., Waldhardt, R., Simmering, D., 2013. Relating canopy reflectance to the vegetation composition of mountainous grasslands in the Greater Caucasus. Agric. Ecosyst. Environ. 177, 101–112. doi:10.1016/j.agee.2013.05.017

Martens, H., Martens, M., 2000. Modified Jack-knife estimation of parameter uncertainty in bilinear modelling by partial least squares regression (PLSR). Food Qual. Prefer. 11, 5–16.

McGill, B.J., Enquist, B.J., Weiher, E., Westoby, M., 2006. Rebuilding community ecology from functional traits. Trends Ecol. Evol. 21, 178–185.

McGwire, K., Minor, T., Fenstermaker, L., 2000. Hyperspectral mixture modeling for quantifying sparse vegetation cover in arid environments. Remote Sens. Environ. 72, 360–374.

McIntyre, S., Lavorel, S., 2001. Livestock grazing in subtropical pastures: steps in the analysis of attribute response and plant functional types. J. Ecol. 89, 209–226.

Middleton, E.M., 1991. Solar zenith angle effects on vegetation indices in tallgrass prairie. Remote Sens. Environ. 38, 45–62. doi:10.1016/0034-4257(91)90071-D

Mutanga, O., Adam, E., Adjorlolo, C., Abdel-Rahman, E.M., 2015. Evaluating the robustness of models developed from field spectral data in predicting African grass foliar nitrogen concentration using WorldView-2 image as an independent test dataset. Int. J. Appl. Earth Obs. Geoinformation 34, 178–187. doi:10.1016/j.jag.2014.08.008

Mutanga, O., Skidmore, A.K., Prins, H.H.T., 2004. Predicting in situ pasture quality in the Kruger National Park, South Africa, using continuum-removed absorption features. Remote Sens. Environ. 89, 393–408. doi:10.1016/j.rse.2003.11.001

Myneni, R.B., Ross, J., Asrar, G., 1989. A review on the theory of photon transport in leaf canopies. Agric. For. Meteorol. 45, 1–153. doi:10.1016/0168-1923(89)90002-6

Næs, T., Martens, H., 1984. Multivariate calibration. II. Chemometric methods. Trends Anal. Chem. 3, 266–271. doi:10.1016/0165-9936(84)80044-8

Norman, J.M., Welles, J.M., Walter, E.A., 1985. Contrasts among bidirectional reflectance of leaves, canopies, and soils. IEEE Trans. Geosci. Remote Sens. 23, 659–667. doi:10.1109/TGRS.1985.289384

Numata, I., Roberts, D.A., Chadwick, O.A., Schimel, J.P., Galvao, L.S., Soares, J.V., 2008. Evaluation of hyperspectral data for pasture estimate in the Brazilian Amazon using field and imaging spectrometers. Remote Sens. Environ. 112, 1569–1583. doi:10.1016/j.rse.2007.08.014

O`Mara, F.P., 2012. The role of grasslands in food security and climate change. Ann. Bot. 110, 1263–1270. doi:10.1093/aob/mcs209

Oldeland, J., Dorigo, W., Lieckfeld, L., Lucieer, A., Jürgens, N., 2010. Combining vegetation indices, constrained ordination and fuzzy classification for mapping semi-natural vegetation units from hyperspectral imagery. Remote Sens. Environ. 114, 1155–1166. doi:10.1016/j.rse.2010.01.003

Ollinger, S.V., 2011. Sources of variability in canopy reflectance and the convergent properties of plants. New Phytol. 189, 375–394. doi:10.1111/j.1469-8137.2010.03536.x

OSM [OpenStreetMap], 2014. OpenStreetMap [WWW Document]. URL http://www.openstreetmap.org (accessed 10.10.14).

Paruelo, J.M., Golluscio, R.A., Guerschman, J.P., Cesa, A., Jouve, V.V., Garbulsky, M.F., 2004. Regional scale relationships between ecosystem structure and functioning: the case of the Patagonian steppes. Glob. Ecol. Biogeogr. 13, 385–395. doi:10.1111/j.1466-822X.2004.00118.x

Patenaude, G., Milne, R., Dawson, T.P., 2005. Synthesis of remote sensing approaches for forest carbon estimation: reporting to the Kyoto Protocol. Environ. Sci. Policy 8, 161–178. doi:10.1016/j.envsci.2004.12.010

Peñuelas, J., Filella, I., 1998. Visible and near-infrared reflectance techniques for diagnosing plant physiological status. Trends Plant Sci. 3, 151–156. doi:10.1016/S1360-1385(98)01213-8

Peñuelas, J., Filella, I., Biel, C., Serrano, L., Savè, R., 1993. The reflectance at the 950–970 nm region as an indicator of plant water status. Int. J. Remote Sens. 14, 1887–1905.

Peñuelas, J., Gamon, J.A., Fredeen, A.L., Merino, J., Field, C.B., 1994. Reflectance indices associated with physiological changes in nitrogen- and water-limited sunflower leaves. Remote Sens. Environ. 48, 135–146. doi:10.1016/0034-4257(94)90136-8

Peñuelas, J., Pinol, J., Ogaya, R., Filella, I., 1997. Estimation of plant water concentration by the reflectance water index WI (R900/R970). Int. J. Remote Sens. 18, 2869–2875. doi:10.1080/014311697217396

Peñuelas, P., Filella, I., Lloret, P., Munoz, F., Vilajeliu, M., 1995. Reflectance assessment of mite effects on apple trees. Int. J. Remote Sens. 16, 2727–2733. doi:10.1080/01431169508954588

Pimentel, D., 2006. Soil erosion: a food and environmental threat. Environ. Dev. Sustain. 8, 119–137. doi:10.1007/s10668-005-1262-8

Pinter, P.J., Jackson, R.D., Elaine Esra, C., Gausman, H.W., 1985. Sun-angle and canopy-architecture effects on the spectral reflectance of six wheat cultivars. Int. J. Remote Sens. 6, 1813–1825. doi:10.1080/01431168508948330

Poças, I., Cunha, M., Pereira, L.S., 2012. Dynamics of mountain semi-natural grassland meadows inferred from SPOT-VEGETATION and field spectroradiometer data. Int. J. Remote Sens. 33, 4334–4355. doi:10.1080/01431161.2011.645084

Pontes, L.S., Carrere, P., Andueza, D., Louault, F., Soussana, J.F., 2007. Seasonal productivity and nutritive value of temperate grasses found in semi-natural pastures in Europe: responses to cutting frequency and N supply. Grass Forage Sci. 62, 485–496.

Pontes, L.S., Louault, F., Carrere, P., Maire, V., Andueza, D., Soussana, J.-F., 2010. The role of plant traits and their plasticity in the response of pasture grasses to nutrients and cutting frequency. Ann. Bot. 105, 957–965. doi:10.1093/aob/mcq066

Poorter, H., De Jong, R., 1999. A comparison of specific leaf area, chemical composition and leaf construction costs of field plants from 15 habitats differing in productivity. New Phytol. 143, 163–176. doi:10.1046/j.1469-8137.1999.00428.x

Posse, G., Cingolani, A.M., 2004. A test of the use of NDVI data to predict secondary productivity. Appl. Veg. Sci. 7, 201–208. doi:10.1658/1402-2001(2004)007[0201:ATOTUO]2.0.CO;2

Price, K.P., Crooks, T.J., Martinko, E.A., 2001. Grasslands across time and scale: a remote sensing perspective. Photogramm. Eng. Remote Sens. 67, 414–420.

Psomas, A., Kneubühler, M., Huber, S., Itten, K., Zimmermann, N.E., 2011. Hyperspectral remote sensing for estimating aboveground biomass and for exploring species richness patterns of grassland habitats. Int. J. Remote Sens. 32, 9007–9031. doi:10.1080/01431161.2010.532172

Psomas, A., Zimmermann, N.E., Kneubühler, M., Kellenberger, T., Itten, K., 2005. Seasonal variability in spectral reflectance for discriminating grasslands along a dry-mesic gradient in Switzerland, in: Proceedings of 4th EARSeL Workshop on Imaging Spectroscopy, New Quality in Environmental Studies. pp. 655–656.

R Development Core Team, 2015. R: A language and environment for statistical computing. R Foundation for Statistical Computing, Vienna, Austria.

Rahman, A.F., Gamon, J.A., 2004. Detecting biophysical properties of a semi-arid grassland and distinguishing burned from unburned areas with hyperspectral reflectance. J. Arid Environ. 58, 597–610. doi:10.1016/j.jaridenv.2003.12.005

Ramoelo, A., Skidmore, A.K., Cho, M.A., Mathieu, R., Heitkönig, I.M.A., Dudeni-Tlhone, N., Schlerf, M., Prins, H.H.T., 2013. Non-linear partial least square regression increases the estimation accuracy of grass nitrogen and phosphorus using in situ hyperspectral and environmental data. ISPRS J. Photogramm. Remote Sens. 82, 27–40. doi:10.1016/j.isprsjprs.2013.04.012

Ramoelo, A., Skidmore, A.K., Schlerf, M., Mathieu, R., Heitkönig, I.M.A., 2011. Water-removed spectra increase the retrieval accuracy when estimating savanna grass nitrogen and phosphorus concentrations. ISPRS J. Photogramm. Remote Sens. 66, 408–417. doi:10.1016/j.isprsjprs.2011.01.008

Redshaw, E.S., Weisenburger, R.D., Mathison, G.W., Milligan, L.P., 1986. Near infrared reflectance spectroscopy for predicting forage composition and voluntary consumption and digestibility in cattle and sheep. Can. J. Anim. Sci. 66, 103–115. doi:10.4141/cjas86-012

Reid, R.L., Jung, G.A., Puoli, J.R., Cox-Ganser, J.M., Scott, L.L., 1992. Nutritive quality and palatability of switchgrass hays for sheep: effects of cultivar, nitrogen fertilization, and time of adaptation. J. Anim. Sci. 70, 3877–3888. doi:10.2527/1992.70123877x

Richter, K., Hank, T.B., Mauser, W., 2012. Derivation of biophysical variables from earth observation data: validation and statistical measures. J. Appl. Remote Sens. 6, 063557-1-063557-21. doi:10.1117/1.JRS.6.063557

Ripple, W.J., 1986. Spectral reflectance relationships to leaf water stress. Photogramm. Eng. Remote Sens. 52, 1669–1675.

Ritchie, J.T., NeSmith, D.S., 1991. Temperature and crop development, in: Hanks, J., Ritchie, J.T. (Eds.), Modeling Plant and Soil Systems. ASA, CSSA, SSSA, Madison, WI, USA, pp. 5–29.

Roberts, D.A., Numata, I., Holmes, K., Batista, G., Krug, T., Monteiro, A., Powell, B., Chadwick, O.A., 2002. Large area mapping of land-cover change in Rondonia using multitemporal spectral mixture analysis and decision tree classifiers. J. Geophys. Res. Atmos. 107(D20), 40_1-40_18. doi:10.1029/2001JD000374

Roberts, D.A., Smith, M.O., Adams, J.B., 1993. Green vegetation, nonphotosynthetic vegetation, and soils in AVIRIS data. Airbone Imaging Spectrom. 44, 255–269. doi:10.1016/0034-4257(93)90020-X

Rocchini, D., Balkenhol, N., Carter, G.A., Foody, G.M., Gillespie, T.W., He, K.S., Kark, S., Levin, N., Lucas, K., Luoto, M., Nagendra, H., Oldeland, J., Ricotta, C., Southworth, J., Neteler, M., 2010. Remotely sensed spectral heterogeneity as a proxy of species diversity: recent advances and open challenges. Spec. Issue Adv. Ecol. Remote Sens. Glob. Change 5, 318–329. doi:10.1016/j.ecoinf.2010.06.001

Roelofsen, H., van Bodegom, P., Kooistra, L., Witte, J.P., 2013. Trait estimation in herbaceous plant assemblages from in situ canopy spectra. Remote Sens. 5, 6323–6345. doi:10.3390/rs5126323

Rollin, E.M., Milton, E.J., 1998. Processing of high spectral resolution reflectance data for the retrieval of canopy water content information. Remote Sens. Environ. 65, 86–92. doi:10.1016/S0034-4257(98)00013-3

Ross, J., 1981. The radiation regime and architecture of plant stands. Kluwer, Dodrecht, The Netherlands.

Rossini, M., Cogliati, S., Meroni, M., Migliavacca, M., Galvagno, M., Busetto, L., Cremonese, E., Juliatta, T., Siniscalco, C., Morra di Cella, U., Colombo, R., 2012. Remote sensing-based estimation of gross primary production in a subalpine grassland. Biogeosciences 9, 2565–2584. doi:10.5194/bg-9-2565-2012

Rouse Jr., J., Haas, R., Schell, J., Deering, D., 1974. Monitoring vegetation systems in the Great Plains with ERTS. NASA special publication paper A20 351, 309–317.

Rusch, G.M., Pausas, J.G., Lepš, J., 2003. Plant functional types in relation to disturbance and land use: introduction. J. Veg. Sci. 14, 307–310. doi:10.1658/1100-9233(2003)014[0307:PFTIRT]2.0.CO;2

Ryser, P., 1996. The importance of tissue density for growth and life span of leaves and roots: a comparison of five ecologically contrasting grasses. Funct. Ecol. 10, 717–723. doi:10.2307/2390506

Sampson, P.H., Treitz, P.M., Mohammed, G.H., 2001. Remote sensing of forest condition in tolerant hardwoods: an examination of spatial scale, structure and function. Can. J. Remote Sens. 27, 232–246. doi:10.1080/07038992.2001.10854940

Sánchez-Azofeifa, G.A., Castro, K., Wright, S.J., Gamon, J., Kalacska, M., Rivard, B., Schnitzler, S.A., Feng, J.L., 2009. Differences in leaf traits, leaf internal structure, and spectral reflectance between two communities of lianas and trees: implications for remote sensing in tropical environments. Remote Sens. Environ. 113, 2076–2088. doi:10.1016/j.rse.2009.05.013

Savitzky, A., Golay, M.J.E., 1964. Smoothing and differentiation of data by simplified least squares procedures. Anal. Chem. 36, 1627–1639. doi:10.1021/ac60214a047

Schaepman, M.E., Ustin, S.L., Plaza, A.J., Painter, T.H., Verrelst, J., Liang, S., 2009. Earth system science related imaging spectroscopy—an assessment. Remote Sens Env. 113, S1, S123–S137. doi:10.1016/j.rse.2009.03.001

Schauer, C.S., Bohnert, D.W., Ganskopp, D.C., Richards, C.J., Falck, S.J., 2005. Influence of protein supplementation frequency on cows consuming low-quality forage: performance, grazing behavior, and variation in supplement intake. J. Anim. Sci. 83, 1715–1725. doi:10.2527/2005.8371715x

Schellberg, J., Möseler, B.M., Kühbauch, W., Rademacher, I.F., 1999. Long-term effects of fertilizer on soil nutrient concentration, yield, forage quality and floristic composition of a hay meadow in the Eifel mountains, Germany. Grass Forage Sci. 54, 195–207. doi:10.1046/j.1365-2494.1999.00166.x

Schellberg, J., Pontes, L.S., 2012. Plant functional traits and nutrient gradients on grassland. Grass Forage Sci. 67, 305–319. doi:10.1111/j.1365-2494.2012.00867.x

Schlerf, M., Atzberger, C., Hill, J., 2005. Remote sensing of forest biophysical variables using HyMap imaging spectrometer data. Remote Sens. Environ. 95, 177–194. doi:10.1016/j.rse.2004.12.016

Schlerf, M., Atzberger, C., Hill, J., Buddenbaum, H., Werner, W., Schüler, G., 2010. Retrieval of chlorophyll and nitrogen in Norway spruce (Picea abies L. Karst.) using imaging spectroscopy. Int. J. Appl. Earth Obs. Geoinformation 12, 17–26. doi:10.1016/j.jag.2009.08.006

Schmidt, K., Skidmore, A., Kloostermann, E., Van Oosten, H., Kumar, L., Janssen, J., 2004. Mapping coastal vegetation using an expert system and hyperspectral imagery. Photogramm. Eng. Remote Sens. 70, 703–716.

Schmidt, K.S., Skidmore, A.K., 2003. Spectral discrimination of vegetation types in a coastal wetland. Remote Sens. Environ. 85, 92–108. doi:10.1016/S0034-4257(02)00196-7

Schmidtlein, S., 2005. Imaging spectroscopy as a tool for mapping Ellenberg indicator values. J. Appl. Ecol. 42, 966–974. doi:10.1111/j.1365-2664.2005.01064.x

Schmidtlein, S., Feilhauer, H., Bruelheide, H., 2012. Mapping plant strategy types using remote sensing. J. Veg. Sci. 23, 395–405. doi:10.1111/j.1654-1103.2011.01370.x

Schmidtlein, S., Oldenburg, C., Feilhauer, H., 2015. Package autopls. Partial least square regression with backward selection of predictors. [WWW Document]. URL https://cran.r-project.org/web/packages/autopls/index.html (accessed 7.1.17).

Schmidtlein, S., Sassin, J., 2004. Mapping of continuous floristic gradients in grasslands using hyperspectral imagery. Remote Sens. Environ. 92, 126–138. doi:10.1016/j.rse.2004.05.004

Schut, A.G.T., Ketelaars, J.J.M.H., Meulemann, J., Kornet, J.G., Lockhorst, C., 2002. Novel imaging spectroscopy for grass sward characterization. Biosyst. Eng. 82, 131–141. doi:10.1006/bioe.2002.0060

Schut, A.G.T., Lokhorst, C., Hendriks, M.M.W.B., Kornet, J.G., Kasper, G., 2005. Potential of imaging spectroscopy as tool for pasture management. Grass Forage Sci. 60, 34–45.

Schut, A.G.T., Van Der Heijden, G.W.A.M., Hoving, I., Stienezen, M.W.J., Van Evert, F.K., Meuleman, J., 2006. Imaging spectroscopy for on-farm measurement of grassland yield and quality. Agron. J. 98, 1318–1325.

Serrano, L., Peñuelas, J., Ustin, S.L., 2002. Remote sensing of nitrogen and lignin in mediterranean vegetation from AVIRIS data: decomposing biochemical from structural signals. Remote Sens. Environ. 81, 355–364. doi:10.1016/S0034-4257(02)00011-1

Serrano, L., Ustin, S.L., Roberts, D.A., Gamon, J.A., Peñuelas, J., 2000. Deriving water content of chaparral vegetation from AVIRIS data. Remote Sens. Environ. 74, 570–581. doi:10.1016/S0034-4257(00)00147-4

Shaver, G.R., Street, L.E., Rastetter, E.B., Van Wijk, M.T., Williams, M., 2007. Functional convergence in regulation of net CO2 flux in heterogeneous tundra landscapes in Alaska and Sweden. J. Ecol. 95, 802–817.

Shen, M., Tang, Y., Klein, J., Zhang, P., Gu, S., Shimono, A., Chen, J., 2008. Estimation of aboveground biomass using in situ hyperspectral measurements in five major grassland ecosystems on the Tibetan Plateau. J. Plant Ecol. 1, 247–257. doi:https://doi.org/10.1093/jpe/rtn025

Shibayama, M., Akiyama, T., 1986. A spectroradiometer for field use. Radiometric estimation of nitrogen levels in field canopies. Jpn. J. Crop Sci. 55, 439–445.

Shibayama, M., Wiegand, C.L., 1985. View azimuth and zenith, and solar angle effects on wheat canopy reflectance. Remote Sens. Environ. 18, 91–103. doi:10.1016/0034-4257(85)90040-9

Sibanda, M., Mutanga, O., Rouget, M., 2016. Discriminating rangeland management practices using simulated HyspIRI, Landsat 8 OLI, Sentinel 2 MSI, and VENµS spectral data. IEEE J. Sel. Top. Appl. Earth Obs. Remote Sens. 9, 3957–3969.

Sibanda, M., Mutanga, O., Rouget, M., Odindi, J., 2015. Exploring the potential of in situ hyperspectral data and multivariate techniques in discriminating different fertilizer treatments in grasslands. J. Appl. Remote Sens. 9, 096033–096033.

Sims, D.A., Gamon, J.A., 2002. Relationships between leaf pigment content and spectral reflectance across a wide range of species, leaf structures and developmental stages. Remote Sens. Environ. 81, 337–354. doi:10.1016/S0034-4257(02)00010-X

Šmarda, P., Hejcman, M., Březinová, A., Horová, L., Steigerová, H., Zedek, F., Bures, P., Hejcmanová, P., Schellberg, J., 2013. Effect of phosphorus availability on the selection of species with different ploidy levels and genome sizes in a long-term grassland fertilization experiment. New Phytol. 200, 911–921. doi:10.1111/nph.12399

Smith, M.L., Martin, M.E., Plourde, L., Ollinger, S.V., 2003. Analysis of hyperspectral data for estimation of temperate forest canopy nitrogen concentration: comparison between an airborne (AVIRIS) and a spaceborne (Hyperion) sensor. IEEE Trans. Geosci. Remote Sens. 41, 1332–1337.

Stagakis, S., Markos, N., Sykioti, O., Kyparissis, A., 2010. Monitoring canopy biophysical and biochemical parameters in ecosystem scale using satellite hyperspectral imagery: an application on a Phlomis fruticosa Mediterranean ecosystem using multiangular CHRIS/PROBA observations. Remote Sens. Environ. 114, 977–994. doi:http://dx.doi.org/10.1016/j.rse.2009.12.006

Starks, P.J., Zhao, D., Phillips, W.A., Coleman, S.W., 2006. Herbage mass, nutritive value and canopy spectral reflectance of bermudagrass pastures. Grass Forage Sci. 61, 101–111. doi:10.1111/j.1365-2494.2006.00514.x

Steiner, U., Buerling, K., Oerke, E.-C., 2008. Sensor use in plant protection. Gesunde Pflanz. 60, 131–141.

Steininger, M.K., 2000. Satellite estimation of tropical secondary forest above-ground biomass: Data from Brazil and Bolivia. Int. J. Remote Sens. 21, 1139–1157. doi:10.1080/014311600210119

Stevens, A., Ramirez-Lopez, L., 2013. An introduction to the prospectr package. R package Vignette. R package version 0.1.3. [WWW Document]. URL https://cran.r-project.org/web/packages/prospectr/vignettes/prospectr-intro.pdf (accessed 1.31.17).

Svoray, T., Perevolotsky, A., Atkinson, P.M., 2013. Ecological sustainability in rangelands: the contribution of remote sensing. Int. J. Remote Sens. 34, 6216–6242. doi:10.1080/01431161.2013.793867

Thenkabail, P.S., 2003. Biophysical and yield information for precision farming from near-real-time and historical Landsat TM images. Int. J. Remote Sens. 24, 2879–2904.

Thenkabail, P.S., 2001. Optimal hyperspectral narrowbands for discriminating agricultural crops. Remote Sens. Rev. 20, 257–291. doi:10.1080/02757250109532439

Thenkabail, P.S., Enclona, E.A., Ashton, M.S., Legg, C., De Dieu, M.J., 2004a. Hyperion, IKONOS, ALI, and ETM+ sensors in the study of African rainforests. Remote Sens. Environ. 90, 23–43. doi:10.1016/j.rse.2003.11.018

Thenkabail, P.S., Enclona, E.A., Ashton, M.S., Van Der Meer, B., 2004b. Accuracy assessments of hyperspectral waveband performance for vegetation analysis applications. Remote Sens. Environ. 91, 354–376. doi:10.1016/j.rse.2004.03.013

Thenkabail, P.S., Lyon, J.G., Huete, A., 2012. Hyperspectral remote sensing of vegetation. Taylor & Francis, Boca Raton, FL, USA.

Thenkabail, P.S., Smith, R.B., De Pauw, E., 2002. Evaluation of narrowband and broadband vegetation indices for determining optimal hyperspectral wavebands for agricultural crop characterization. Photogramm. Eng. Remote Sens. 68, 607–622.

Thenkabail, P.S., Smith, R.B., De Pauw, E., 2000. Hyperspectral vegetation indices and their relationships with agricultural crop characteristics. Remote Sens. Environ. 71, 158–182. doi:10.1016/S0034-4257(99)00067-X

Theurillat, J.-P., Guisan, A., 2001. Potential impact of climate change on vegetation in the European Alps: a review. Clim. Change 50, 77–109.

Tilman, D., Cassman, K.G., Matson, P.A., Naylor, R., Polasky, S., 2002. Agricultural sustainability and intensive production practices. Nature 418, 671–677. doi:10.1038/nature01014

Trigg, S., Flasse, S., 2000. Characterizing the spectral-temporal response of burned savannah using in situ spectroradiometry and infrared thermometry. Int. J. Remote Sens. 21, 3161–3168. doi:10.1080/01431160050145045

Trombetti, M., Riaño, D., Rubio, M.A., Cheng, Y.B., Ustin, S.L., 2008. Multi-temporal vegetation canopy water content retrieval and interpretation using artificial neural networks for the continental USA. Remote Sens. Environ. 112, 203–215. doi:10.1016/j.rse.2007.04.013

Tucker, C.J., 1977. Asymptotic nature of grass canopy spectral reflectance. Appl. Opt. 16, 1151–1156.

Underwood, E., Ustin, S., Dipietro, D., 2003. Mapping nonnative plants using hyperspectral imagery. Remote Sens. Environ. 86, 150–161. doi:10.1016/S0034-4257(03)00096-8

USGS [United States Geological Survey] (ed.), 2016. Using the USGS spectral viewer. Relative spectral response of the Landsat 7 sensor [WWW Document]. Using USGS Spectr. Viewer Relat. Spectr. Response Landsat 7 Sens. URL http://landsat.usgs.gov/instructions.php (accessed 11.4.16).

Ustin, S.L., 2013. Remote sensing of canopy chemistry. Proc. Natl. Acad. Sci. U. S. A. 110, 804–805.

Ustin, S.L., Gamon, J.A., 2010. Remote sensing of plant functional types. New Phytol. 186, 795–816. doi:10.1111/j.1469-8137.2010.03284.x

Ustin, S.L., Gitelson, A.A., Jacquemoud, S., Schaepman, M., Asner, G.P., Gamon, J.A., Zarco-Tejada, P., 2009. Retrieval of foliar information about plant pigment systems from high resolution spectroscopy. Remote Sens. Environ. 113, S.1, S67–S77. doi:http://doi.org/10.1016/j.rse.2008.10.019

Vallentine, J.F., 1990. Grazing management. 2nd ed. Academic Press, San Diego, CA, USA.

van der Heijden, G.W.A.M., Clevers, J.G.P.W., Schut, A.G.T., 2007. Combining close-range and remote sensing for local assessment of biophysical characteristics of arable land. Int. J. Remote Sens. 28, 5485–5502. doi:10.1080/01431160601105892

van Leeuwen, W.J.D., Huete, A., 1996. Effects of standing litter on the biophysical interpretation of plant canopies with spectral indices. Remote Sens. Environ. 55, 123–134.

van Soest, P.J., Robertson, J.B., Lewis, B.A., 1991. Methods for dietary fiber, neutral detergent fiber, and nonstarch polysaccharides in relation to animal nutrition. J. Dairy Sci. 74, 3583–3597. doi:10.3168/jds.S0022-0302(91)78551-2

Velthof, G.L., Oenema, O., 1995. Nitrous oxide fluxes from grassland in the Netherlands: I. Statistical analysis of flux-chamber measurements. Eur. J. Soil Sci. 46, 533–540. doi:10.1111/j.1365-2389.1995.tb01349.x

Verrelst, J., Geerling, G.W., Sykora, K.V., Clevers, J.G.P.W., 2009. Mapping of aggregated floodplain plant communities using image fusion of CASI and LiDAR data. Int. J. Appl. Earth Obs. Geoinformation 11, 83–94. doi:10.1016/j.jag.2008.09.001

Verstraete, M.M., Pinty, B., Myneni, R.B., 1996. Potential and limitations of information extraction on the terrestrial biosphere from satellite remote sensing. Remote Sens. Environ. 58, 201–214.

Vinzi, V.E., Chin, W.W., Henseler, J., Wang, H.E., 2010. Handbook of partial least squares. Concepts, methods, and applications. Springer, Heidelberg, London, Dordrecht, New York.

Violle, C., Navas, M.-L., Vile, D., Kazakou, E., Fortunel, C., Hummel, I., Garnier, E., 2007. Let the concept of trait be functional! Oikos 116, 882–892. doi:10.1111/j.0030-1299.2007.15559.x

Wang, F.-M., Huang, J.-F., Wang, X.-Z., 2008. Identification of optimal hyperspectral bands for estimation of rice biophysical parameters. J. Integr. Plant Biol. 50, 291–299. doi:10.1111/j.1744-7909.2007.00619.x

Wang, Q., Adiku, A., Tenhunen, J., Granier, A., 2005. On the relationship of NDVI with leaf area index in a deciduous forest site. Remote Sens. Environ. 94, 244–255. doi:10.1016/j.rse.2004.10.006

Wardlow, B.D., Egbert, S.L., Kastens, J.H., 2007. Analysis of time-series MODIS 250 m vegetation index data for crop classification in the U.S. Central Great Plains. Remote Sens. Environ. 108, 290–310. doi:10.1016/j.rse.2006.11.021

Weiher, E., Werf, A., Thompson, K., Roderick, M., Garnier, E., Eriksson, O., 1999. Challenging Theophrastus: a common core list of plant traits for functional ecology. J. Veg. Sci. 10, 609–620.

Welch, B.L., 1938. The significance of the difference between two means when the population variances are unequal. Biometrika 29, 350–362.

West, G.B., Brown, J.H., Enquist, B.J., 1997. A general model for the origin of allometric scaling laws in biology. Science 276, 122. doi:10.1126/science.276.5309.122

West, J.S., Bravo, C., Oberti, R., Lemaire, D., Moshou, D., McCartney, H.A., 2003. The potential of optical canopy measurement for targeted control of field crop diseases. Annu. Rev. Phytopathol. 41, 593–614.

Westoby, M., Eldridge, D., Freudenberger, D., 1999. The LHS strategy scheme in relation to grazing and fire. Presented at the VIth International Rangeland Congress, Townsville, AU, pp. 893–896.

Westoby, M., Falster, D.S., Moles, A.T., Vesk, P.A., Wright, I.J., 2002. Plant ecological strategies: some leading dimensions of variations between species. Annu. Rev. Ecol. Syst. 33, 125–159. doi:10.1146/annurev.ecolsys.33.010802.150452

Wickham, H., Chang, W., 2016. ggplot2. Create elegant data visualisations using the grammar of graphics [WWW Document]. URL https://cran.r-project.org/web/packages/ggplot2/index.html (accessed 7.1.17).

Widlowski, J.-L., Pinty, B., Gobron, N., Verstraete, M.M., Diner, D.J., Davis, A.B., 2004. Canopy structure parameters derived from multi-angular remote sensing data for terrestrial carbon studies. Clim. Change 67, 403–415. doi:10.1007/s10584-004-3566-3

Wold, S., Sjöström, M., Eriksson, L., 2001. PLS-regression: a basic tool of chemometrics. PLS Methods 58, 109–130. doi:10.1016/S0169-7439(01)00155-1

Wright, I.J., Reich, P.B., Cornelissen, J.H.C., Falster, D.S., Garnier, E., Hikosaka, K., Lamont, B.B., Lee, W., Oleksyn, J., Osada, N., Poorter, H., Villar, R., Warton, D.I., Westoby, M., 2005. Assessing the generality of global leaf trait relationships. New Phytol. 166, 485–496. doi:10.1111/j.1469-8137.2005.01349.x

Xavier, A.C., Rudorff, B.F.T., Moreira, M.A., Alvarenga, B.S., de Freitas, J.G., Salomon, M.V., 2006. Hyperspectral field reflectance measurements to estimate wheat grain yield and plant height. Sci. Agric. 63, 130–138.

Yasuda, T., Shiyomi, M., Takahashi, S., 2003. Differences in spatial heterogeneity at the species and community levels in semi-natural grasslands under different grazing intensities. J. Jpn. Soc. Grassl. Sci. Jpn. 49, 101–108.

Yoder, B.J., Pettigrew-Crosby, R.E., 1995. Predicting nitrogen and chlorophyll content and concentrations from reflectance spectra (400–2500 nm) at leaf and canopy scales. Remote Sens. Environ. 53, 199–211. doi:10.1016/0034-4257(95)00135-N

Zhang, C., Kovacs, J.M., Wachowiak, M.P., Flores-Verdugo, F., 2013. Relationship between hyperspectral measurements and mangrove leaf nitrogen concentrations. Remote Sens. 5, 891–908. doi:10.3390/rs5020891

Zhao, D., Starks, P.J., Brown, M.A., Phillips, W.A., Coleman, S.W., 2007. Assessment of forage biomass and quality parameters of bermudagrass using proximal sensing of pasture canopy reflectance. Grassl. Sci. 53, 39–49. doi:10.1111/j.1744-697X.2007.00072.x

Zutta, B., 2003. Assessing vegetation functional type and biodiversity in Southern California using spectral reflectance. M. Sc. thesis. California State University, Los Angeles, CA, USA.

7   Appendices

*Table A 1. Performance of the fifteen VIs for distinguishing the five grassland communities in Growth 1 and Growth 2 (Welch test with α= 0.9; * p < 0.1, ** p < 0.05,*

		nWI	nREP	LCI	nSIPI	nWC	nNDLI	nNDNI	nLCI	NDVI	nGNDVI	nNDVI	GNDVI	nPRI	nNPCI	nNPQI
Growth 1	nWI	-	-	**	**	***	***	***	***	***	***	***	***	***	***	***
	nREP	-	-	-	*	**	**	***	***	***	***	***	***	***	***	***
	LCI	**	-	-	-	-	-	**	***	***	***	***	***	***	***	***
	nSIPI	**	*	-	-	-	-	-	**	**	**	**	***	***	***	***
	nWC	***	**	-	-	-	-	-	-	*	*	*	**	***	***	***
	nNDLI	***	**	-	-	-	-	-	-	*	*	*	**	***	***	***
	nNDNI	***	***	**	-	-	-	-	-	-	-	-	-	*	**	***
	nLCI	***	***	***	**	-	-	-	-	-	-	-	-	**	**	***
	NDVI	***	***	***	**	*	*	-	-	-	-	-	-	*	**	***
	nGNDVI	***	***	***	**	*	*	-	-	-	-	-	-	*	*	***
	nNDVI	***	***	***	**	*	*	-	-	-	-	-	-	-	**	***
	GNDVI	***	***	***	***	**	**	-	-	-	-	-	-	-	**	***
	nPRI	***	***	***	***	***	***	*	**	*	*	-	-	-	-	-
	nNPCI	***	***	***	***	***	***	**	**	**	*	**	**	-	-	-
	nNPQI	***	***	***	***	***	***	***	***	***	***	***	***	-	-	-

		nREP	nWI	LCI	nSIPI	nWC	nNDNI	nNPCI	nGNDVI	nNDLI	nLCI	nNDVI	GNDVI	NDVI	nPRI	nNPQI
Growth 2	nREP	-	-	-	-	*	**	***	***	***	***	***	***	***	***	***
	nWI	-	-	-	-	-	*	**	**	**	**	**	***	***	***	***
	LCI	-	-	-	-	-	*	***	**	**	***	***	***	***	***	***
	nSIPI	-	-	-	-	-	-	**	**	**	***	***	***	***	***	***
	nWC	*	-	-	-	-	-	*	-	-	**	**	**	***	***	***
	nNDNI	**	*	**	-	-	-	-	-	-	-	-	-	-	**	**
	nNPCI	***	**	***	**	*	-	-	-	-	-	-	-	-	***	***
	nGNDVI	***	**	**	**	-	-	-	-	-	-	-	-	-	*	**
	nNDLI	***	**	**	**	-	-	-	-	-	-	-	-	-	*	*
	nLCI	***	**	***	***	**	-	-	-	-	-	-	-	-	**	***
	nNDVI	***	**	***	***	**	-	-	-	-	-	-	-	-	***	***
	GNDVI	***	***	***	***	**	-	-	-	-	-	-	-	-	*	**
	NDVI	***	***	***	***	***	-	-	-	-	-	-	-	-	*	*
	nPRI	***	***	***	***	***	**	***	*	*	**	***	*	*	-	-
	nNPQI	***	***	***	***	***	**	***	**	*	***	***	**	*	-	-

Table A 2. Averages and standard deviations of the Compressed Sward Height (CSH) measurements for 2013 and 2014.

Year	Growth	T∑ (°C·d)	CSH (cm)	SD (CSH)
2013	1	947	20.59	10.63
		964	6.49	2.51
	2	1077	4.62	2.15
		1378	6.98	2.95
2014	1	464	5.52	2.93
		560	7.75	4.23
		757	18.12	8.47
		883	17.72	10.09
		1017	17.18	9.64
		1307	24.5	18.21
	2	210	5.17	1.18
		804	10.54	5.37
		972	12.94	4.90
		1174	13.28	4.97
		1353	11.21	4.57

Figure A 1. The crane system installed at the Rengen Grassland Experiment (adapted, Photo: Vittek, M., 2013).

Figure A 2. Aerial imagery of the Rengen Grassland Experiment on October 2014. Optical differences between the single grassland plots are observed (Photo: Bareth, G., 2014).

Table A 3. Band selection frequency. Band regions were expressed in 30 nm wide intervals. Count represents the average frequency of single bands for detecting the 23 PFTs of each band region.

Bands (nm)	Rank	Count	Bands (nm)	Rank	Count
1551-1580	1	12	995-1024	28	4
1581-1610	2	9	2001-2030	29	3
365-394	3	9	845-874	30	3
1115-1144	4	8	905-934	31	3
665-694	5	7	1055-1084	32	3
515-544	6	7	2031-2060	33	3
635-664	7	7	425-454	34	3
1611-1640	8	6	725-754	35	2
1205-1234	9	6	2301-2330	36	2
935-964	10	6	2271-2300	37	2
1731-1760	11	5	2241-2270	38	2
1701-1730	12	5	1671-1700	39	2
1145-1174	13	5	2121-2150	40	2
1085-1114	14	4	605-634	41	2
1175-1204	15	4	785-814	42	2
695-724	16	4	965-994	43	2
1325-1354	17	4	1235-1264	44	2
395-424	18	4	2331-2360	45	2
1761-1790	19	4	2061-2090	46	2
1025-1054	20	4	1295-1324	47	2
815-844	21	4	455-484	48	2
1641-1670	22	4	575-604	49	2
485-514	23	4	875-904	50	2
755-784	24	4	2181-2210	51	1
1265-1294	25	4	2151-2180	52	1
2091-2120	26	4	2211-2240	53	1
545-574	27	4			